Radiometric Measurement of Thermodynamic Temperatures in the Temperature Range from 419 °C to 660 °C for an Improved Temperature Scale

vorgelegt von

M.Sc.
Narudom Noulkhow
aus Suratthani (Thailand)

Der Fakultät II - Mathematik und Naturwissenschaften
der Technischen Universität Berlin
zur Erlangung des akademischen Grades
Doktor der Ingenieurwissenschaften
-Dr.-Ing.-

genehmigte Dissertation

Promotionsausschuss:

Vorsitzender: Prof. Dr. U. Woggon
Berichter/Gutachter: Prof. Dr. A. Hoffmann
Berichter/Gutachter: Prof. Dr. C. Thomsen

Tag der wissenschaftlichen Aussprache: 10. Dezember 2009

Berlin 2009

D 83

Abstract

The International Temperature Scale of 1990 (ITS-90), as a practical temperature scale, is a very good approximation of the true thermodynamic temperature. It is based on the phase transition temperatures of its defining fixed-points and interpolating and extrapolating instruments for the temperature measurement between and above these fixed-points. However, at the time the ITS-90 was established, the freezing points of tin and zinc had been measured twice, in 1976 and in 1989 at the National Institute of Standard and Technology (NIST) with a gas thermometer, and at a reference temperature of 730 K these two measurements gave significantly different results of 30 mK. Since no primary thermometry other than gas thermometry was available at that time in this temperature range, the Consultative Committee for Thermometry (CCT) decided to use the average value between these two measurements for the reference temperature of the ITS-90 at 730 K with a standard uncertainty of 15 mK with respect to thermodynamic temperature. This uncertainty is passed on and increases for the thermodynamic temperature determination of fixed-points with higher temperatures by radiation thermometry. In order to prepare a new improved practical temperature scale anticipated for the year 2011, possible deviations of the ITS-90 from the thermodynamic temperature have to be investigated with an accurate primary thermometry method, independent from gas thermometry.

This work contributes to solve the problem of the systematic deviation of 30 mK between the two gas thermometry measurements of the reference temperature at 730 K by applying absolute radiation thermometry as an independent primary thermometry method. To achieve this, two narrow-bandwidth filter radiometers based on InGaAs photodiodes working at 1300 nm and 1550 nm were realized and a double heat-pipe blackbody radiator was used as a high-accuracy source of thermal radiation in the temperature range from 692 K to 933 K. This temperature range covers the important zinc-fixed-point (692.677 K) and aluminum-fixed-point (933.473 K).

The filter radiometers were calibrated in terms of their spectral irradiance responsivity traceable to the most accurate primary detector standard, a cryogenic electrical substitution radiometer. A newly developed tuneable laser- and monochromator based - cryogenic radiometer facility allowed to reduce the relative standard uncertainty of the near infrared spectral responsivity scale to 0.03%. For the determination of the deviation of the ITS-90 temperature from the thermodynamic temperature a standard uncertainty of about 30 mK at 692 K and 60 mK at 933 K was achieved. With these radiometric measurements the set of gas thermometry measurements by Edsinger and Schooley in 1989 clearly agrees, while the gas thermometry results by Guildner und Edsinger in 1979 disagree.

Zusammenfassung

Die internationale Temperaturskala von 1990 (ITS-90) ist als praktische Temperaturskala eine sehr gute Näherung der thermodynamischen Temperatur. Sie basiert auf den Phasenübergangstemperaturen definierender Fixpunkte und Messverfahren der Inter- und Extrapolation für die Temperaturmessung zwischen und oberhalb dieser Fixpunkte. Zu der Zeit als die ITS-90 erstellt wurde, wurde die Erstarrungstemperatur von Zinn und Zink zweimal (1976 und 1989) am National Institute of Technology (NIST) mit einem Gasthermometer gemessen. Zwischen diesen beiden Messungen bestand ein signifikanter Unterschied von 30 mK bei einem Referenzwert von 730 K. Da zum damaligen Zeitpunkt und in diesem Temperaturbereich keine andere, von der Gasthermometrie unabhängige, primärthermometrische Methode zur Verfügung stand, wurde vom Consultative Committee for Thermometry (CCT) für die ITS-90 als primärthermometrischer Referenzwert bei 730 K der Mittelwert der beiden Messungen, mit einer Unsicherheit bezüglich der thermodynamischen Temperatur von 15 mK festgelegt. Durch die quadratische Fehlerfortpflanzung wirkt sich die Unsicherheit des Referenzwertes bezüglich der thermodynamischen Temperatur im Hochtemperaturbereich besonders deutlich aus. Für eine neue, verbesserte praktische Temperaturskala, müssen mögliche Abweichungen der ITS-90 von der thermodynamischen Temperatur mit genauen primärthermometrischen Methoden untersucht werden, die von der Gasthermometrie unabhängig ist.

Diese Arbeit trägt dazu bei, mit einer von der Gasthermometrie unabhängigen primärthermometrischen Methode, der spektralradiometrischen Messung thermodynamischer Temperaturen an einem Schwarzen Strahler, das Problem der systematischen Abweichung zwischen den beiden gasthermometrisch am NIST bestimmten Werten für die thermodynamische Temperatur des ITS-90-Referenzwertes zu lösen. Dazu wurden zwei schmalbandige Filterradiometer, die auf InGaAs Photodioden basieren mit den Schwerpunktwellenlängen 1300 nm und 1550 nm aufgebaut und ein Doppel-Wärmerohr-Hohlraumstrahler wurde als genaue Quelle von thermischer Strahlung im Temperatursbereich zwischen dem Zink-Fixpunkt (692.677 K) und dem Aluminium-Fixpunkt (933.473 K) eingesetzt.

Die Filterradiometer wurden bezüglich ihrer der spektralen Bestrahlungsstärke-empfindlichkeit kalibriert, d.h. rückgeführt auf ein bei sehr tiefen Temperaturen betriebenes (~5 K) elektrisches Substitutionsradiometer (Kryoradiometer) als Detektor-Primärnormal. An einem neuentwickelten Laser- und Monochromator gestützten Kryoradiometermessplatzes konnte die relative Standardunsicherheit der spektralen Empfindlichkeitskala im nahen Infrarot um den Faktor 6 auf 0.03% verringern werden. Bei der Bestimmung der Abweichung zwischen der ITS-90 Temperatur und der thermodynamischen Temperatur wurde eine Standard-unsicherheit von 30 mK bei 692 K und 60 mK bei 933 K erzielt.

Das Ergebnis dieser Arbeit für die thermodynamische Temperatur des Referenzwertes stimmt mit dem von Edsinger und Schooley 1989 am NIST erzielten Resultat sehr gut überein. Das Ergebnis von Guildner und Edsinger 1976 am NIST hingegen weicht signifikant davon ab.

Contents

List of Abbreviations

BIPM	Bureau International des Poids et Mesures, International Bureau of Weights and Measures (the international body responsible for metrology)
CCT	Comité Consultatif de Thermometrie, Consultative Committee on Thermometry (a consultative committee of the BIPM)
CGPM	Conférence Générale des Poids et Mesures, General Conference on Weights and Measures (held every 4 years at BIPM by representatives of the governments of all member states)
CODATA	Committee on Data for Science and Technology
CRI	Cambridge Research and Instrumentation (New type of cryogenic radiometer applied in this work)
CVGT	Constant volume gas thermometer
DCGT	Dielectric-constant gas thermometer
DVM	Digital volt meter
EPT-76	The 1976 Provisional 0.5 K to 30 K Temperature Scale
ESR	Electrical substitution radiometer
FIR	Far-infrared
FP	Fixed-point
FR	Filter radiometer
FWHM	Full width at half maximum
He-Ne laser	Helium-neon laser
IPTS-48	The International Practical Temperature Scale of 1948
IPTS-68	The International Practical Temperature Scale of 1968
IPTS-68(75)	the International Practical Temperature Scale of 1968 in the Amended Edition of 1975
ITS-27	The International Temperature Scale of 1927

ITS-48	The International Temperature Scale of 1948
ITS-90	International Temperature Scale of 1990
InGaAs	Indium gallium arsenide
LABB	Large aperture area blackbody
NIR	Near-infrared
NIST	National Institute of Standards and Technology, USA
PID controller	Proportional–integral–derivative controller
PTB	Physikalisch-Technische Bundesanstalt
RTCR	Radiation thermometry cryogenic radiometer
Si	Silicon
SI	Systéme International d'Unités, International System of Units
SPRT	Standard platinum resistance thermometer
TPW	The triple point of water
UV	Ultraviolet

Parts of this work have been published in the following publications:

1. N. Noulkhow, R. D. Taubert, P. Meindl and J. Hollandt, Infrared Filter Radiometers for Thermodynamic Temperature Determination below 660 °C, International Journal of Thermophysics, vol. 30, pp.131-143, 2009

2. N. Noulkhow, R. D. Taubert, P. Meindl, L. Werner, J. Hollandt, High-Accuracy Thermodynamic Temperature Measurements with Near Infrared Filter Radiometers, Proceedings of the 10th International Conference on Infrared Sensors & Systems, IRS^2 2008, pp. 219-224, pub. AMA Service GmbH, ISBN 978-3-9810993-3-1, 2008

3. N. Noulkhow, R. D. Taubert, P. Meindl, L. Werner, and J. Hollandt, Application of Absolutely Calibrated Near Infrared Filter Radiometers for High-Accuracy Thermodynamic Temperature Measurements, Proceedings of the 10th international conference on new developments and applications in optical radiometry, NEWRAD 2008, pp. 281-282, 2008

4. P. Meindl, N. Noulkhow, A. E. Klinkmüller, U. Johannsen, L. Werner, New PTB detector calibration capability for spectral responsivity in the NIR range, Proceedings of the 9th International Conference on Infrared Sensors & Systems, IRS^2 2006, pp. 213-215, pub. AMA Service GmbH, ISBN 978-3-9810993-0-0, 2006

5. A. E. Klinkmüller, P. Meindl, U. Johannsen, N. Noulkhow, and L. Werner, Improved NIR spectral responsivity scale of the PTB and implications for radiation thermometry, Proceedings of the 9th international conference on new developments and applications in optical radiometry, NEWRAD 2005, pp. 115, 2005

Chapter I

Introduction

The economic globalization requires an increased competitive capability and plays an important role in the optimization of production processes. In order to optimize a production process, it needs the measurement and regulation of all quantities which influence it. One of the most frequently measured quantity is temperature [**1**]. Therefore, a highly accurate and reproducible measurement of temperature traceable to the International Temperature Scale is mandatory in order to optimize the productivity and to fulfill the quality control requirements. In addition to industry, the accurate measurement of temperature in climate research and environmental protection is of crucial importance [**2**]. In the framework of climate modeling, long-term temperature measurements in conjunction with other relevant parameters and the resulting scientific prediction influence long-term political and economical decisions [**3**]. Therefore in 1999 the 21st Conference Generale des Poids et Mesures (CGPM) recommended to disseminate the thermodynamic temperature for studies of earth resources in order to guarantee permanent, world-wide comparable results of temperature measurements and the linkage to other well-characterized SI units [**4**].

The thermodynamic temperature is measured by primary thermo-meters [**5,6,7,8,9,10**]. However, it is difficult and very time-consuming to measure the thermodynamic temperature directly. Since 1927 internationally-agreed temperature scales are used for practical temperature measurements as a very good approximation of the thermodynamic temperature [**11**] and the currently agreed best approximation of the thermodynamic temperature is the International Temperature Scale of 1990 (ITS-90) [**12**]. The International Temperature Scales consist of a set of fixed-points and adequate interpolation and extrapolation instruments. For high accuracy temperature measurements, it is very important to assign accurate thermodynamic temperature values to these fixed-points as well as to have suitable

interpolation and extrapolation instruments in order for the practical temperature scale to be a good approximation of the thermodynamic temperature.

At the time ITS-90 was defined, the freezing points of tin and zinc had been measured twice, in 1976 [**13**] and 1989 [**5**], with a gas thermometer, at the National Institute of Standard and Technology (NIST). However, at the reference temperature of 730 K these two measurements gave significantly different results of 30 mK. At that time, in this temperature range no other kind of primary thermometer, which is independent from the gas thermometry, was available. Thus the Consultative Committee for Thermometry (CCT) used the average value between this two measurements with a standard uncertainty 15 mK for the reference temperature of the ITS-90 of 730 K [**14**]. This uncertainty is passed on and increases with the thermodynamic temperature determination of fixed-points with higher temperatures by radiation thermometry [**15,16,17,18**]. Therefore for an improved future temperature scale, the deviations of the fixed-point temperatures of the ITS-90 from the thermodynamic temperature (T-T_{90}) have to be determined with an accurate primary thermometry method, independent from the gas thermometry.

By using blackbody radiators as the primary standard sources of optical radiation from the ultraviolet (UV) to the far-infrared (FIR) spectral region in radiometry [**19,20**], the thermodynamic temperature of the blackbodies can be determined precisely by measuring the spectral irradiance of the blackbody via the Planck's law. Thereby the emissivity of the blackbody should be well known. Therefore the absolute radiometry of high quality blackbodies is the alternative primary thermometric method for the determination of T-T_{90}. This method applies an absolutely calibrated detector and the suitable type of detector for this method is a filter radiometer.

At the Physikalisch-Technische Bundesanstalt (PTB) absolutely calibrated filter radiometers based on silicon photodiodes (Si-FRs) are routinely used since more than ten years for the determination of the thermodynamic temperature of blackbodies in the range from about 3000 °C down to about 419 °C (the zinc-fixed-point, Zn-FP) [**21**]. The calibrations of these Si-FRs are traceable to a cryogenic electrical substitution radiometer which is the most accurate primary standard at PTB for the measurement of radiant power [**22,23,24**].

However, the determination of the thermodynamic temperature below 500 °C by using the Si-FRs becomes a difficult task due to their too low signal-to-noise ratio. To overcome this problem, in a first step the PTB has developed the first filter radiometer based on indium gallium arsenide photodiodes (InGaAs-FR) with a center wavelength at 1595 nm and a bandwidth (FWHM) of 100 nm [**21**]. This filter radiometer was absolutely calibrated in terms of spectral irradiance responsivity against the single InGaAs photodiode which was previously calibrated against the RTCR in terms of its spectral responsivity. Nevertheless the spectral responsivity maintained on this InGaAs photodiode is an interpolated scale of the near-infrared (NIR) spectral responsivity (950 nm to 1650 nm) [**23**] and has an uncertainty of more than one order of magnitude higher than the spectral responsivity scale maintained on Si-trap detectors [**24**]. The uncertainty of this NIR spectral responsivity scale is the main contribution to the standard uncertainty of the InGaAs filter radiometer calibration. As a consequence the standard uncertainty of the thermodynamic temperature determination applying this filter radiometer at the gas thermometry reference temperature (730 K) of the ITS-90 was about 104 mK [**21**]. Due to this relatively large uncertainty, the results for the thermodynamic temperature measured with this InGaAs filter radiometer could not yet be used for the investigation the accuracy of ITS-90 by with the determination of T-T_{90}.

To solve this problem, with this work the uncertainty of the spectral responsivity scale in the wavelength range from 950 nm to 1650 nm was significantly reduced through a newly developed tuneable laser- and monochromator-based cryogenic radiometer facility. Furthermore, two new InGaAs filter radiometers were built. These filter radiometers were optimized with respect to their bandwidth and center wavelength for a calibration with the lowest possible uncertainties, which is mandatory for high-accuracy radiometric temperature measurements. Finally they were successfully applied to measure T-T_{90} with an accuracy which allows to decide between the two conflicting two gas thermometry measurement at NIST.

This work is presented in 5 chapters. First the different primary thermometric methods to measure thermodynamic temperature and the International Temperature Scale are introduced (Chapter 2). Then the objectives for this thesis are formulated (Chapter 3). Chapter 4 describes the necessary improvement of the spectral responsivity scale in the NIR wavelength range for the transfer detectors applied in this work. Chapter 5 describes the design and the absolute calibration of the new

filter radiometers used in this work in terms of their spectral irradiance responsivity. Finally, the investigation of the accuracy of the ITS-90 temperature with these filter radiometers and the comparison of the radiometric results with the gas thermometry results are given in Chapter 6.

Chapter II

Theory and measurement concept

2.1 Thermodynamic temperature

The thermodynamic temperature *T* is the absolute measure of temperature and the basic thermodynamic quantity. It occurs in most relations between other thermodynamic quantities such as the equation of state. Temperature governs heat transfer between two systems in thermal contact, the efficiency of heat engines and the emission of heat radiation, and in statistical thermodynamics it is a parameter of probability distributions.

Many industrial production processes e.g. metal, glass or semiconductor production, chemical processes or food preparation are strongly influenced by temperature. Therefore, they can be compared only if they are determined at the same temperature. This reasons makes temperature besides time the most frequently measured physical quantity [**1**] and several million temperature sensors and temperature measuring devices are being newly installed worldwide every year.

The thermodynamic temperature is one of the seven base quantities of the International System of Units (SI) (see table 2.1). Temperature is an intensive quantity in contrast to other base quantities in SI which are extensive quantities e.g. mass or length. This mean temperature does not have the property of additivity i.e. we cannot realize the temperature 2*T* by joining two systems of temperature *T*. Therefore a temperature scale is needed to define the measurement of temperatures. In order to measure the temperature, a thermometer based on the change of a physical property of a material due to the temperature change in a reproducible way must be applied.

Table 2.1: Base units of the International System of Units (SI)

Base quantity	SI base unit	
	Name	Symbol
Mass	kilogram	kg
Length	meter	m
Time	second	s
Electric current	ampere	A
Thermodynamic temperature	kelvin	K
Amount of substance	mole	mol
Luminous intensity	candela	cd

The first device to measure temperature seems to have been invented by Galileo Galilei between 1592 and 1603. This instrument consisted of a glass bulb connected to a long tube immersed in a liquid. The liquid column in the tube rose or fell as a function of the ambient temperature. In the absence of any graduation it is better to call the instrument a thermoscope. About 1650, the members of the Florentine Academy of Sciences made the first thermometer consisting of a spiral-shaped tube with a closed end and a graduation. However, no numbers were ascribed to the graduation marks.

To standardize thermometers and temperature measurement the need arose to define temperature fixed-points. After first attempts in the late seventeenth century, Daniel Gabriel Fahrenheit from Danzig (now Gdansk in Poland) described in 1724 the mercury-in-glass thermometer and associated three temperature fixed-points with the device: a mixture of ice, water and ammonium chloride was taken as the zero point, a mixture of ice and water was taken as 32°, and the human body temperature was taken as 96°. The unit of the temperature scale was defined as degree Fahrenheit with the symbol °F. Another development of the mercury-in-glass thermometer was done by the Swedish astronomer and physicist Anders Celsius. In 1742, he assigned 0° as the freezing temperature of water and 100° as the temperature of boiling water. The region between these two points was divided into 100 equal steps. The temperature unit of the scale was defined as degree Celsius, symbol °C. The Celsius scale is used nowadays throughout science and in most countries.

A new temperature scale based on the second law of thermodynamics using the absolute zero temperature and one additional temperature fixed-point was proposed by William Thomson (later well known as Lord Kelvin) as early as 1854. About a hundred years later, in 1948, the 10th General Conference on Weights and Measures of the Metre Convention followed this suggestion. As the fixed point, the triple point of water (TPW) was chosen. The TPW is the unique point in the phase diagram where vapour, fluid and ice coexist (see figure 2.1). The triple-point temperature T_{TPW} was assigned the temperature 273.16 K, so that the unit of temperature, the Kelvin (symbol K), becomes

$$1\ \mathrm{K} = T_{TPW} / 273.16. \qquad 2.1$$

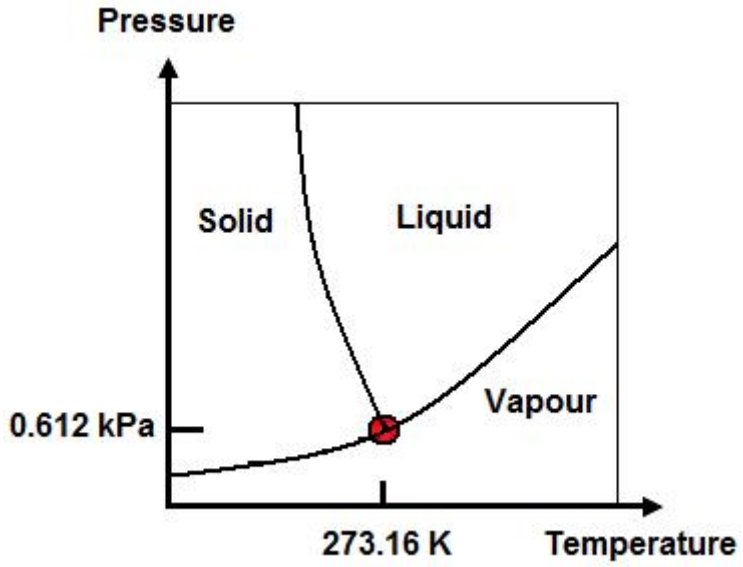

Figure 2.1 : Schematic diagram of the triple point of water (TPW)

The numerical value 273.16 was chosen for the TPW to be in as close agreement as possible with the degree Celsius used before, which was one hundredth of the temperature difference between the boiling point and the melting point of water at normal atmospheric pressure, p_{atm}= 101.325 kPa. In everyday life (and in the temperature range above 0°C, also in thermometry) the degree Celsius with the unit symbol °C is still in use though only as a specific name for the Kelvin for the statement of Celsius temperatures *t*. As the melting temperature of water at atmospheric pressure is slightly lower than the triple point temperature (the triple point pressure is only 0.612 kPa), the relation

$$t\,/°C = T\,/K - 273.15 \qquad 2.2$$

is valid if t and T designate the same temperature. The Celsius temperature scale is thus a Kelvin temperature scale with the zero point shifted to 273.15 K. Accordingly, a given temperature difference has the same numerical value in both the Kelvin and the Celsius scales:

$$\Delta t\,/°C = \Delta T/K. \qquad 2.3$$

2.2 Measurement of the thermodynamic temperature

Thermodynamic temperatures can be measured absolutely by methods which are described by physical equations of the type $f(T, A_i, \alpha_k) = 0$, whereas A_i are the temperature independent measurands [**26**] of the method and α_k are natural constants. One group of methods for the determination of the thermodynamic temperature is by using the physical properties of the ideal gas which is dependent from the temperature. The most important methods for this determination are:

- **Constant volume gas thermometer (CVGT) :**The CVGT is one of the most familiar thermodynamic thermometer [**27**]. It is based on the equation of state for an ideal gas (equation 2.4). The CVGT was also used for the establishment of the thermodynamic basis of the International Temperature Scale of 1990 (ITS-90) in the temperature range up to 730 K [**5,13**].

$$PV = nN_A kT \qquad 2.4$$

P is the pressure (Pa)

V is the volume (m^3)

n is the number of moles (mol)

N_A is the Avogadro's number (6.0221 x 10^{23} mol^{-1})

k is the Boltzmann constant (1.3806505 x 10^{-23} $J{\cdot}K^{-1}$)

T is the thermodynamic temperature (K)

The accuracy of the CVGT is limited at higher temperature due to sorption effects and increasing thermal expansion [**28**].

- **Acoustic gas thermometer :** For an ideal gas, the relation between the acoustic velocity and the thermodynamic temperature can be written as equation 2.5 [**27**]. This method is used as the primary thermometry method in the range from 90 K to 800 K [**6,25,29,30**].

$$c_s = \sqrt{\frac{\gamma RT}{M}} \qquad 2.5$$

c_s is the acoustic velocity

γ is the adiabatic index which is $\frac{C_P}{C_V}$

R is the universal gas constant [8.314 472 (15) J·mol^{-1}·K^{-1}]

T is the thermodynamic temperature (K)

M is the molar mass for the gas (kg·mol^{-1})

C_P is the heat capacity at constant pressure (J·K^{-1})

C_V is the heat capacity at constant volume (J·K^{-1})

- **Dielectric-constant gas thermometer (DCGT) :** An alternative form of the gas thermometer is the dielectric-constant gas thermometer (DCGT). The basic idea of DCGT is to replace the density in the state equation of a gas by the dielectric constant and to measure the change in electrical capacity of a gas-filled capacitor for different pressure levels. The dielectric constant of an ideal gas is given by the relation :

$$\varepsilon = \varepsilon_0 + \alpha_0 \frac{N}{V} \qquad 2.6$$

where ε_0 is the exactly known electric constant, α_0 is the static electric dipole polarizability of the atoms, N is the number of gas particles and V is the volume of gas, i.e. the state equation of an ideal gas can be written in the form

$$P = \frac{kT(\varepsilon - \varepsilon_0)}{\alpha_0} \qquad 2.7$$

where P is the pressure, k and T is the Boltzmann constant and thermodynamic temperature respectively [**28**].

Hitherto the DCGT has been applied for the measurement of the thermodynamic temperature in the low temperature range between 4 K to 27 K [**7**]. At higher temperatures the DCGT will lose accuracy due to the loss of sensitivity and compressibility changes [**27**].

There are two other types of thermometers, which do not depend on the gas laws, and have been applied for the thermodynamic temperature measurement over wide temperature ranges. These are the electronic noise thermometer (Nyquist law). and the two types of radiation thermometers, the spectral radiation thermometer (Planck law) and the total radiation thermometer (Stefan-Boltzmann law) :

- **Noise thermometer :** the measurement of the Johnson noise in a resistor allows the determination of thermodynamic temperatures using the Nyquist equation, but because of the small voltages involved it has always been a very difficult method to implement. The noise thermometer is based on the temperature dependence of the mean square noise voltage $\langle U^2 \rangle$ developed in a resistor. Nyquist derived equation 2.8 from thermodynamic calculations [**31**]:

$$\left\langle U^2 \right\rangle = 4kTR\Delta f \qquad 2.8$$

valid for frequencies f **<<** kT/h , where R is a frequency independent resistance, f is the bandwidth and h is Planck's constant.

The noise thermometer has been variously applied in the few mK temperature range to temperatures of more than 1700 K [**8**].

- **Radiation thermometer :** The thermodynamic temperature can be determined by measurement of the total radiation of a blackbody, described by the Stefan-Boltzmann law [**9,22**], or the spectral radiance, described by the Planck radiation law [**10,32**].

- **Total radiation thermometer:** The accurate measurement of the total radiation emitted from a blackbody has become possible only with the development of the cryogenic radiometer [**28**]. The total radiant exitance $M(T)$ of a blackbody at a temperature T is given by equation 2.9.

$$M(T) = \frac{2\pi^5 k^4}{15h^3c^2} T^4 = \sigma T^4 \qquad 2.9$$

where σ is the Stefan–Boltzmann constant and c is the speed of light in vacuum. The total radiation thermometer is used for the determination of the thermodynamic temperature in the temperature range from 143 K to 505 K [**22**,**33**,**34**].

- **Spectral radiation thermometer:** The spectral radiation thermometer is used for the determination of the thermodynamic temperature by using Planck's formula (equation 2.10) which describes the emitted spectral radiance of electromagnetic radiation at each wavelengths from a black body at temperature T, $L_{\lambda,\mathrm{BB}}(\lambda,T)$:

$$L_{\lambda,\mathrm{BB}}(\lambda,T) = \frac{2\pi c^2}{n^2\lambda^5} \cdot \frac{1}{e^{\frac{hc}{n\lambda kT}} - 1} \cdot \frac{1}{\pi\Omega_0} \qquad 2.10$$

where Ω_0 is the solid angle and equal 1 sr, n is the refractive index of air, λ is the wavelength and h and k are the Planck constant and the Boltzmann constant respectively. The spectral radiation thermometer is also used to define the ITS-90 in the temperature range above the freezing point of silver (1234.93 K) [**28**].

2.3 The International Temperature Scale

In principle, temperature is defined completely by thermodynamics laws. However the temperature measurements with the thermometers based on thermodynamic laws are too complex, time-consuming and expensive for practical everyday temperature measurements. Therefore in 1927 the General Conference on Weights and Measures (CGPM) adopted an empirical temperature scale that is sufficiently reproducible to meet the increasing demand for simplified but reliable and world wide comparable temperature measurements in science and industry. The scale is based on a number of reproducible temperatures fixed points, to which numerical values of thermodynamic temperatures were assigned. The CGPM also defined standard instruments to be calibrated at these fixed points. The calibration of these standard instruments furnished the constants for the formulae defining temperatures in the various temperature ranges between the fixed points. This detailed set of instructions was called the International Temperature Scale of 1927 (ITS-27) [**35**]. The scale is revised periodically to ensure that it is a close approximation of the corresponding thermodynamic temperatures and covers a wide temperature range in practice. According to the technological and scientific progress, the International Temperature Scale is revised from time to time and there are a series of further international temperature scales, which are the International Temperature Scale of 1948 (ITS-48) [**36**], the 1958 ^{4}He Vapor Pressure Scale of Temperature [**37**], the International Practical Temperature Scale of 1948 (IPTS-48) [**38**], the 1962 ^{3}He Vapor Pressure Scale of Temperature [**39**], the International Practical Temperature Scale of 1968 (IPTS-68) [**40**], the International Practical Temperature Scale of 1968 in the Amended Edition of 1975 [IPTS-68(75)] [**41**], the 1976 Provisional 0.5 K to 30 K Temperature Scale (EPT-76) [**42**] and the current official temperature scale, which is the International Temperature scale of 1990 (ITS-90) [**12**]. The ITS-90 defines both International Kelvin Temperatures (T_{90}) and International Celsius Temperatures (t_{90}). It is an equipment calibration standard for making measurements on the Kelvin and Celsius temperature scales to which accredited laboratories refer to in calibration certificates and is to be used for practical temperature measurements.

The ITS-90 [**12,43**] came into effect on 1 January 1990. It improves the accuracy and reproducibility of temperature measurements in comparison with the IPTS-68 and the EPT-76, e.g. it prescribes more accurate instruments. The ITS-90 extends upwards from 0.65 K to the highest temperature practically measurable in

terms of the Planck radiation law using monochromatic radiation. It is based on 17 well-reproducible thermodynamic states of equilibrium as the defining fixed points;

boiling points: helium (He) and equilibrium hydrogen (e-H_2).

triple points: equilibrium hydrogen (e-H_2), neon (Ne), oxygen (O_2), argon (Ar), mercury (Hg), water (H_2O).

melting point of gallium (Ga)

freezing points: indium (In), tin (Sn), zinc (Zn), aluminium (Al), silver (Ag), gold (Au), copper (Cu).

Table 2.2: Defining fixed-points of the ITS-90. The symbols are denote as: V: vapour pressure point; T: triple point (temperature at which the solid liquid and vapour phases are in equilibrium); G: gas thermometer point; M, F: melting point, freezing point (temperature, at a pressure of 101325 Pa, at which the solid and liquid phases are in equilibrium). All substances except ^{3}He are of natural isotopic composition, e-H_2 is hydrogen at the equilibrium concentration of the ortho- and para-molecular forms.

	Temperature			
Number	T_{90}/K	t_{90}/ºC	Substance	State
1	3 to 5	-270.15 to -268.15	He	V
2	13.8033	-259.3467	e-H_2	T
3	~17	~-256.15	e-H_2 (or He)	V (or G)
4	~20.3	~-252.85	e-H_2 (or He)	V (or G)
5	24.5561	-248.5939	Ne	T
6	54.3584	-218.7916	O_2	T
7	83.8058	-189.3442	Ar	T
8	234.3156	-38.8344	Hg	T
9	273.16	0.01	H_2O	T
10	302.9146	29.7646	Ga	M
11	429.7485	156.5985	In	F
12	505.078	231.928	Sn	F
13	692.677	419.527	Zn	F
14	933.473	660.323	Al	F
15	1234.93	961.78	Ag	F
16	1337.33	1064.18	Au	F
17	1357.77	1084.62	Cu	F

On these states of fixed-point the numerical values of the temperature T_{90} are assigned. These are values that have been determined by measurements of the corresponding thermodynamic temperatures T in several national metrology institutes [**14**]. The defining fixed points are listed in table 2.2. The ITS-90 has been constructed in such a way that, throughout its range, for any given temperature the numerical value of T_{90} is a close approximation to the numerical value of T by using the instruments to interpolate the temperature T_{90} between these defining fixed points. Compared to direct measurements of the thermodynamic temperatures T, measurements of T_{90} are more easily made, are more precise and are highly reproducible. A schematic of the defining fixed points with the interpolation instruments of the ITS-90 is shown in figure 2.2.

The helium vapour-pressure scales from 0.65K to 5K are quasi-continuous fixed points, T_{90} values are defined via vapour pressure versus temperature relations for ^{3}He and ^{4}He [**12**].

For contact thermometry, temperatures between the fixed points at higher temperatures are defined by means of interpolating instruments calibrated at the fixed points. From the readings of these thermometers the temperature T_{90} is calculated using specified interpolating equations. The interpolating instruments are the CVGT for the temperature between 3.0 K and the triple point of neon (24.5561 K) and the standard platinum resistance thermometer (SPRT) for the temperature between the triple point of equilibrium hydrogen (13.8033 K) and the freezing point of silver (961.78 K).

Non-contact thermometry by application of the Planck radiation law had been used to define T_{90} above the freezing point of silver (1234.93 K). The extrapolation instrument is a radiation thermometer and the specified extrapolating equation is:

$$\frac{L_\lambda(\lambda, T_{90})}{L_\lambda\left(\lambda, T_{90,\mathrm{ref}}\right)} = \frac{\exp(c_2\left[\lambda T_{90,\mathrm{ref}}\right]^{-1}) - 1}{\exp(c_2\left[\lambda T_{90}\right]^{-1}) - 1} \qquad 2.11$$

where $T_{90,\mathrm{ref}}$ refers to any one of the silver, gold and copper freezing points (1234.93 K, 1337.33 K and 1357.77 K respectively), L_λ is the spectral radiance at the wavelength λ and c_2=0.014388 mK.

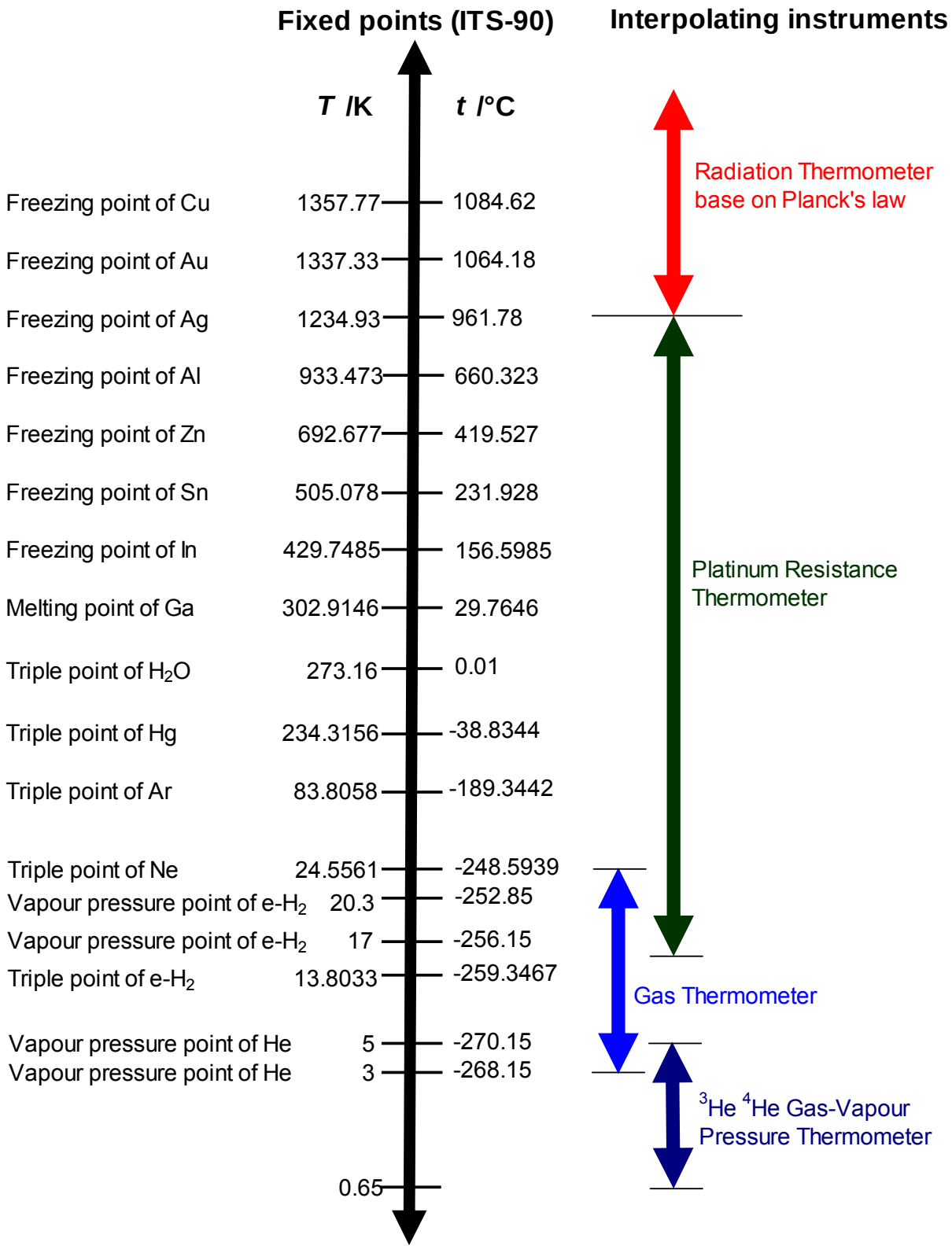

Figure 2.2 : Schematic of the defining fixed points and the interpolating instruments of the ITS-90

2.4 Radiation thermometry

All objects emit radiation by virtue of the motions of the atoms of which they are made, and since the thermal motion of atoms increases with temperature, so does the radiation emitted. Most of the radiation is in the infrared, but as the temperature increases beyond about 700 °C a dull 'red heat' can be seen, which gradually brightens to orange, yellow and finally a brilliant white heat. The effect is very sensitive and radiation thermometry (infrared thermometry, radiation pyrometry) is a powerful method of temperature measurement, even at temperatures down to -60 °C.

2.4.1 Thermal radiation

Thermal radiation is the radiation that the nontransparent body emits at any temperature above 0 K. The radiation is emitted in the form of electromagnetic waves. The radiation is emitted by an object at all wavelengths spanning the electromagnetic spectrum shown in figure 2.3. The short-wavelength end of the spectrum corresponds to high-energy gamma radiation, while the long-wavelength end corresponds to low-energy radio waves. In between these two extremes the spectrum is split roughly into x-ray, ultraviolet radiation, visible light, infrared radiation and microwaves. The visible spectrum between 0.38 μm and 0.78 μm, is only a very narrow portion of the entire spectrum. Radiation thermometry is carried out at wavelengths within the region labeled "Thermal radiation" and is usually restricted to the range between 0.5 μm and 20 μm.

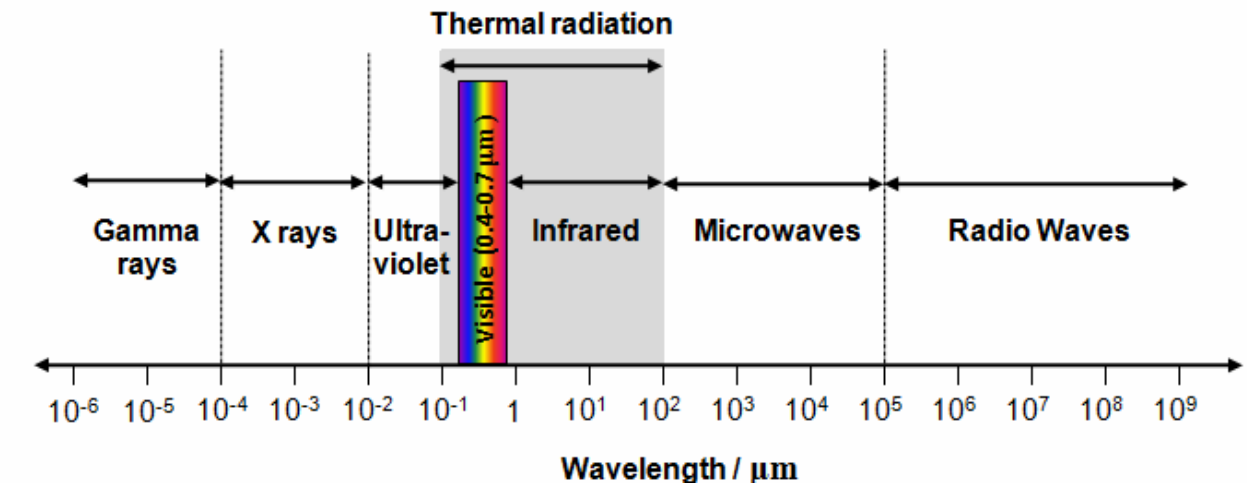

Figure 2.3 : The electromagnetic spectrum

For an arbitrary body at the temperature $T \neq 0$, the energy of the emitted thermal radiation can not be analytically calculated as the function of wavelength. However for a so called blackbody (BB) [**44**] which completely absorbs all incoming radiation and the spectrum of the emitted radiation is independent from the shape and material of the blackbody. The analytical calculation of its emitted radiation was achieved by Max Planck in 1900 [**45**]. The concept of the blackbody was introduced by Gustav Kirchhoff in 1860. He used the blackbody as a radiator with an absorptivity α of unity [**44**]. Based on the second law of thermodynamics, he concluded that the emissivity ε at any wavelength is equal to the absorptivity α for every body at the same wavelength. Since the emissivity represents a measure of the ability of a body to emit thermal radiation, it is unity for a blackbody. Thus at a given temperature, a blackbody emits the highest amount of thermal radiation power per area, solid angle and wavelength interval, the so-called spectral radiance L_λ, and every real body at the same temperature emits a smaller amount of radiation. The ratio of the spectral radiance emitted by a real body to the spectral radiance emitted by a blackbody is called the emissivity of the real body, which is always smaller than unity.

2.4.2 Blackbody radiation

An ideal blackbody is defined as a body that will absorb all incident electromagnetic radiation at all wavelengths and from all directions. Therefore a blackbody is emitting exactly what it absorbs when it is in equilibrium with its surroundings. A blackbody is an idealized object which is a perfect emitter of radiation. For any arbitrary temperature a blackbody will emit more radiation at the a given wavelength than any other object at that same temperature. Although a blackbody is strictly idealized, the concept is very important since it represents a standard against which real objects may be compared. Furthermore, a very good approximation to a blackbody can be achieved in practice by constructing a constant and uniform distributed temperature cavity containing an opening or aperture which is small with respect to the dimensions of the cavity.

Given a cavity with walls at a constant temperature, the atoms in the walls will be constantly agitated because they have a temperature different from 0 K and their vibration is proportional to their temperature. This motion of electrical charges causes electromagnetic waves to be emitted into the cavity. Some of these waves will be

reabsorbed by the atoms in the walls and eventually equilibrium will be reached where the amount of radiation absorbed by the walls is equal to the amount of radiation emitted. Inside the cavity the radiation has to be completely isotropic: that is, the radiation is independent of both direction and position, since otherwise equilibrium could not be reached. If a small hole is made in this cavity, a small part of the blackbody radiation will be emitted. The radiation power emitted by an area element into a solid angle per wavelength interval can be calculated from a statistical analysis of the quantized energy of the atoms in the walls. The equation was first derived by the German physicist Max Planck and the result is known as Planck's law [**45**].

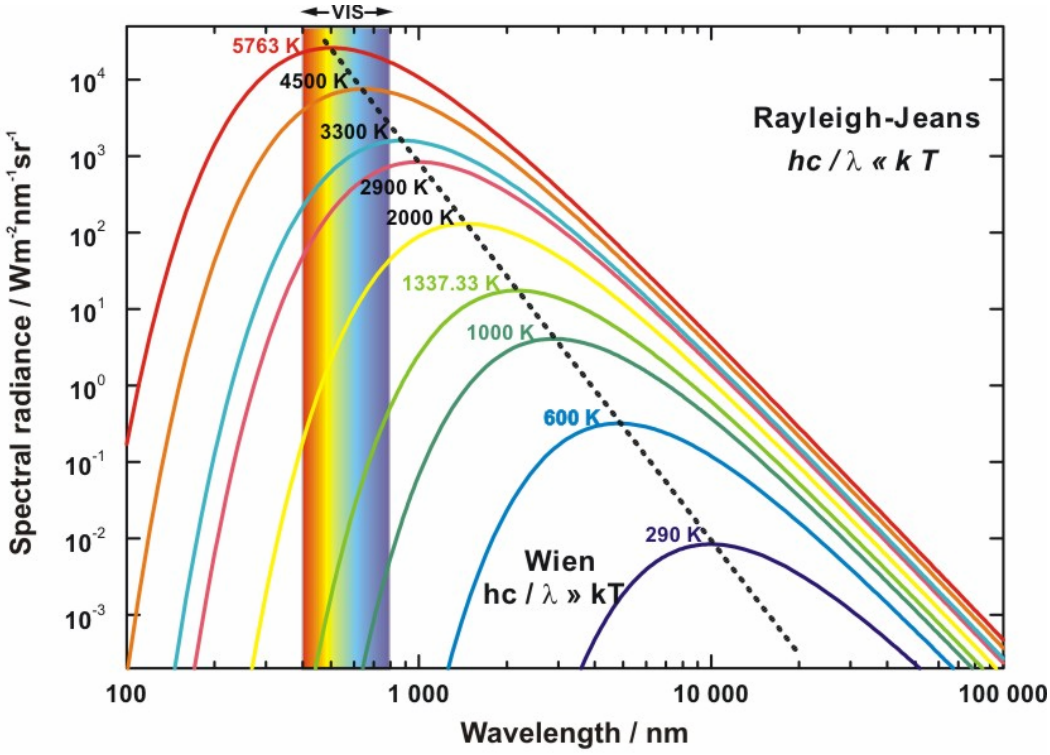

Figure 2.4 : The spectral radiance of the ideal blackbody as the function of wavelength for different temperatures.

The spectral radiance for an ideal blackbody for several temperatures from room temperature (290 K) to the sun's mean surface temperature (5673 K) is shown in the figure 2.4. It can be seen for temperatures below 800 K, almost all of the spectral radiance is emitted in the infrared. As the temperature increases above 800 K, the radiation start to move into the visible region (380 nm to 780 nm) of the spectrum. However, to achieve a sufficiently radiance output from a blackbody in the visible and ultraviolet (190 nm to 380 nm) region, the temperature of the blackbody

must exceed the freezing temperature of gold (1337.33 K). As the temperature increases further, the intensity of the radiation also increases very rapidly. Note that the vertical axis is logarithmic, so that each step on the axis corresponds to an increase by a factor of 10 in the spectral radiance.

An ideal blackbody is a cavity in total thermal equilibrium, with uniform temperature throughout and with only an infinitesimal hole. For a real blackbody it is not possible to meet all of these requirements but will be as close an approximation as possible. Practically made blackbodies can be close to being ideal blackbodies. There are two main kinds of practical blackbodies. The first is the fixed-point blackbody (see figure 2.5) where the cavity of blackbody is surrounded by an ultra-pure metal, which is melted and then refrozen. During the period of melt and freeze the temperature of the metal and the cavity will be constant. The temperature at which this occurs will be the melting respective the freezing temperature of the metal. The international temperature scale defines the melting and the freezing temperatures of certain metals (see table 2.2 : Ga using melting temperature, In, Sn, Zn, Al, Ag, Au and Cu using freezing temperature).

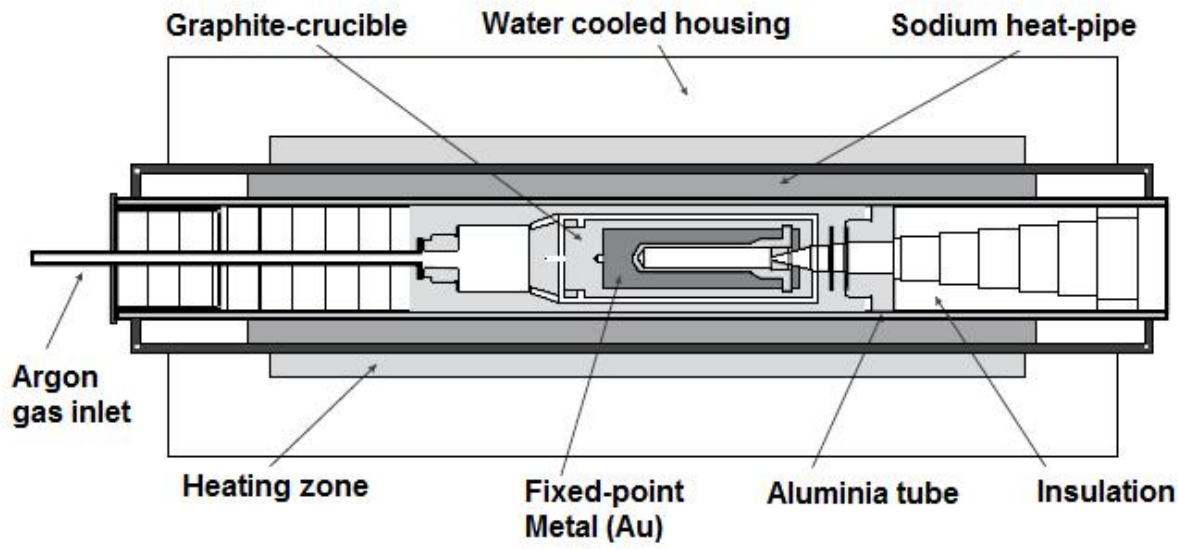

Figure 2.5 : Schematic diagram of the PTB gold fixed-point blackbody [**28**]

The alternative kind of practical blackbody is the variable temperature blackbody. The cavity of the blackbody is heated usually electrically. The temperature of the variable temperature blackbody must itself be measured, and is usually actively stabilized.

2.4.3 Emissivity

The limitation of the real blackbody in contrast to the ideal blackbody is the achievable temperature uniformity and an emissivity lower than unity. The emissivity of the real blackbody is the ratio of energy radiated by the real blackbody to the energy radiated by an ideal blackbody at the same temperature. An ideal blackbody has by definition an emissivity $\varepsilon = 1$ while any real blackbody would have an emissivity $\varepsilon < 1$. A high emissivity of real blackbody can be achieved by two conditions. Firstly, selecting a suitable wall material or coating of high local emissivity. Secondly, by following design principles, so that any light reflected from a surface element is reabsorbed by another surface element of the blackbody or is reflected back onto an absorbing surface. However for the high temperature blackbodies the material options are often limited (i.e. materials that resist high temperatures). Furthermore, emissivity also depends on the internal temperature uniformity of the blackbody, the more uniform the temperature across the blackbody, the more it will be close to a true Planckian radiator.

For radiation thermometry and radiometry, it is very important to determine the emissivity precisely. Nevertheless a high emissivity close to one can usually hardly be measured [**46**]. Therefore, the emissivity of the blackbody can be obtained by calculation using analytical or numerical models [**47**,**48**]. A simple model to estimate the emissivity $\varepsilon_{\text{cavity}}$ of a cylindrical cavity radiator with a wall emissivity $\varepsilon_{\text{wall}}$, a length l and a radius r was given by Bauer and Bischoff in 1970 [**45**] and is shown in equation 2.12.

$$\varepsilon_{\text{cavity}} = 1 - \frac{\varepsilon_{\text{wall}}}{1-\varepsilon_{\text{wall}}} \cdot \frac{1}{\left(1+\frac{l^2}{r^2}\right)} \qquad 2.12$$

2.4.4 Planck's law

The radiation emitted by an object is not distributed uniformly across the entire electromagnetic spectrum, but is concentrated in specific regions as determined by the object's temperature. This is illustrated by the different curves in figure 2.4, which are the spectral radiances of a blackbody at various temperatures as a function of wavelength. The shapes of the blackbody radiation curves in figure 2.4 were known

empirically since the 19th century. However, the classical theories of the time predicted that as the wavelength of the radiation become shorter and shorter, the intensity increased to infinity. The theory was clearly at odds with the observation and this discrepancy was recognized as a crucial problem and was dubbed the ultraviolet catastrophe. In 1900, Max Planck solved the problem and derived an equation for the blackbody curves using concept that the energy exchange of a blackbody wall to its surroundings is not continuous but discrete with the quantum energy hv. With this radiation equation he could explain discrepancies in the spectral distribution of the black-body radiation. His concept would lead to the development of the highly successful theory of quantum physics. His equation is known as "*Planck's law*" and is given by equation 2.13.

$$L_{\lambda,\mathrm{BB}}(\lambda,T)=\frac{c_1}{n^2\lambda^5}\frac{1}{\exp(c_2\left[n\lambda T\right]^{-1})-1} \qquad 2.13$$

where n is the refractive index of air, λ is the wavelength of the radiation in air, and c_1 and c_2 are the first and the second radiation constants respectively (c_1=$2hc^2$, c_2=hc/k). Their currently best measured values are c_1=1.191044×10^{-1} W·m^2 and c_2=0.01438769 m·K [**49**]. For the definition of the temperature scale above the silver fixed point, only the second radiation constant c_2 is required, and the fixed value of c_2=0.014388 m·K is assigned to it in the ITS-90. With the Planck's law (equation 2.13), the spectral radiance of the blackbody ($L_{\lambda,\mathrm{BB}}\left[\lambda,T\right]$) can be directly calculated.

2.4.5 Wien's displacement law

The dotted line joining the peak of each curve in figure 2.4 demonstrates that the peak of the radiation emitted by a blackbody moves to shorter wavelengths with increasing temperature. This shift can be quantified by determining, for a given temperature, the wavelength, $\lambda_{\max}$, that maximizes the spectral radiance expressed by equation 2.13. This can be done using standard techniques of calculus and the result is "Wien's displacement law" [**50**].

$$\lambda_{\max} = \frac{2897.7686(51)}{T}\mu m \qquad 2.14$$

For an object at room temperature (about 290K), equation 2.14 tells us that the maximum spectral radiance occurs at wavelength just shorter than 10 μm, which is well in the infrared and beyond our visual capabilities. However, for a tungsten lamp operating near 3000 K, the peak wavelength is near 1 μm, with large amounts of radiation emitted across the entire visible region such that the lamp appears white. Because of this shift in the peak wavelength with temperature, a suitable radiation detector must be designed with an operating wavelengths to match the desired working temperature range.

2.4.6 Approximations to Planck's law

Planck's law (equation 2.13) is mathematically awkward and does not lend itself to simple manipulation. While it gives an exact description of blackbody radiance across the entire electromagnetic spectrum for all values of temperature, if we apply certain restrictions to the wavelengths and temperatures of interest then we can find simpler laws that approximate well the blackbody curves over these limited ranges.

The most important simplification to Planck's law comes about if we neglect the -1 term of the equation 2.13. This is acceptable when the exponential term is much larger than 1, which in turn requires the quantity $c_2\left[n\lambda T\right]^{-1}$ to be sufficiently larger than 1. For any given temperature, if we restrict the wavelength to be shorter than $\lambda_{\max}$, given by equation 2.14, then $c_2\left[n\lambda T\right]^{-1}$ will be at least 5, and the condition is satisfied. The resulting equation for the blackbody spectral radiance is known as Wien's law and is given by

$$L_{\lambda,\mathrm{BB}}(\lambda,T) = \frac{c_1}{\lambda^5}\exp\left(-\frac{c_2}{\lambda T}\right) \qquad 2.15$$

Provided $\lambda < \lambda_{\max}$, Wien's law is in error by at most 0.7%, and this error decreases with decreasing temperature at a given wavelength. This wavelength region corresponds to the left-hand side of the peaks in the curves of figure 2.4 and is also the region where most radiation thermometry is practiced. Wien's laws is a good approximation when $hc/\lambda >> kT$.

Another approximation of the Planck's law applies to the region where $c_2[n\lambda T]^{-1}$ is much less than 1. This corresponds to very long wavelengths and/or very high temperatures. Using the standard series expansion for the exponential term in equation 2.13 and retaining only the first-order term in $c_2[n\lambda T]^{-1}$, the spectral radiance can be written as a linear function of temperature:

$$L_{\lambda,\mathrm{BB}}(\lambda,T)=\frac{c_1 T}{c_2\lambda^4} \qquad 2.16$$

This is the classical Rayleigh-Jeans law, which gave rise to the "ultraviolet catastrophe". The Rayleigh-Jeans law is valid when $hc/\lambda << kT$.

2.4.7 Total radiation and the Stefan-Boltzmann law

The total radiation of a blackbody $M(T)$ at given temperature is obtained by integrating Planck's law across the entire electromagnetic spectrum, which is equivalent to determining the area under the corresponding curve in figure 2.4 with solid angle of 2π. The result is the Stephan-Boltzmann law [**51**] and is given by

$$M(T)=\int_0^\infty L_{\lambda,\mathrm{BB}}(\lambda,T)d\lambda=\int_0^\infty \frac{c_1}{n^2\lambda^5}\frac{1}{\exp(c_2[n\lambda T]^{-1})-1}d\lambda=\frac{\sigma}{\pi}T^4 \qquad 2.17$$

Where σ is the Stefan-Boltzmann constant with the value 5.670 400(40)×10^{-8} W m^{-2} K^{-4} and T is the thermodynamic temperature of the blackbody. Note that λ is dropped from the bracket of $M(T)$ to indicate that this is the total radiance summed over all wavelength, in contrast to the spectral radiance of equation 2.13, which corresponds to the radiance at the particular wavelength. The Stefan-Boltzmann law declares that the total amount of radiation is proportional to T^4 [**51,52**].

2.5 Requirements for the detectors

The radiation temperature of the blackbody is connected to radiometry by the Planck's law of thermal radiation. The important quantities in radiometry used to characterize the electromagnetic radiation are the following :

- **Radiant flux :** Radiant Flux (Φ) is energy (Q) per unit time (t) that is radiated from a source for optical wavelengths, which are defined to be from $3x10^{11}$ and $3x10^{16}$ Hz. This range is approximately equivalent to wavelengths from 0.01 μm to 1000 μm and includes the regions of the electromagnetic spectrum commonly referred to as Ultra Violet (UV), Visible, and Infra Red (IR). Radiant flux can be formulated as :

$$\Phi = \frac{dQ}{dt} \qquad 2.18$$

The radiant flux is measured in units of Joules per second (J/s), or Watts (W) (A radiant flux of 1 W means that a source produces 1 Joule every second). If we integrate radiant flux over time we obtain the total Energy (Q) output by the source.

- **The solid angle :** The solid angle (Ω) is the angle in three-dimensional space that an object subtends at a point. It is assigned to the angle that, seen from the center of a sphere, includes a given area on the surface (A) of that sphere. The value of the solid angle is numerically equal to the size of that area divided by the square of the radius (r) of the sphere (see equation 2.19).

$$\Omega = \frac{A}{r^2} \qquad 2.19$$

The unit of solid angle is the SI steradian with the unit symbol “sr”. The solid angle is a dimensionless quantity. Since the surface area of a sphere is 4π**,** there are 4π steradians of solid angle in a sphere.

- **Irradiance and spectral irradiance:** Irradiance (E) is the radiometric term for the power of electromagnetic radiation incident on a surface, per unit area. Irradiance is used when the radiation is incident on the surface and defines as the incident flux (Φ) per unit area onto a point or area of a surface (A) as shown in equation 2.20. The SI unit of irradiance is W m^{-2}.

$$E = \frac{d\Phi}{dA} \qquad 2.20$$

Irradiance and radiant exitance are characterized the total amount of radiation at all wavelengths. It is also common to consider each wavelength in the spectrum separately. When this is done for radiation incident on a surface, it is called "spectral irradiance (E_λ)", and has the SI units of $W \cdot m^{-3}$ (or $W \cdot m^{-2} \cdot nm^{-1}$). When a point source radiates light uniformly in all directions and there is no absorption, then the irradiance is inversely proportional to the square of the distance from that source since the total power is constant and it is spread over an area that increases with the square of the distance from the source.

- **Radiance and spectral radiance:** Radiance (L) and spectral radiance (L_λ) are radiometric quantities used to describe the light that passes through or is emitted from a particular area into a particular solid angle. They are the amount of flux (Φ) emitted per unit projected area of surface (A) into a unit solid angle(Ω) in a specified direction (θ) from the perpendicular to the surface. It is usually measured by focussing an area element of the source in a defined geometry. The radiance is defined in equation 2.21 and has the SI units of $W\ m^{-2}\ sr^{-1}$

$$L = \frac{d^2\Phi}{d\Omega dA \cos\theta} \qquad 2.21$$

Radiance characterizes total radiation, while spectral radiance characterizes the light at a single wavelength. The radiance is equal to the integral of all the spectral radiances from a surface. The spectral radiance has the SI unit of $W \cdot sr^{-1} \cdot m^{-3}$ or commonly $W \cdot sr^{-1} \cdot m^{-2}\ nm^{-1}$.

- **Spectral responsivity:** When using detectors in radiometry, an additional important quantity is the detector spectral responsivity. The detector spectral responsivity is the output signal for a given optical flux that is received by the detector. This is usually measured in Ampere pro Watt ($A \cdot W^{-1}$) or Voltage pro Watt ($V \cdot W^{-1}$).

Radiometric methods of measuring temperature, like the radiation thermometric method and the absolute radiometric method, are primary thermometry methods. Both methods measure the thermodynamic temperature rather than ITS-90 temperature. The radiation thermometric methods for temperatures above the silver fixed-point rely on the measurement of spectral radiance ratio with a radiation thermometer of one of the silver, gold or copper fixed-point. The freezing temperatures of these fixed points are defined in the ITS-90. These temperatures were themselves determined by ratios to other fixed-points that could be measured with gas thermometry. At the time the ITS-90 became effective, the freezing points of tin and zinc had only been measured twice, with gas thermometry, at NIST. Unfortunately the two measurements gave significantly different results from 30 mK at the highest common measured temperature of 730 K [**5**,**13**], and for the construction of the ITS-90 the average between the two values had to be applied with an uncertainty of 15 mK. This uncertainty is passed by the error propagation up to higher temperatures. As a consequence, the higher the temperature above the gold point, the less accurate the ITS-90 temperature determination with be. Therefore for a higher thermodynamic accuracy of a future international temperature scale, possible deviations of the ITS-90 temperature from thermodynamic temperature (T-T_{90}) have to be investigated. The method to be used for this investigation must be accurate with an uncertainty of less than 30 mK for the thermodynamic temperature determination at 730 K and independent from gas thermometry. The most suitable method for this investigation is the absolute radiometry which is independent from the gas thermometry and is traceable to an absolute detector standard, the cryogenic radiometer. The system for this method is called in its simplest version: a blackbody, a filter radiometer and a set of two defining apertures with accurately known dimensions. The thermodynamic temperature is directly measured by the measurement of the spectral irradiance of a blackbody with absolutely calibrated filter radiometer and the thermodynamic temperature is calculated iteratively by using Planck's law. Since the determination of the thermodynamic temperature of a blackbody down to the temperature of zinc-fixed-point has to be performed, therefore InGaAs photodiode base filter radiometers have to be used in this work as already explained in chapter 1. The design and the calibration of the filter radiometer is described in chapter 5. The principle geometry of the absolute radiometric method for the thermodynamic temperature determination is shown in figure 2.6.

In order to measure thermodynamic temperatures with the absolute radiometric method, the absolute spectral irradiance responsivity of filter radiometer with sufficient accuracy (better than 0.1%) must be calibrated. This is fulfilled by the calibration of the filter radiometer traceable to the cryogenic radiometer as the primary detector standard. The details of the spectral responsivity respective the spectral irradiance calibration of the detectors used in this work are explained in chapter 4.

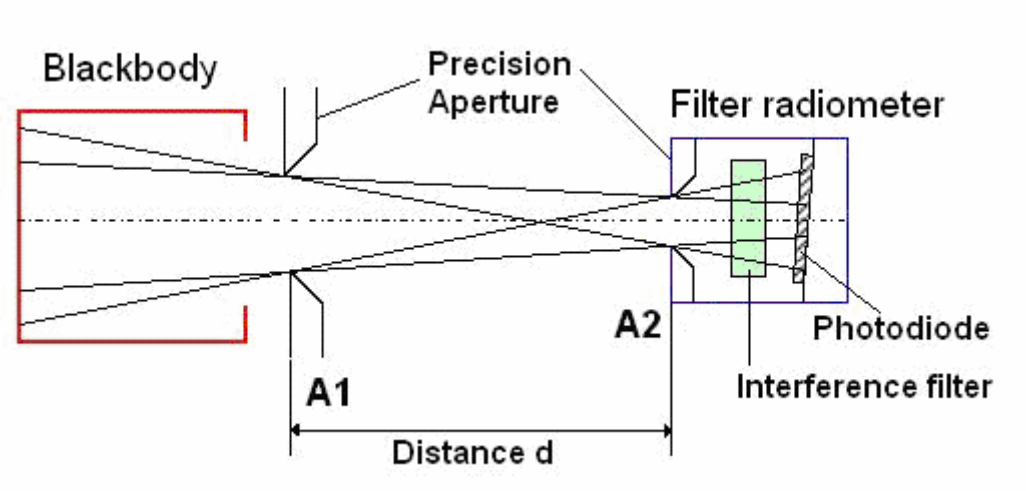

Figure 2.6 : The principle geometry of absolute radiometric method for the thermodynamic temperature measurement

Figure 2.7 illustrates the radiometric chain of the filter radiometer calibration. Basically, the traceable calibration of the filter radiometers are performed in a two step procedure. In a first step, a broadband transfer detector, e.g. an InGaAs photodiode, is calibrated against a cryogenic radiometer which is the primary standard for the measurement of radiant power thereby the spectral responsivity of the transfer detectors related to radiant power is determined [**23,24,53,54,55**]. In the second step, the transfer detector is used to continuously calibrate the filter radiometers at a spectral comparator facility [**56**]. In this step the sensitive area of the transfer detector for spectral responsivity is limited with a precision, diamond turned aperture with a nominal diameter of ca. 3 mm. By this, the transfer detector for spectral responsivity is transferred into a transfer detector for spectral irradiance responsivity and has been used for the calibration of filter radiometer. With this calibration procedure the filter radiometers are traceable to the SI unit Ampere.

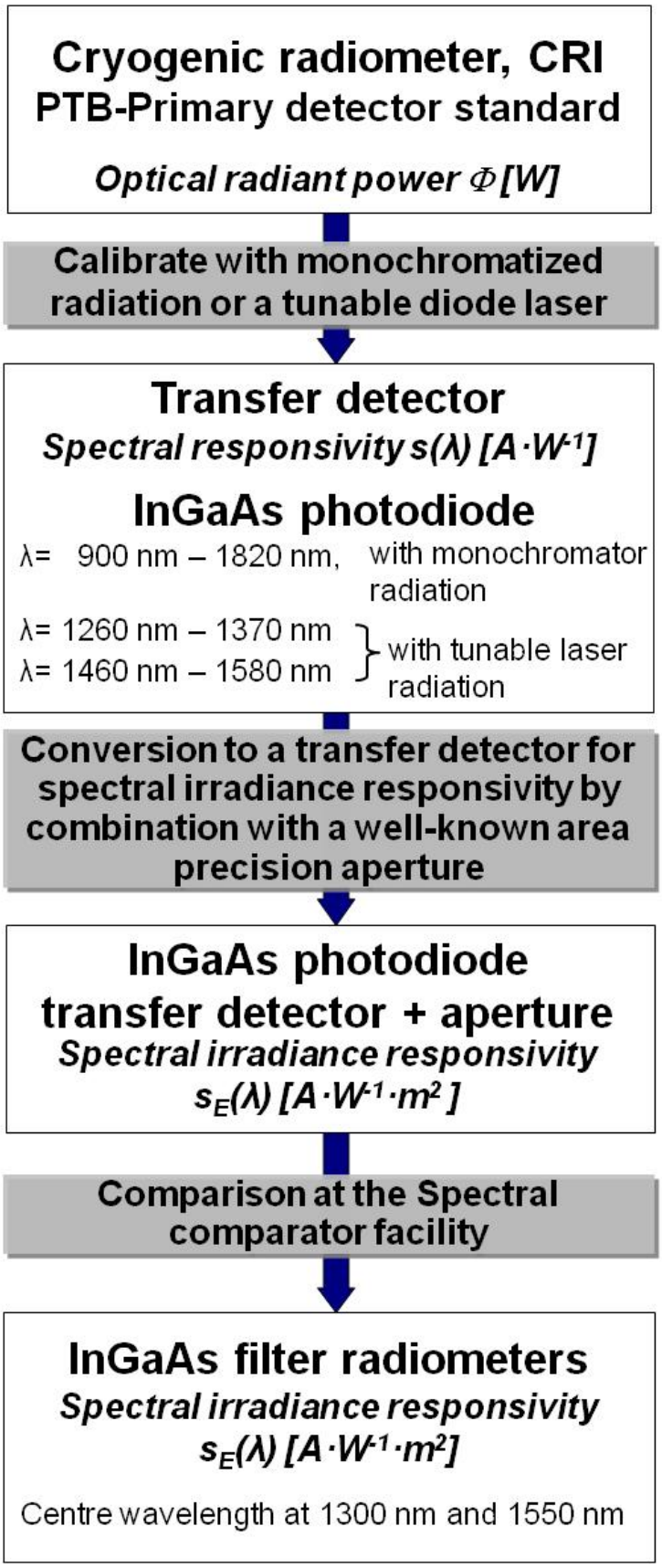

Figure 2.7 : Radiometric calibration chain of the InGaAs filter radiometers used in this work.

Chapter III

Objective of this work

The assigned temperature values of the high temperature fixed-points of the ITS-90 i.e. the freezing temperatures of aluminum (Al : 933.473 K), silver (Ag : 1234.93), gold (Au : 1337.33) and copper (Cu : 1375.77 K) are based on radiance ratio measurements of the radiance of a variable temperature blackbody at the temperature of 730 K and the radiance of each fixed-point blackbody [**16**,**17**]. At the time the ITS-90 was established the thermodynamic temperature at this reference point (730 K) had been measured twice using gas thermometry at NIST with a significant temperature difference of 30 mK between the two measurements [**5**,**13**]. At that time, no other kind of primary thermometer, which was independent from the gas thermometry, was available for this temperature range to investigate the observed systematic difference. Therefore the average value between these two measurements with a standard uncertainty of 15 mK had been used by the CCT as the reference temperature (at 730 K) for the ITS-90 [**14**]. This thermodynamic uncertainty of 15 mK is passed on and increases by the radiance ratio method for the temperature measurements of the thermodynamic temperature determination of the high temperature fixed points of the ITS-90. It sums up to 40 mK at the Ag-fixed-point and 50 mK at the Au-fixed-point. In order to improve the accuracy of the ITS-90 for the realization of a new International Temperature Scale, the correct value of the ITS-90 reference point has to be identified by the determination of the deviation between the thermodynamic temperature and the ITS-90 temperature (T-T_{90}) with a primary thermometry method which is independent from the gas thermometry.

The principle aim of this work is to solve the systematic deviation of 30 mK at 730 K between the two gas thermometry measurements at the NIST for the establishment of an improved temperature scale, by the measurement of T-T_{90} with an absolute radiometric method using InGaAs filter radiometer. Furthermore the results from this work can be used to prove the application of the detector-based radiation thermometry as an alternative primary thermometric method for the

realization of a temperature scale from the Zn-fixed-point (692.677 K) to the Al-fixed-point (933.473 K). To achieve these objective the following steps have been done:

- First, the uncertainty of the NIR spectral responsivity scale had to be significantly reduced to the same order of magnitude as the spectral responsivity scale maintained in the visible spectral range on Si trap detectors. This was one of the main challenges of this work due to the fact that the PTB NIR spectral responsivity scale already had the worldwide highest accuracy and the uncertainty still had to be further reduced by at least a factor of four. In order to reach this aim, a new cryogenic radiometer facility for the high accuracy calibration of the NIR spectral responsivity had to be established. The details of this work are explained in chapter 4.
- In the next step, in order to take advantage from this improved NIR spectral responsivity scale, two new InGaAs filter radiometers were constructed with optimized center wavelengths at 1300 nm and 1550 nm and bandwidths (FWHM) of 50 nm. These two new InGaAs filter radiometers were calibrated against an InGaAs photodiode based transfer detector. The transfer detector was calibrated at the new cryogenic radiometer facility. In terms of their spectral irradiance resposivity the filter radiometers were calibrated at the PTB spectral comparator facility. The design and the calibration procedure of these two InGaAs filter radiometers is explained in chapter 5.
- The calibrated InGaAs filter radiometers have been used directly after their calibration to determine the possible deviation between the thermodynamic temperature T and the ITS-90 temperature T_{90}, (T-T_{90}), applying them in front of a large-area, double sodium heat-pipe blackbody (LABB) as a high-accuracy source of spectral irradiance. The experimental setup, the measurement procedure and the results of these determinations are described in chapter 6. The results from these determinations can be used to identify the correct thermodynamic temperature value at the reference temperature of the ITS-90 at 730 K in order to improve the thermodynamic accuracy of the ITS-90. This information is of fundamental importance for the realization of the new, improved International Temperature Scale anticipated for the year 2011.

Chapter IV

Measurement of the spectral responsivity in the NIR spectral range

4.1 Transfer detector

Suitable transfer detectors for the spectral responsivity in the near-infrared (NIR) wavelength range from 950 nm to 1650 nm are single InGaAs photodiodes. The spectral responsivity homogeneity of the transfer detector is one of the most important factors for a transfer standard to be used as a spectral irradiance responsivity standard. Additionally, a high shunt resistance of the transfer detector is necessary to reduce the noise signal. The transfer standards used in this work were two different windowless InGaAs photodiodes (GAP5000-Germanium Power Devices, FD5000W-Fermionics) with a 5 mm diameter sensitive area with a shunt resistance of more than 10 MΩ, which were previously characterized in respect to homogeneity of the spectral responsivity at 1300 nm and 1550 nm (figure 4.1).

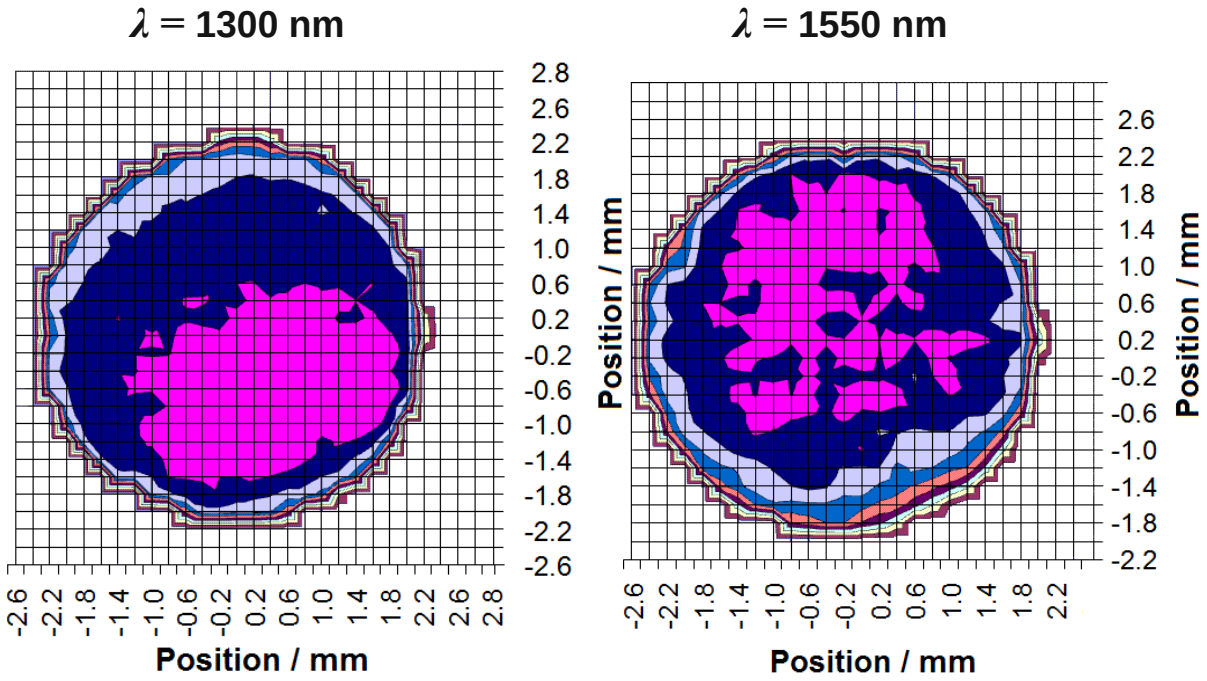

Figure 4.1 : Mapping of the spectral responsivity over the sensitive area of the detector at the wavelengths 1300 nm and 1550 nm of an InGaAs photodiode transfer detector (FD5000W). One change in color represents a relative change of $1x10^{-3}$ in spectral responsivity.

The measurement of the spectral responsivity homogeneity of the transfer detectors was performed at the spectral comparator facility of PTB [**65**]. An 0.3 mm diameter spot was applied to scan the sensitive area of the InGaAs photodiodes transfer detectors. The homogeneity of the transfer detector shown in figure 4.1 is for both wavelengths better than $3x10^{-3}$.

4.2 Cryogenic radiometer

The cryogenic electrical substitution radiometer is the most accurate primary detector standard for the measurement of optical radiant power. It is based on the substitution of optical power by electrical power.

The operating principle of a cryogenic radiometer is shown in figure 4.2. A cavity absorber is used to minimize the reflection losses in the wavelength range from the ultraviolet to the infrared. The cavity absorber is operated near liquid helium temperature (4.2 K) to improve the sensitivity and achieve high accuracy of the cryogenic radiometer. In the first step of the operation, the absorber is electrically heated to the working temperature (bias heating).

In the second step, the radiant power (Φ) falls into the cavity absorber. The working temperature (T_{abs}) is kept constant, so that the electrical power (P_{el}) is reduced by the eqivalent value of the incident radiant power.

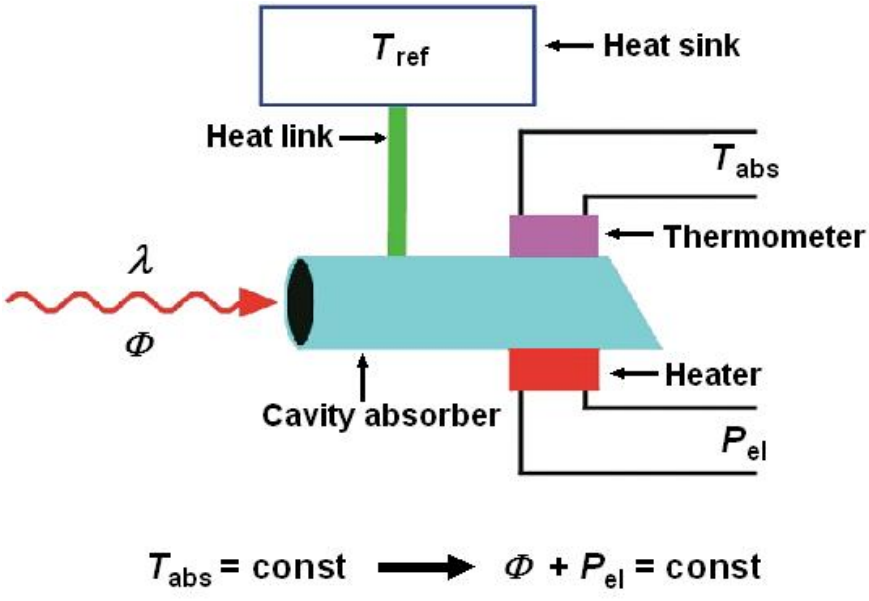

Figure 4.2 : Basic a principle of a cryogenic radiometer

The cryogenic radiometer is operated at a temperature below 20 K (ca.-253 °C). In this temperature range the sensivity of the cryogenic radiometer is improved by three orders of magnitude compared to room temperature operation because of the decrease in copper's specific heat. Therefore the time required to reach thermal equilibrium also decreases, allowing the measurements to be performed in a short time. With this reduction in specific heat, cavities can be used to improve the absorption of the optical radiation. Additionally, in this temperature range superconducting leads can be used, which removes the lead "self-heating". Thus the equivalence of the optical- and the substituted electrical power has been improved. Furtheremore, a cold cavity absorber is surrounded by a cold shielding, thus the radiative transfer between the shields and the detector is minimized. Since a cryogenic radiometer is operated under vacuum, there is no heat conduction or convection losses. This means that a cryogenic radiometer can be 50 times more accurate [**57**] than a room temperature electrical substitution radiometer.

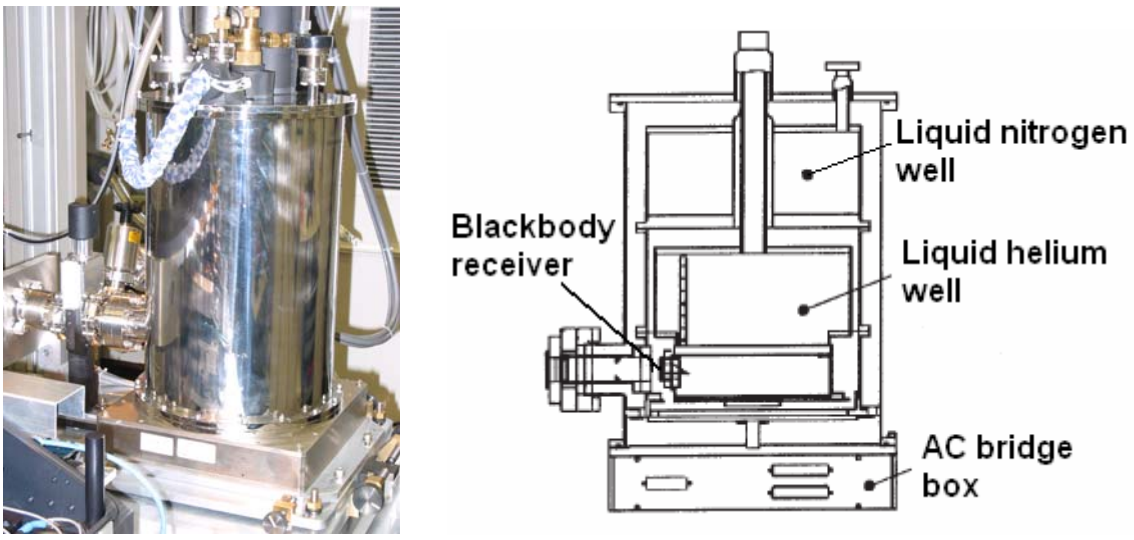

Figure 4.3 : The photo and the sketch of the cryogenic radiometer (Cambridge Research & Instrumentation Inc., type CryoRad II)

The cryogenic radiometer used in this work is a CryoRad II from Cambridge Research & Instrumentation Inc. (figure 4.3). It has a specified wavelength range for operation from 200 nm to 50 µm. The cavity absorptance is 0.99984 at 632.8 nm and has been measured by the manufacturer [**58**]. The absorptance of the cavity coating does not change significantly with wavelength up to 1700 nm [**58**]. The cavity has a responsivity of about 2.38 $K \cdot mW^{-1}$, a time constant of 3.5 s and a diameter of 7 mm. An aperture of 5.4 mm diameter is mounted in front of the cavity.

Table 4.1: The principle characteristics of the cryogenic radiometer used in this work.

Specification of cryogenic radiometer type: CryoRad II	
Spectral range	200 nm to 50 µm
Aperture diameter	5.4 mm
Response time (1/e)	3.5 s
Receiver responsivity	2.38 K/mW
Power range	10 µW to 500 µW
Receiver absorptance	0.999840 ± 0.0000033

4.3 Apparatus

For this work, a new facility for the calibration of the NIR spectral responsivity of detectors in the wavelength range from 950 nm to 1650 nm has been established to meet the low uncertainty requirement for application of InGaAs filter radiometers in radiation thermometry [**53,54**]. The facility serves to calibrate the spectral responsivity of a detector by comparison to the cryogenic radiometer. It consists of a prism-grating double monochromator, a mirror imaging system, a cryogenic radiometer CryoRad II and the detector positioning system. The schematic diagram of the new detector calibration facility is shown in figure 4.4. Originally, the system was optimized for calibrations in the UV range [**59**]. In order to perform calibrations in the NIR, only the radiation source, the grating, and the monitor detector had to be changed. The entire optical path is set up in gas- and light-tight boxes that can be purged with nitrogen to reduce the H_2O-absorption in the NIR wavelength range.

4.3.1 Radiation source

A tungsten halogen lamp serves as a radiation source for the calibration of the spectral responsivity in the wavelength range between 900 nm and 1820 nm. Figure 4.5 shows the radiant power from a tungsten halogen lamp as a function of wavelength. The available radiant power in this wavelength range is about 1 µW to 2 µW within a bandwidth of 8.3 nm. If more radiant power is needed, a tunable diode laser can be attached to the system through an optical fiber. By this very small uncertainties are possible for the responsivity calibration of InGaAs diodes. Different tuneable lasers with wavelength ranges from 1260 nm to 1370 nm and 1460 nm to 1580 nm have been used in this work.

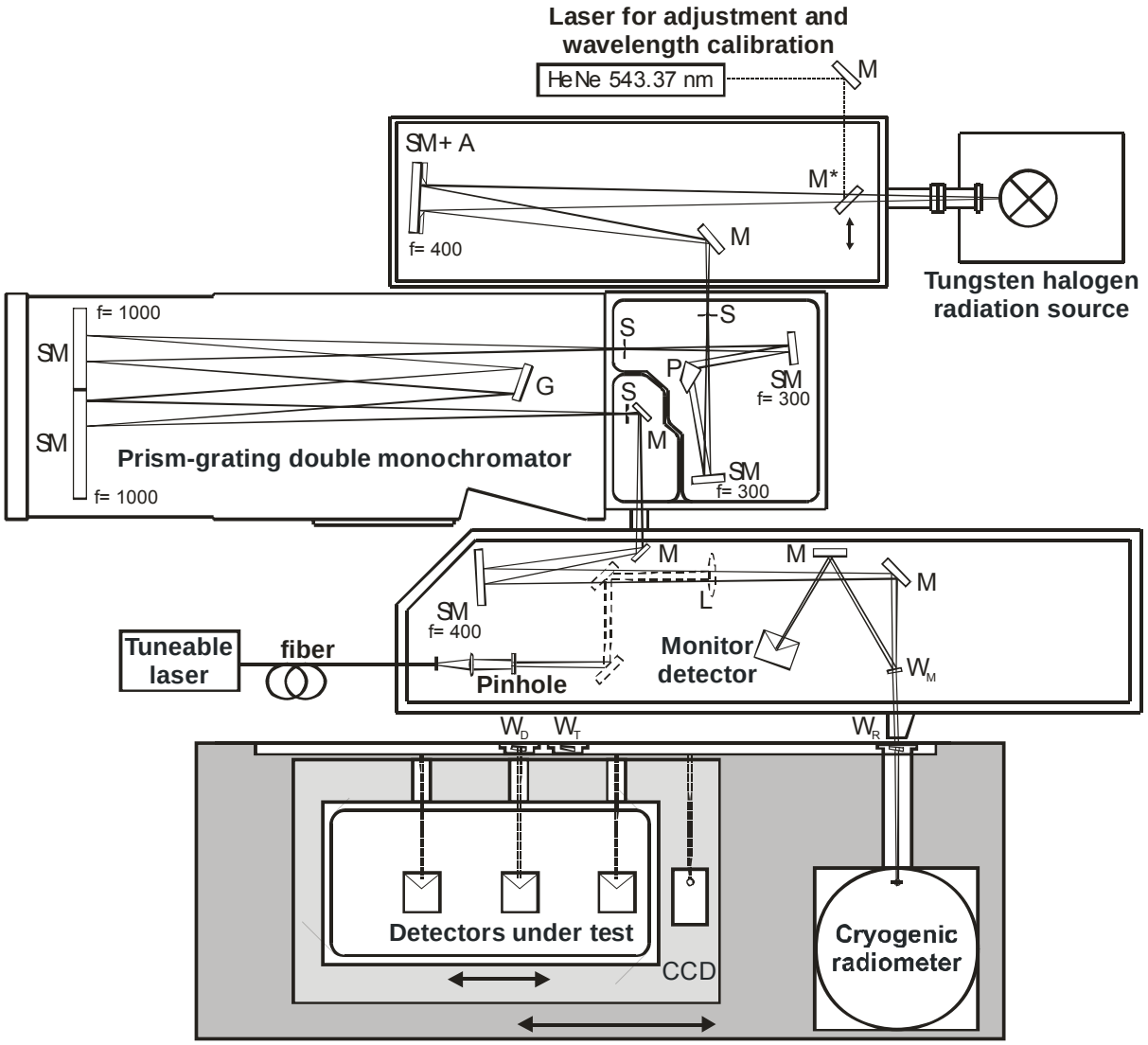

Figure 4.4 : Schematic diagram of the new detector calibration facility

4.3.2 Optical components

The optical system of the detector calibration facility is optimized to achieve a high incident radiant power on the detectors, therefore the aim was to use high reflection optical elements as well as a small number of optical elements. The optical components labeled in figure 4.4 are ; M: plane mirrors; SM: spherical mirrors (focal lengths are stated in mm); M*: removable mirror only in use for adjustment and wavelength calibration; A: f/40 aperture in front of the collecting mirror; S: circular apertures of 1.25 mm diameter used as monochromator slits; P: Pellin-Broca prism made of fused silica; G: NIR grating; W: wedged windows of the same type where W_M is used to couple out the monitor beam, W_R is the vacuum sealing window in front of the cryogenic radiometer which is rotated by 180° with respect to W_M, W_D is

an additional window to obtain the same optical path at the cryogenic radiometer and the detectors under test; W_T is the position in which W_R is placed for measuring the ratio of the window transmittances W_D to W_R.

Additional plane mirrors and two achromatic lenses are used to insert the radiation of tuneable diode laser into the optical system instead of the monochromatised radiation of the tungsten halogen lamp.

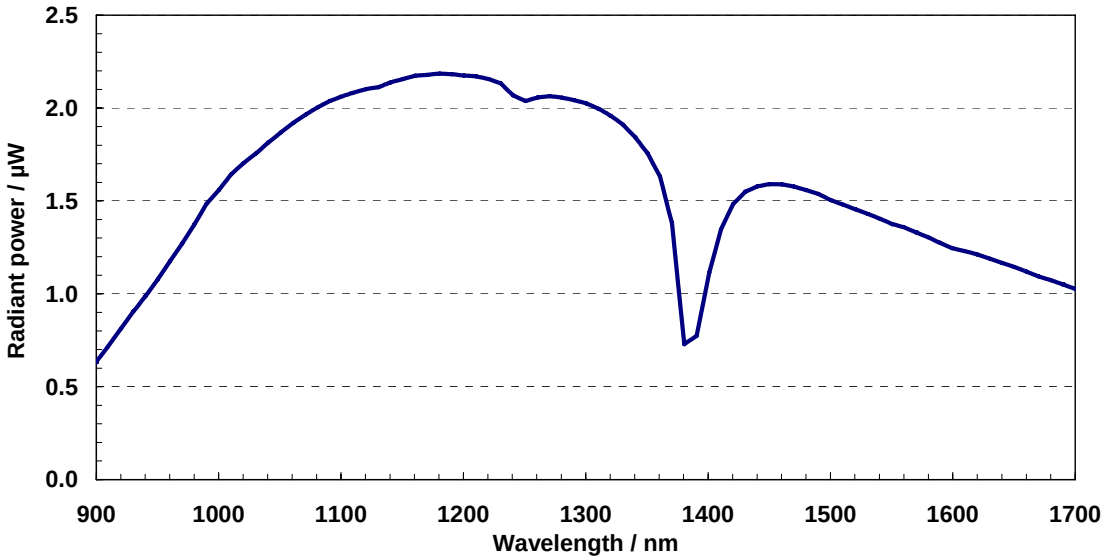

Figure 4.5 : The radiant power from the tungsten halogen lamp in wavelength range from 900 nm to 1700 nm. The radiant power falls off around the wavelength 1380 nm as a consequence of OH-absorption in the quartz glass of the monochromator prism.

4.3.3 Monochromator

A prism-grating double monochromator is used for wavelength selection. The grating monochromator is based on a gas-tight 1 m focal length Czerny-Turner type grating monochromator. A 0.3 meter focal length prism monochromator is placed in front of the grating monochromator and serves as a predisperser to minimize stray light. A grating with a line density of 600 mm^{-1} was chosen to achieve a spectral bandwidth of 1 nm. The circular apertures with diameter of 1.25 mm are used as the entrance and exit slits of the monochromator as a replacement for the original slits. Thereby the exit slit of the prism monochromator acts simultaneously as entrance slit for the grating monochromator. The exit aperture of the grating monochromator is finally imaged onto the detector under test. The image is magnified to a diameter of 2.6 mm.

The wavelength calibration of the monochromator is obtained by measuring different diffraction orders of the He-Ne laser (wavelength in the air : 543.37 nm) e.g. by measurement of the zero and the first order of diffraction. From this the distance between adjacent grooves of grating d can be determined by the grating equation:

$$\frac{n\lambda}{d} = \sin(\alpha) + \sin(\beta) \quad \text{where} \quad \beta = \alpha + \varepsilon \qquad 4.1$$

n is the order (of diffraction)
λ is the wavelength
d is the distance between adjacent grooves of grating
α is the angle of incidence
β is the angle of the diffracted beam
ε is the angle between incidence and the diffracted beam

For the application of the grating equation the directions of the incident and diffracted beam are determined. The direction of the incident beam is determined with the autocollimation method (the diffracted beam is in the same position with the incident beam, i.e. α = 0°). For other angles, α can be measured using the absolute angle encoder of the grating. The angle ε is calculated by the measuring of the grating angle at the first order of diffraction, thereby ε = 2α. The angle of the grating can be precisely adjusted and measured with an uncertainty of a few arcsecond by the help of an angle decoder placed directly on the grating axes.

Any requested wavelength of the grating angle can be calculated and aligned by using the grating equation (equation 4.1). By measuring the rotation angles of the prism and of the grating using absolute angle encoders, the wavelength can be determined reliably. The relative standard uncertainty of the wavelength in the NIR wavelength range (950 nm to 1650 nm) by using the described method above is below 3×10^{-4}.

4.3.4 Positioning system

A motorized stage allows to position the cryogenic radiometer as well as the detectors to be calibrated into the beam. In this way, the detectors and the cryogenic radiometer are irradiated at the same position of the beam during the measurement. Three detectors can be calibrated side by side. Each of them is mounted in a rotary stage, and calibrations are performed at three different angles in order to determine

the dependence on the polarization of the radiation used and to calculate the detector responsivity to non-polarized radiation (see figure 4.6).

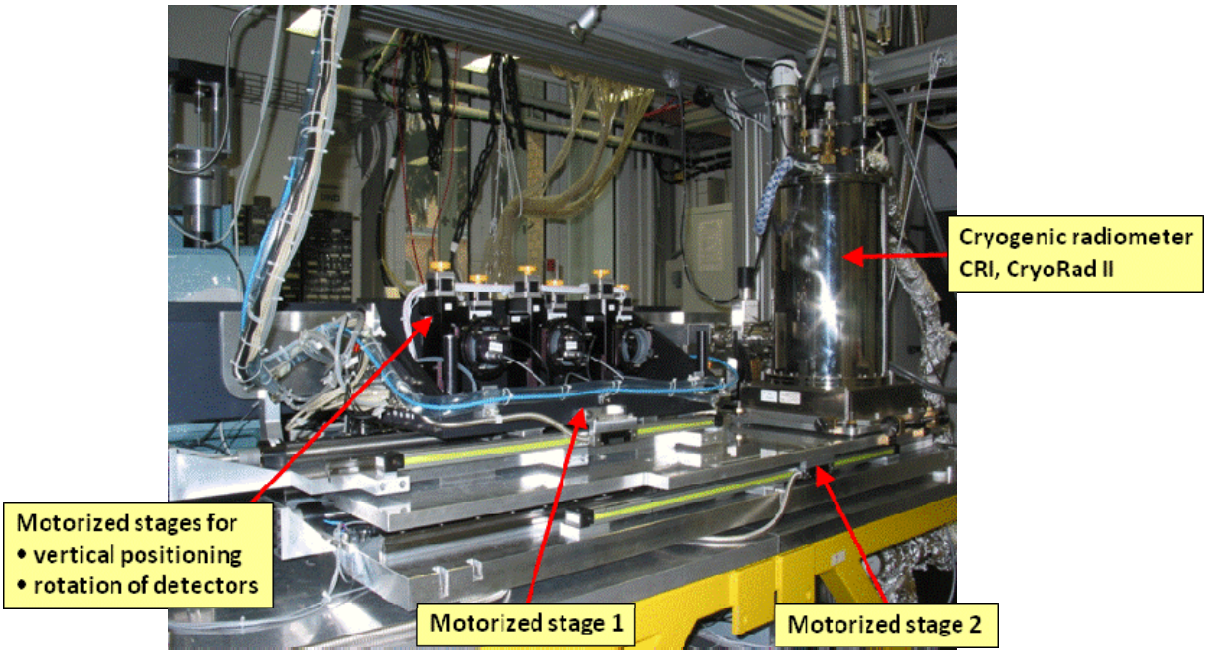

Figure 4.6 : Photography of the new detector calibration facility using in this work. The detectors to be calibrated (InGaAs photodiodes) are mounted in the rotary motorized stages. This stage allow the detectors to position in vertical direction and to rotate in different angle around an optical axis. The motorized stage 1 serves to position the detectors in horizontal direction as well as the motorized stage 2 which serves to position the cryogenic radiometer in horizontal direction.

4.3.5 Monitor detector

A single InGaAs photodiode (GAP5000-Germanium Power Devices) is used as a monitor detector to correct for power variations of the tuneable laser or tungsten halogen lamp during the measurements with the cryogenic radiometer and the detectors under test. The monitor detector is irradiated by a beam reflected from a wedged plate of fused silica (W_M in figure 4.4). Wedged plates of the same kind but rotated by 180° are placed in front of the cryogenic radiometer and in front of the detectors under test in order to have the same parallel beam displacement at any wavelength in both cases.

4.4 High accuracy calibration of InGaAs transfer-detectors

4.4.1 Spectral responsivity measurement

The InGaAs photodiode transfer detectors are calibrated by measuring their electrical signal when inserted into the beam from the monochromator or the tunable laser at the same position where the radiant power of the beam is determined by the cryogenic radiometer. The spectral responsivity of the detectors $s(\lambda)$ as a function of wavelength is defined by equation 4.2

$$s(\lambda) = \left[\frac{I_{\mathrm{Det}}}{P_{\mathrm{Cryorad}}} \right]_{\lambda} \qquad 4.2$$

I_{Det} is the signal of the detector (typically the photo current)

P_{Cryorad} is the radiant power (measured by cryogenic radiometer)

λ is the effective wavelength

In order to correct for possible variations of the radiant power between the cryogenic radiometer measurement and the detector measurement which are typically in order of 10^{-3}, the signal of a monitor detector is simultaneously measured and used to correct these variations. The spectral responsivity redefines as:

$$s(\lambda) = \left[\frac{I_{\mathrm{Det}}}{I_{\mathrm{Mon}}^{\mathrm{Det}}} \right] \cdot \left[\frac{I_{\mathrm{Mon}}^{\mathrm{Cryorad}}}{P_{\mathrm{Cryorad}}} \right] \qquad 4.3$$

$I_{\mathrm{Mon}}^{\mathrm{Det}}$ is the signal of the monitor detector during detector measurement

$I_{\mathrm{Mon}}^{\mathrm{Cryorad}}$ is the signal of the monitor detector during cryogenic radiometer measurement

The spectral responsivity of the InGaAs transfer detectors was measured in the wavelength range from 950 nm to 1650 nm by using the monochromatized radiation from a tungsten halogen lamp. Additionally measurement were performed with tuneable diode laser sources throughout two limited wavelength ranges from

1260 nm to 1370 nm and 1460 nm to 1580 nm. The measured spectral responsivity of the InGaAs transfer-detector is shown in the figure 4.7.

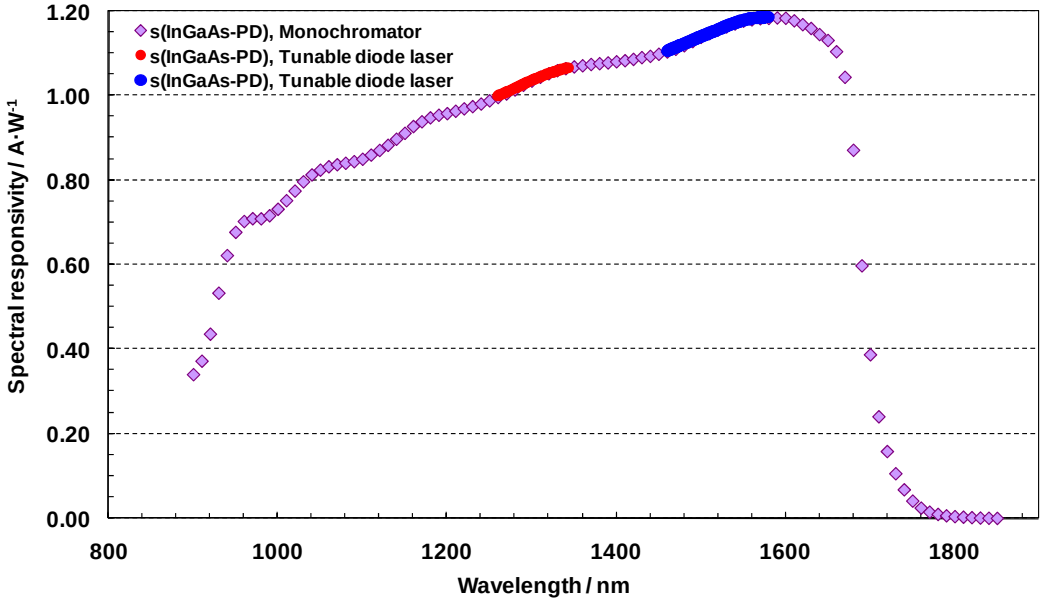

Figure 4.7 : The spectral responsivity of an InGaAs photodiode denote as s(InGaAs-PD) used as a transfer-standard calibrated by using a tungsten halogen lamp and tuneable diode lasers as radiation source on the detector calibration facility.

4.4.2 Polarization effects

The spectral responsivity of a detector is sensitive to the polarization of the incident radiation coming from the radiation source, $s(\alpha)$, and can be defined as

$$s(\alpha) = s_0 + s_1 \cdot \sin(2(\alpha + \varphi)) \qquad 4.4$$

where s_0 is the spectral responsivity of a detector for a non-polarized radiation source, s_1 is the amplitude of the spectral responsivity for a polarized radiation source, α is the angle of the detector to the polarized radiation source and φ is the off-set of the installed angle of a detector. In order to solve equation 4.4 for the three unknown parameters s_0, s_1 and φ, the value of $s(\alpha)$ for 3 angles of α are measured. When these three angles are evenly distributed, i.e. -60°, 0° and 60° of detector rotation with respect to the optical axis, the uncertainty of s_0 is minimized. Furthermore, s_0 is the withmetic mean of the spectral responsivities at -60°, 0° and 60° (see figure 4.8).

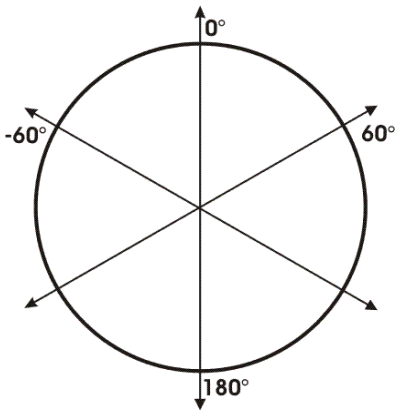

Figure 4.8 : Three measurement angles (-60°, 0°, 60°) of detector rotation in order to correct for polarization effects during the calibration of the detector.

4.4.3 Positioning of the detectors

The detectors are automatically centred with respect to the beam at each wavelength. The detector center is taken as the midpoint between the positions at which the detector signal drops down to 50% in both the vertical and horizontal directions. No spatial beam instability has been observed. The uncertainty of the detector centering is better than 50 μm. The uncertainty of the spectral responsivity measurement due to the uncertainty of the center position of the detector is typically between $2x10^{-4}$and $4x10^{-4}$ depending on the type of the detector.

4.4.4 Detector temperature

The detectors are calibrated at a controlled temperature of 25 °C to minimize temperature dependent effects. The temperature control includes the box in which the detectors are placed during the measurement. The stepping motors inside this box are additionally cooled to obtain stable conditions. The relative uncertainty of the spectral responsivity measurement due to the uncertainty of the temperature dependence of the detector is smaller than $5x10^{-5}$ [**23**] in wavelength range from 950 nm to 1650 nm.

4.4.5 Window transmittance

A window W_R is used to seal the vacuum around the radiometer cavity (in figure 4.4). A second window of identical specifications W_D is placed in front of the detector under test to obtain the same optical path. The ratio of the window transmittance is measured at all wavelengths several times before, during and after

each calibration at each wavelength by moving the window W_R to position W_T. The windows are irradiated at the same area and under the same angle of incidence during detector calibration and measurement of the window transmittance (figure 4.9).

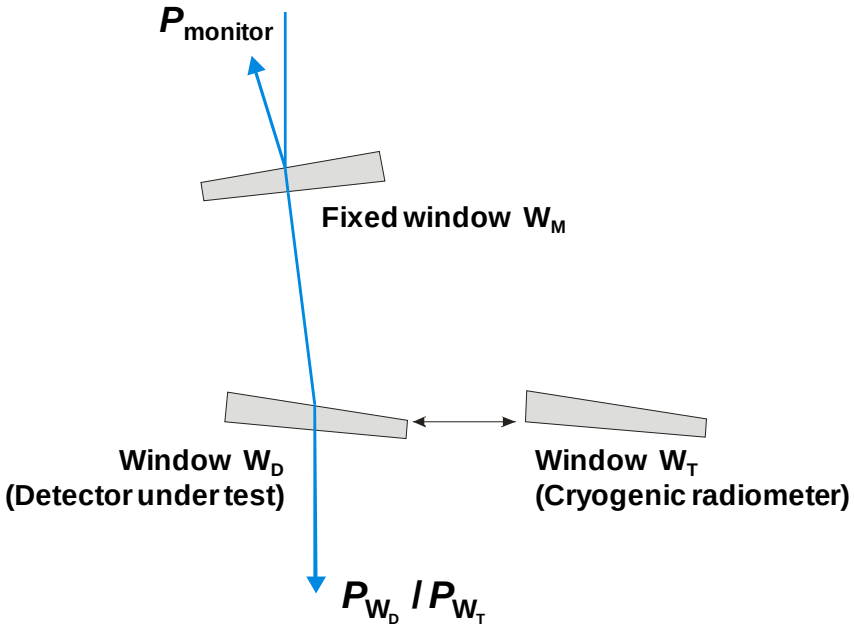

Figure 4.9 : Measurement of the window transmittance ratio

$$\frac{T_{W_D}}{T_{W_T}}(\lambda) = \frac{P_{W_D}}{P_{monitor,W_D}} \cdot \frac{P_{monitor,W_T}}{P_{W_T}} \qquad 4.5$$

$\frac{T_{W_D}}{T_{W_T}}(\lambda)$ is the ratio of the transmittances of the windows in front of the detector under test and the cryogenic radiometer

P_{W_D} is the signal of the detector under test during measurement of the window W_D

$P_{monitor,W_D}$ is the signal of the monitor detector during measurement of the window W_D

P_{W_T} is the signal of the detector under test during measurement of the window W_T

$P_{monitor,W_T}$ is the signal of the monitor detector during measurement of the window W_T

The uncertainty contribution due to the window transmittance is estimated by the standard deviation of the transmittance measurements. The relative uncertainty is about 3×10^{-4} when a tungsten halogen lamp is used as a radiation source. By using

more radiant power (e.g. a tuneable diode laser), the relative uncertainty is reduced to about $1x10^{-4}$. Figure 4.10 shows the ratio of window transmittances for all calibrated wavelength.

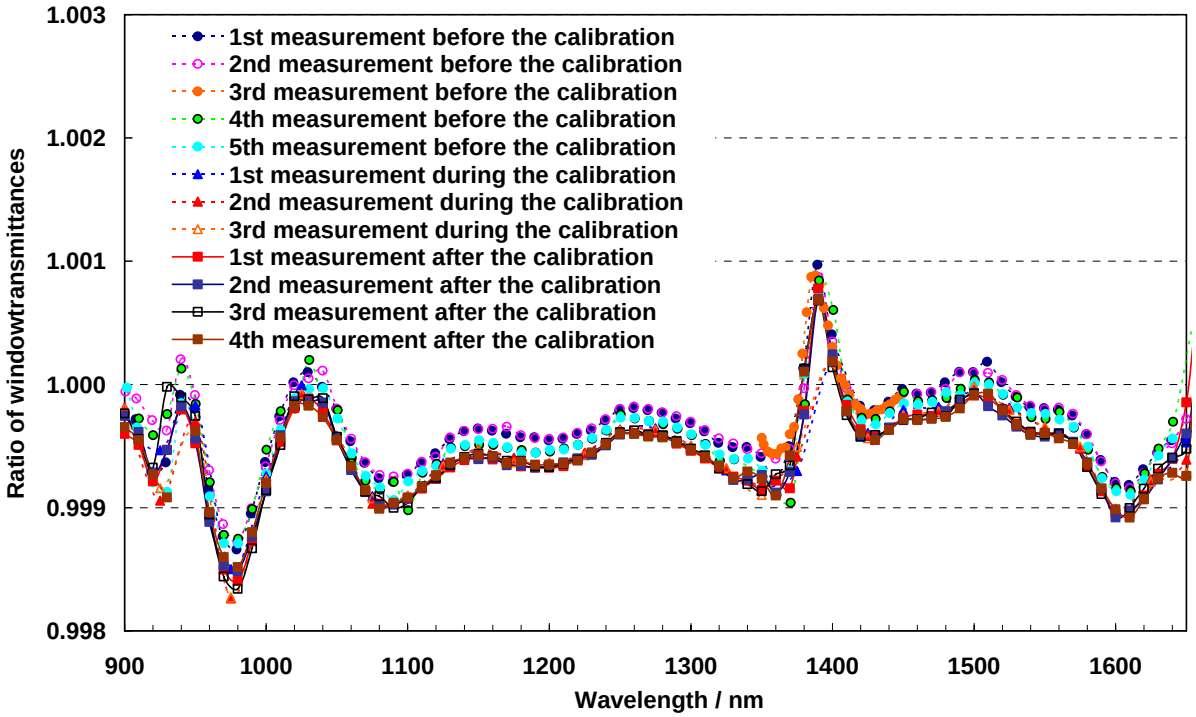

Figure 4.10 : The ratio of window transmittances measured before, during and after each calibration at each wavelength.

4.5 Improvement of spectral responsivity calibration in the NIR spectral range

The previous spectral responsivity scale maintained on InGaAs photodiodes [**23**] in the NIR wavelength range (950 nm to 1650 nm) had an uncertainty more than one order of magnitude higher than the spectral responsivity scale maintained on trap detectors with silicon photodiodes in the wavelength range from 500 nm to 900 nm [**24**]. Hitherto, the spectral responsivity scale was realized by calibrating InGaAs photodiodes at four laser lines using the PTB laser-based radiation thermometry cryogenic radiometer (RTCR) and interpolating the spectral responsivity with thermal detectors [**23**]. However, the interpolation with conventional thermal detectors is very time-consuming and of limited accuracy. Modeling of the spectral responsivity between widely separated laser-based calibrations, as is the case for Si trap detectors in the visible [**24**], is not possible for InGaAs photodipdes because of the lack of an accurate model of the responsivity for the detectors commonly used in the NIR wavelength range. Therefore, in order to reach higher accuracy, the quasi-

continuous calibration with the newly set-up calibration facility by a monochromator based cryogenic radiometer throughout the spectral region of interest has been chosen.

The new NIR spectral responsivity scale has been improved to meet the demand for the InGaAs filter radiometers applied to the thermodynamic temperature determination. The spectral responsivity scale between 950 nm and 1650 nm was realized by calibrating InGaAs photodiodes against a cryogenic radiometer at arbitrary wavelengths by using tungsten halogen lamp as a radiation source. Moreover, the lowest possible uncertainties can be reached by using more radiant power (more detail in section 4.6). Consequently, the cryogenic radiometer facility has been extended by using tuneable laser radiation in certain wavelength range (1260 nm to 1370 nm and 1460 nm to 1580 nm). The relative difference between the spectral responsivity scale of an InGaAs transfer-detector calibrated at the new detector calibration facility (with CRI cryogenic radiometer) and the previous spectral responsivity scale of an InGaAs transfer-detector calibrated at the RTCR is illustrated in figure 4.11.

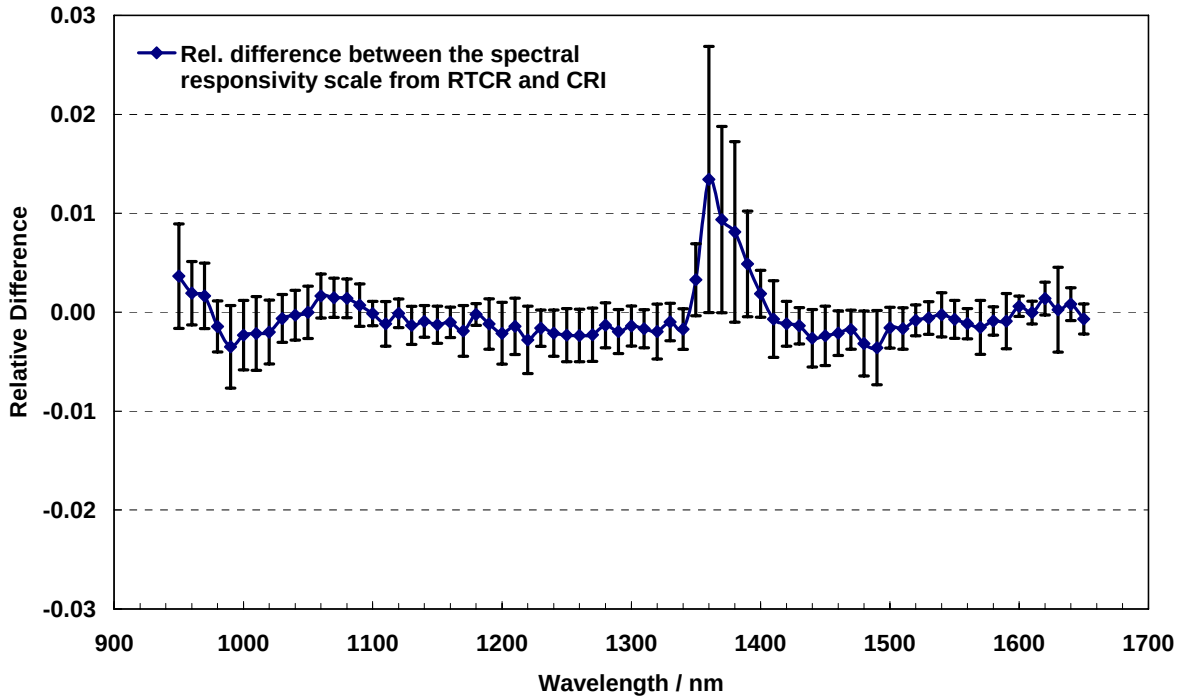

Figure 4.11 : Relative difference of the spectral responsivity scale of the InGaAs transfer-detector realized at the new detector calibration facility (with CRI cryogenic radiometer) and at the RTCR. The error bars denote the uncertainty (k=1) of the relative difference between both scales.

The uncertainty of the relative difference between both scales increases at wavelengths from 1360 nm to 1380 nm as a consequence of OH-absorption in the quartz glass of the monochromator prism at the new detector calibration facility during the calibration.

With the new development of a tuneable laser- and monochromator-based cryogenic radiometer facility the relative standard uncertainty of the NIR spectral responsivity scale has been significantly reduced (figure 4.12). By using monochromatized radiation of a tungsten halogen lamp, a relative standard uncertainty of about $1x10^{-3}$ has been achieved for the spectral responsivity between 950 nm and 1650 nm. In the limited wavelength range from 1260 nm to 1370 nm and 1460 nm to 1580 nm, the uncertainty was reduced to about $3x10^{-4}$ by using tuneable diode laser sources.

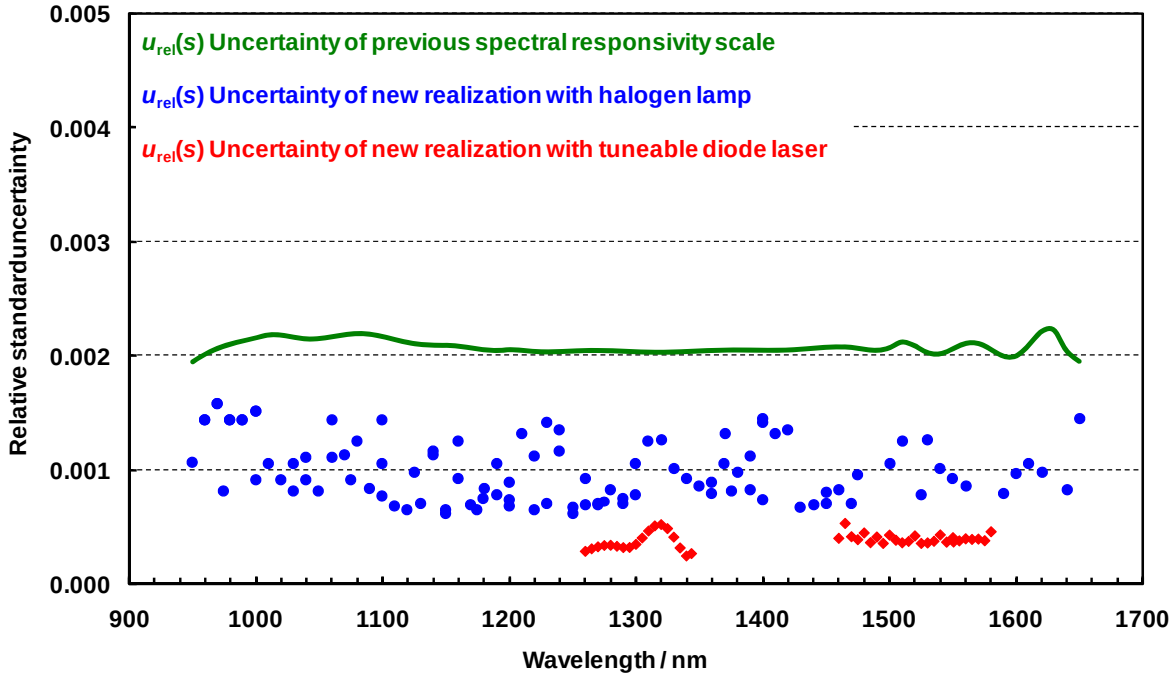

Figure 4.12 : The relative standard uncertainty of the spectral responsivity of the InGaAs transfer-detector by using tungsten halogen lamp and tuneable diode lasers as a light source at the new cryogenic radiometer facility, also shown is the uncertainty of the spectral responsivity of the previous realization.

4.6 Uncertainty of the spectral responsivity

During the calibration of the spectral responsivity of the transfer detector (single InGaAs photodiode) at the new cryogenic radiometer facility the following uncertainty contributions have been considered:

4.6.1 Non-equivalence

The position of the electrical heating and the position of the heating by the radiating power of the CRI cryogenic radiometer are in different positions. If the cavity of the cryogenic radiometer has a small temperature gradient, this non-equivalence will be one of the uncertainty contributions of the calibration. For the determination of this uncertainty, a second heater is placed at the cavity (see figure 4.13), so that the difference amount of the electrical heating can be determined. The uncertainty contribution due to this effect is found to be smaller than 1×10^{-5}.

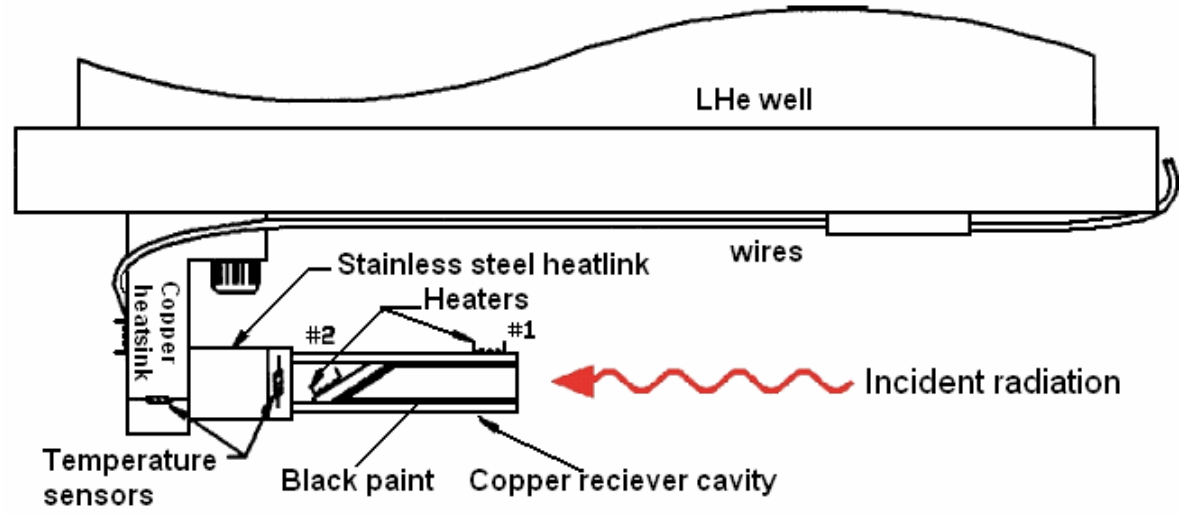

Figure 4.13 : Arrangement of the cryogenic radiometer cavity, the temperature sensors and the heaters (sketch from the manual) [**58**]

4.6.2 Absorption of the cavity

The uncertainty due to the absorption of the cavity in the applied spectral range in this calibration according to the measurement from the manufacturer is about 3×10^{-6} [**60**].

4.6.3 Uncertainty of electrical power measurement

The uncertainty originating from the electric power measurement is typically about 1.5×10^{-4} and maximum 3×10^{-3}. For the applied measurement heating power range in this calibration, this uncertainty contribution is about 1.5×10^{-4} (figure 4.14).

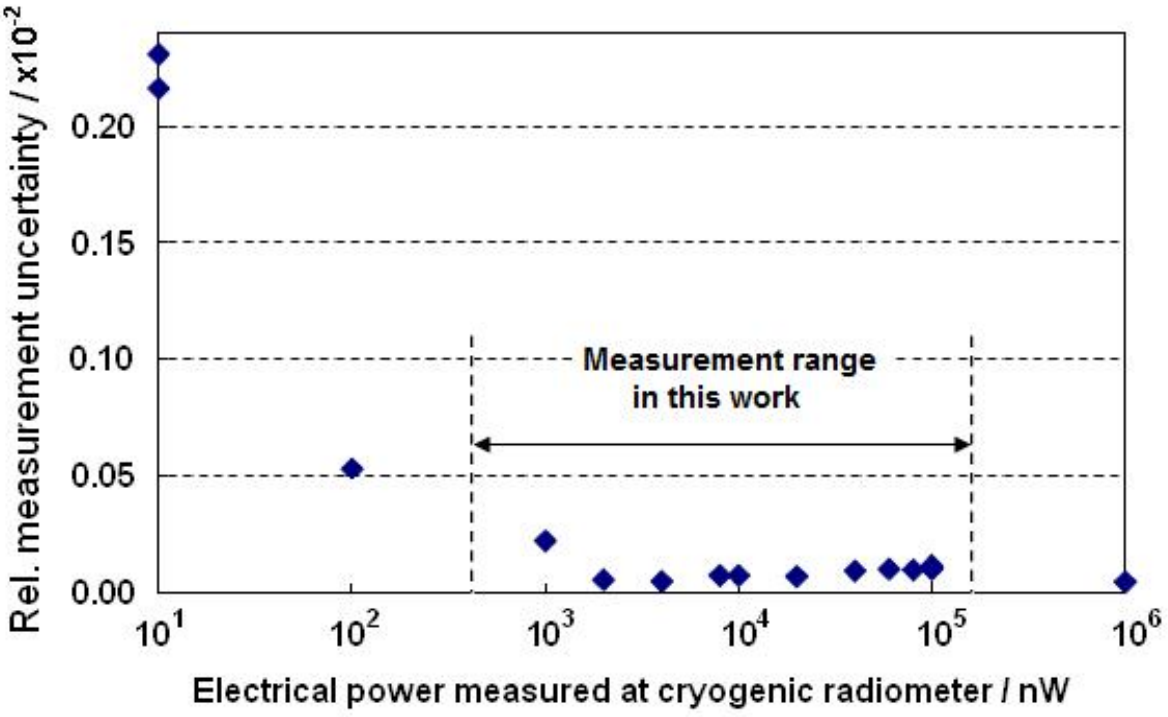

Figure 4.14 : Uncertainty of electrical power measurement [**60**]

4.6.4 Instability of the cryogenic radiometer due to noise of the temperature controller of the cryogenic radiometer

The relative uncertainty contribution according to the instability of the cryogenic radiometer due to noise of the temperature controller of the cryogenic radiometer is shown in figure 4.15. This uncertainty depends substantially on the radiant power input. It is inversely proportional to the radiant power. In order to identify the minimum radiant power necessary for a valid measurement, the parameter set for the automatic temperature controller of cryogenic radiometer is determined. Figure 4.16 shows the behavior of the temperature controller for different parameter sets.

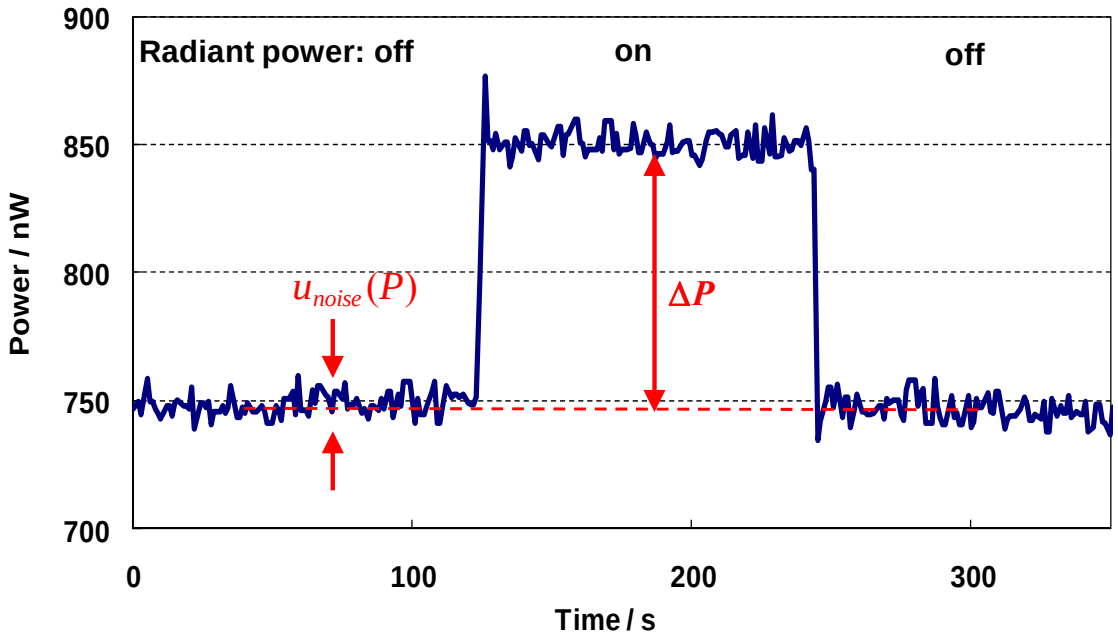

Figure 4.15 : Uncertainty contribution due to noise of the temperature controller of the cryogenic radiometer, $u_{\mathrm{noise}}(P)$ and ΔP is denoted as the radiant power.

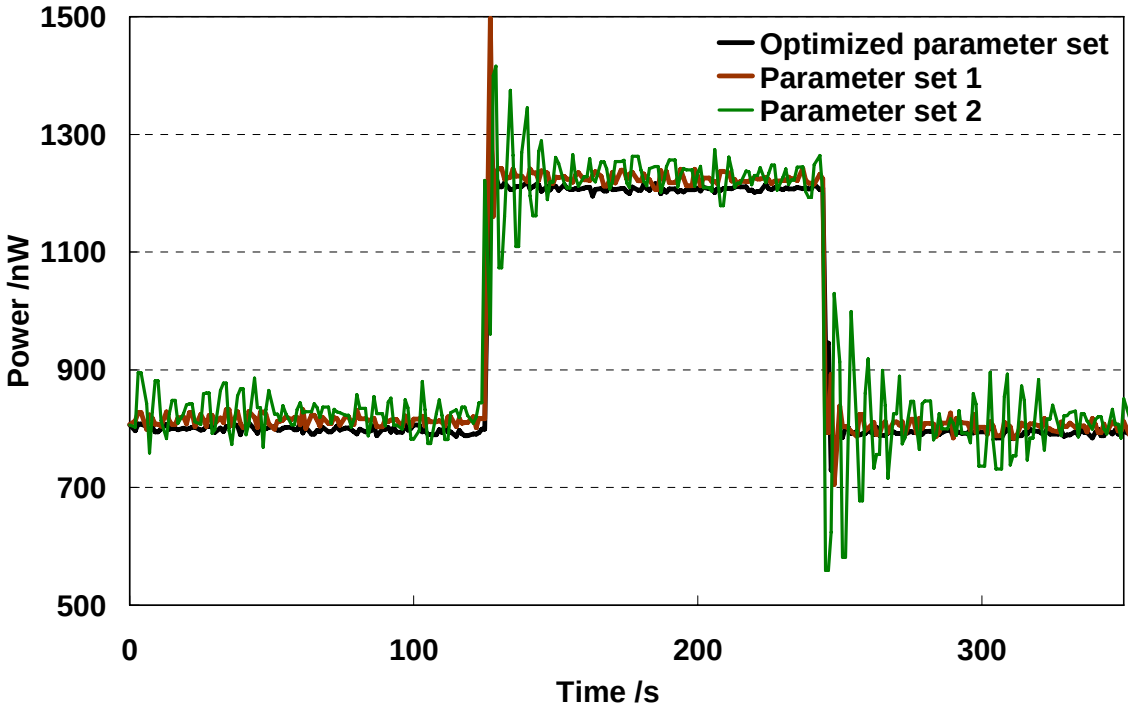

Figure 4.16 : The behavior of the temperature controller with different operating parameter sets. After the irradiation of the cavity approximately 125 seconds, the temperature controller regulates back the heating power with the same amount of the radiant power. The noise can be minimized by changing the operating parameter set of the temperature controller. The parameter set 1 and 2 are recommended from the manufacturer [**60**]

The relative measurement uncertainty decreases rapidly with increasing of the radiant power (see figure 4.17). A radiant power of at least 2 µW is necessary in order to bring this relative uncertainty contribution down to below $1x10^{-3}$. Figure 4.17 also shows the advantage when using a tunable diode laser as a radiant power source.

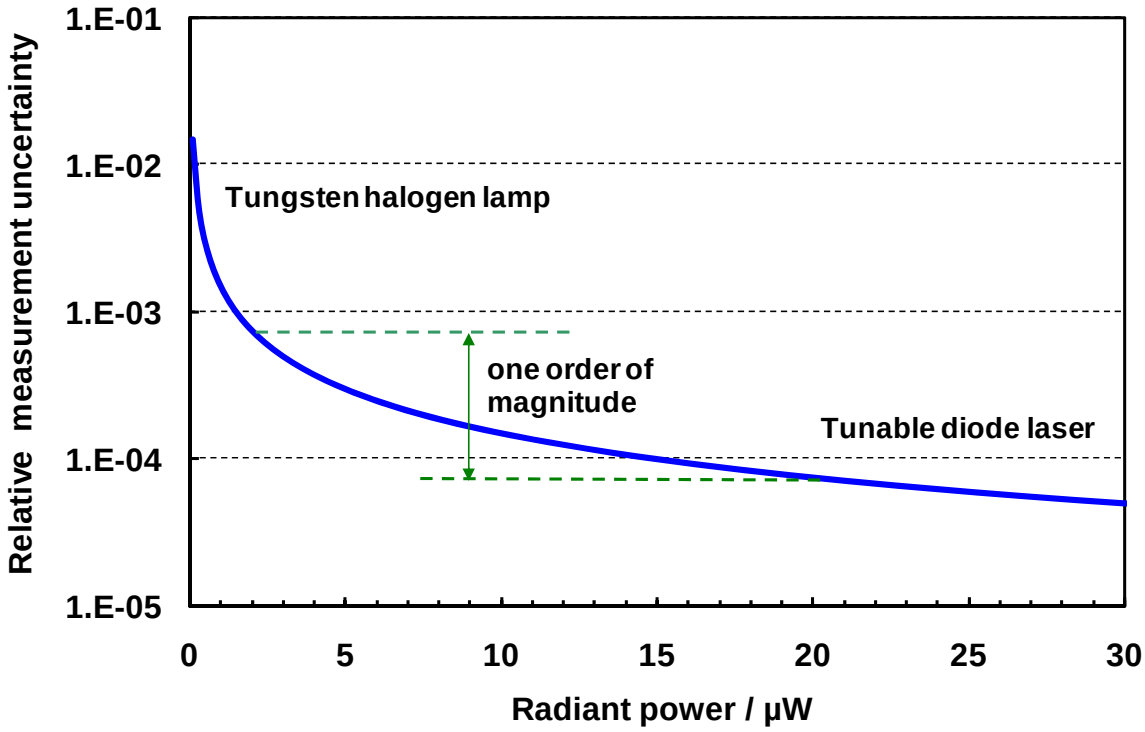

Figure 4.17 : The measurement uncertainty contribution due to noise of the temperature controller of the cryogenic radiometer. The radiant power of the tunable diode laser is significantly higher than from the tungsten halogen lamp, thereby decreases the measurement uncertainty by one order of magnitude.

4.6.5 Instability of the cryogenic radiometer due to drift of background radiation

The drift of the background radiation is typically less than 20 nW in 10 min (figure 4.18) but in some case it can be clearly larger e.g. in the first hours after the fill up of the liquid helium and nitrogen. To prevent this drift the measurement cannot be done before three hours after filling up helium and nitrogen.

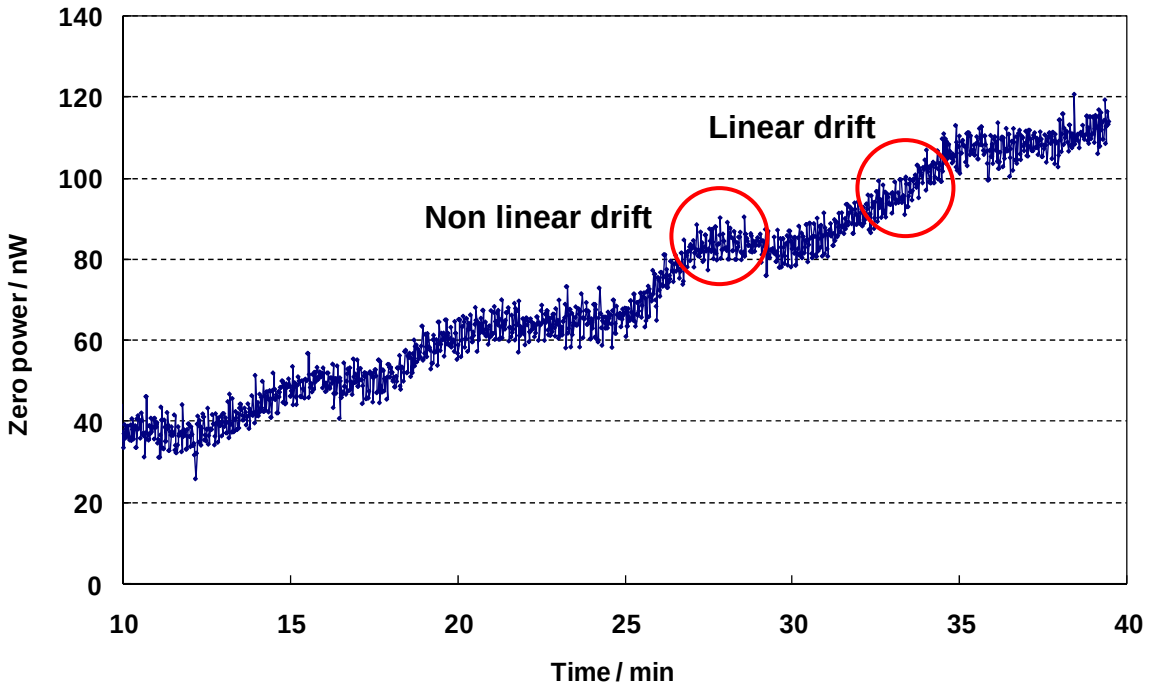

Figure 4.18 : Typical Instability of the cryogenic radiometer due to drift of background radiation.

There are two types of the drift of the background radiation. One is the linear drift and another one is the non-linear drift. With regard to the linear drift, the electrical substitution measurement for the particular radiant power consists of three electric heating power measurements : one measurement during the irradiation (P_{on}) of the cavity and two additional measurements before and after the irradiation (P_{off}) (figure 4.19). The radiant power (ΔP) is then calculated as the difference between the mean heating power before and after the irradiation and the heating power during the irradiation (equation 4.6),

$$\Delta P = \langle P_{\mathrm{on}} \rangle - \langle P_{\mathrm{off}} \rangle = \langle P_{\mathrm{on}} \rangle - \langle P_{\mathrm{off}} \rangle_1 - \left(\langle P_{\mathrm{off}} \rangle_2 - \langle P_{\mathrm{off}} \rangle_1 \right) \cdot \frac{t_{\mathrm{on}} - t_1}{t_2 - t_1} \qquad 4.6$$

Where t_{on} is the mean time during the irradiation, t_1 and t_2 are the mean time before and after irradiation respectively.

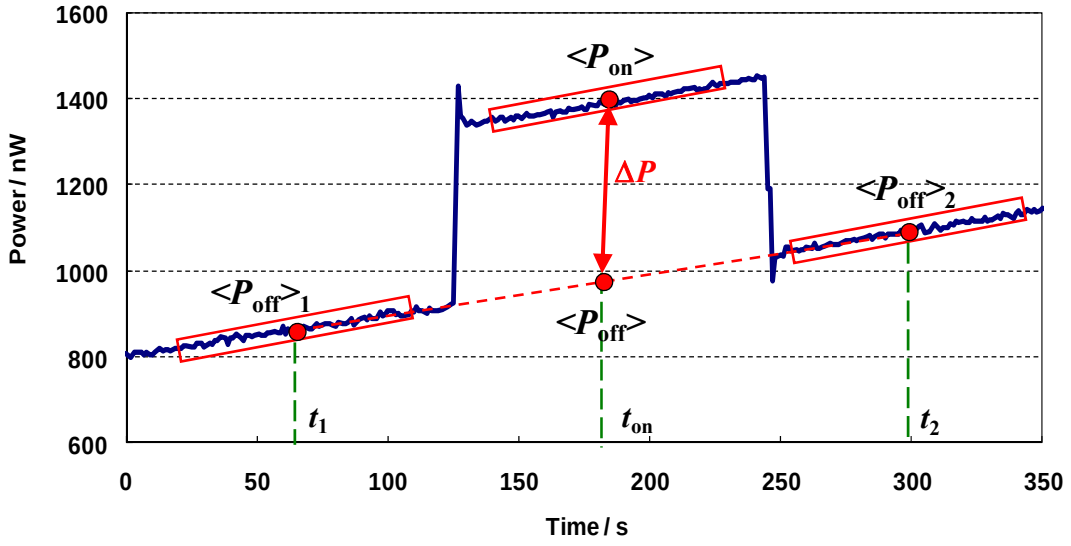

Figure 4.19 : Radiant power measurement with the correction of the linear drift of the zero point.

Not only linear drifts occur during the radiant power measurement also non-linear drifts. A non-linear drift takes place when the drift rate changes during the measurement of the radiant power. The correction by using equation 4.6 is incomplete in this case. For this reason, a second radiant power measurement is performed, both measurements are averaged, and the difference between the two measurements is included in the uncertainty of the mean radiant power (figure 4.20).

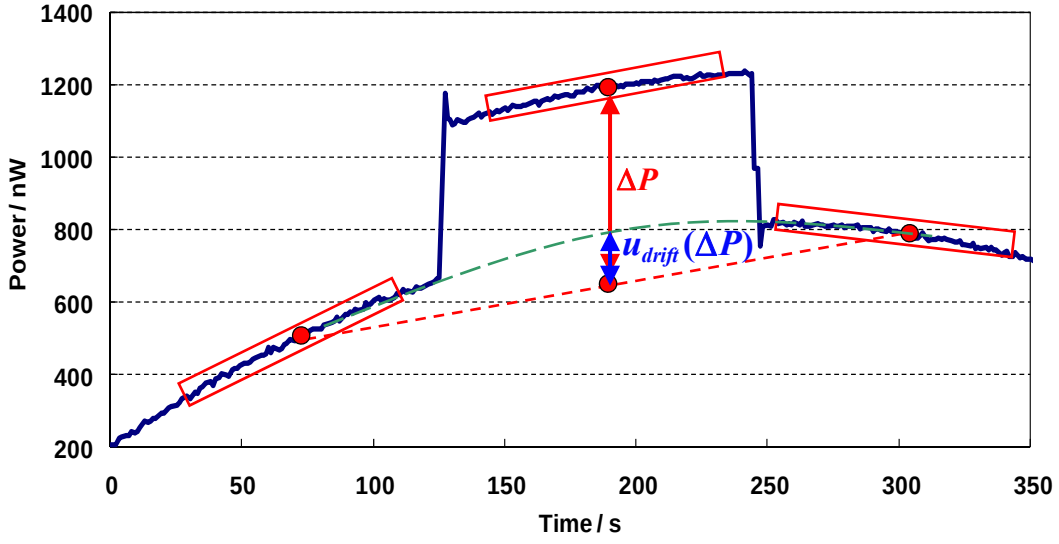

Figure 4.20 : Measurement uncertainty due to the non linear drift of the zero point.

The relative significance of this uncertainty contribution increases with decreasing radiant power. With an insufficient radiant power (1µW), this additional relative uncertainty may become a few parts in 10^3.

Uncertainty of the calibration:

The uncertainty contribution for the measurement of the spectral responsivity at a wavelength of 1550 nm using the monochromatized radiation of a halogen lamp or laser radiation is shown in table 4.2. The uncertainty of the transfer detectors spectral responsivity is significantly improved using laser radiation. Thereby the uncertainty contribution due to the instability of the cryogenic radiometer decreases to about $1x10^{-4}$ which is about one order of magnitude smaller compared to the use of a halogen lamp. Moreover, when using laser radiation the uncertainty of the window transmittance correction can be reduced, and the wavelength uncertainty can be neglected.

The uncertainty according to the non-uniformity of the detector must additionally be taken into consideration when using the transfer detectors to calibrate a filter radiometer (figure 4.1). The uncertainty contribution associated with the non-uniformity of the detector is dependent on the wavelength and the beam profile actually used at the filter radiometer calibration.

The homogeneity of the detector's spectral responsivity is separately measured, and the correlated uncertainty is numerically calculated. This calculation takes into account the difference in beam size and beam profile at the spectral responsivity calibration facility and at the filter radiometer calibration facility. Furthermore, the calculation takes into account the weighting of the uncertainty due to the filter transmittance. The contribution of the uncertainty of the spectral responsivity of the transfer detector to the uncertainty of the filter radiometer calibration has to be calculated for each individual filter radiometer.

For the calibration of InGaAs transfer-detectors in the wavelength range from 950 nm to 1650 nm by using the monochromatized radiation from a tungsten halogen lamp a relative standard uncertainty about 0.1% is achieved (see table 4.2). The uncertainty of this calibration is dominated by the cryogenic radiometer instability ascribed to a drift. The contribution to the overall relative uncertainty decreases with increasing radiant power. The second largest contribution is the uncertainty

associated with the window transmittance correction. Furthermore, the uncertainty of the wavelength of the monochromatized radiation gives a significant contribution. With the tuneable diode lasers the calibration of the InGaAs photodiodes can be performed throughout two limited wavelength ranges (1260 nm to 1370 nm and 1460 nm to 1580 nm). The much higher radiation power and the narrow bandwidth reduce the uncertainty of the measurement of the spectral responsivity to $2x10^{-4}$-$3x10^{-4}$ [**61**]. This uncertainty of the InGaAs transfer-detector is now comparable with the uncertainty of Si trap transfer-detectors.

Table 4.2: The uncertainty budget of the spectral responsivity calibration of an InGaAs photodiode at 1550 nm by using monochromatized radiation of a tungsten halogen lamp or tuneable laser radiation.

Source of uncertainty	$\Delta s/s$ **(x10^4)**	
	Tungsten halogen lamp	**Tuneable diode laser**
Instability of cryogenic radiometer (noise, drift)	7.5	1.1
Uncertainty in wavelength	3.0	0.1
Window transmittance	3.0	1.0
Uncertainty of electric power measurement	1.5	1.5
Detector temperature	0.5	0.5
Cavity absorptance and nonequivalence of power measurement	0.3	0.3
Stray light	0.2	0.2
Combined relative standard uncertainty of spectral responsivity at beam position	8.8	2.2
Typical contribution of the nonuniformity of the transfer detector	3.0	2.0
Combined relative standard uncertainty of spectral responsivity	9.3	3.0

Chapter V

InGaAs filter radiometers

5.1 Design

The thermodynamic temperature of a blackbody can be measured directly with low measurement uncertainties by applying radiometric methods using filter radiometers (FRs) and Plancks law of thermal radiation. In radiometry, filter radiometers are used as transfer standards for the measurement of the spectral irradiance [**62,63**]. For this work, two new InGaAs filter radiometers have been built. The basic components are a precision aperture, an interference filter as the wavelength selecting element and a windowless InGaAs photodiode as the optical radiation detector. All components are installed in a temperature controlled brass housing. A schematic cross section of the new filter radiometers is given in figure 5.1.

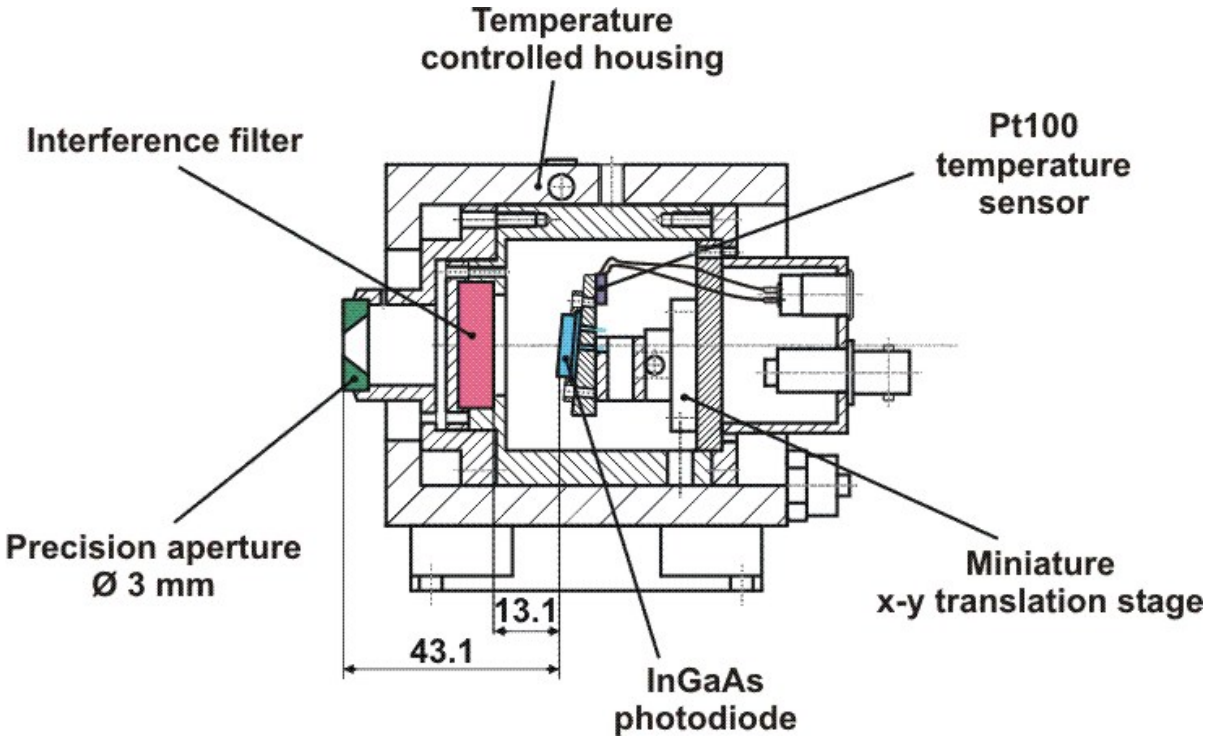

Figure 5.1 : Schematic cross section of a new InGaAs filter radiometer

5.1.1 Precision aperture

Filter radiometer are used as the detector for the measurement of the spectral irradiance in absolute radiometry. For this measurement the geometry of the measurement setup, consisting of two precision apertures, the blackbody aperture, the filter radiometer aperture and the distance between two apertures must be known very accurately. The precision apertures are used to define the solid angle and the field of view. Figure 5.2 shows the principle features of the precision aperture. The most important criteria for the usability of a precision aperture is the edge of the aperture, the ideal is the knife edge structure.

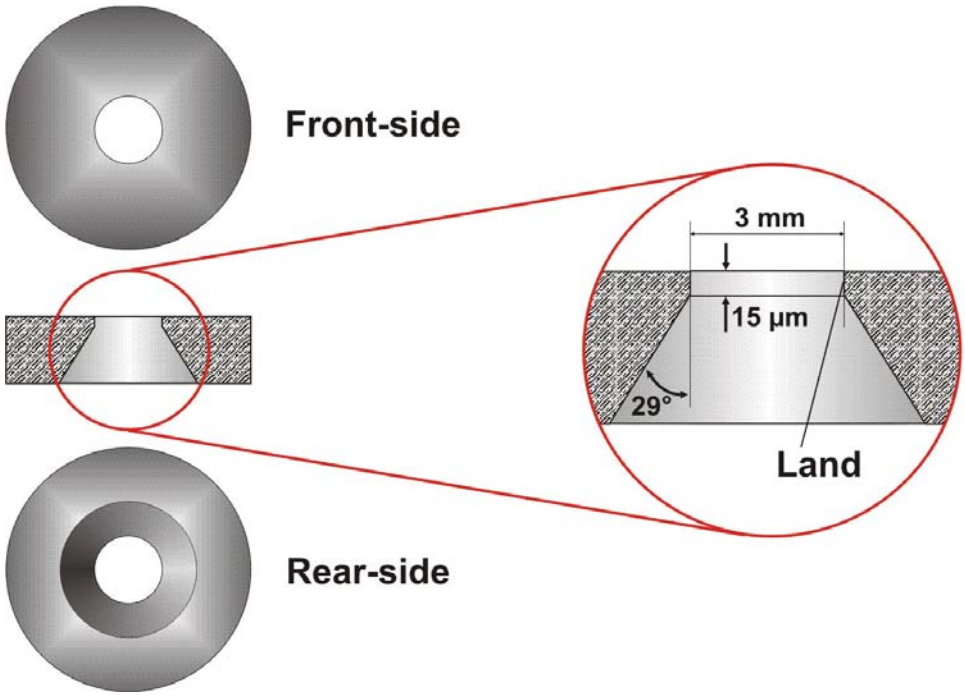

Figure 5.2 : Schematic diagram of a precision aperture assembled in the InGaAs filter radiometer. The inset shows the detailed structure of the edge which is most important for the usability of the optical precision aperture.

The knife edge of the aperture is structured as thin as possible with 90° angle of the remaining cylindrical part, i.e. the land to ensure an effective optical area independent of the angular distribution of the incoming radiation and the collected radiation is independent on the distance between aperture and detector inside the filter radiometer (i.e. InGaAs photodiode) as shown in figure 5.3. To obtain a nearly perfect edge structure the land of the aperture must be as small as possible, in the order of 10 µm to 20 µm and as steep as possible. Such an edge is not obtainable by

commercial manufacturing. One of the promising technical solution is diamond turning of the apertures. The ideal material to structure such an aperture has been found to be aluminium or copper.

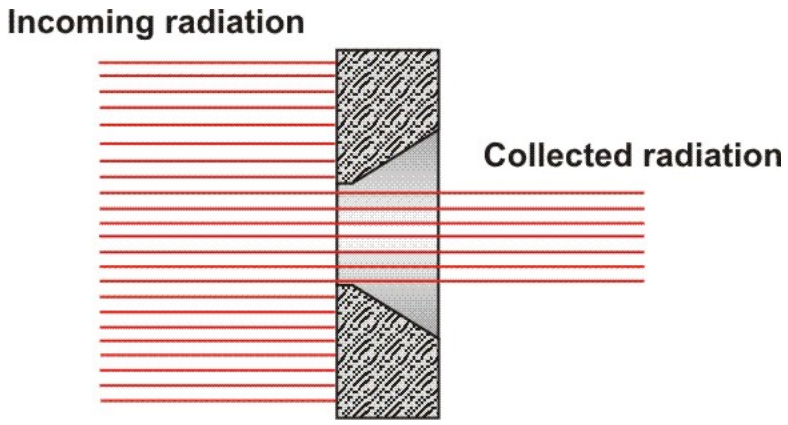

Figure 5.3 : Far-field approximation of an ideal knife edge structure of precision aperture

The aperture of the new InGaAs filter radiometer used in this work is an aluminium, diamond turned aperture with a knife edge and has a diameter of 3 mm to ensure that all of collected radiation is coming across the 5 mm diameter detector (InGaAs photodiode). This aperture defines the effective area of the detector for a homogeneous radiation field. The aperture land is manufactured with a very small thickness (ca. 15 µm) to minimize the reflections from the land onto the detector. In order to minimize the inter-reflections between the aperture and the interference filter, an opening angle of 29° relative to the optical axis has been chosen on the tapered rear-side of the aperture (see figure 5.2).

5.1.2 Interference filter

The interference filter used in the filter radiometer defines the spectral bandpass for the measurement of a broadband source e.g. by the application of the filter radiometer to determine the temperature of the blackbody radiation. The first InGaAs filter radiometer of PTB used for the thermodynamic temperature determination before this work has an interference filter with a center wavelength of 1595 nm and a bandwidth (FWHM) of 100 nm [**21**]. However the uncertainty of the thermodynamic temperature determination with this filter radiometer is still too large for the investigation of the thermodynamic accuracy of the ITS-90 due to the bandpass of the interference filter near to the band-gap wavelength of the InGaAs photodiode

resulting in a high temperature coefficient. To resolve this problem and to take advantage from the improved realization of the NIR spectral responsivity scale, two new InGaAs filter radiometers were built with optimized center wavelengths and bandwidths to avoid the limitations of the first InGaAs filter radiometer.

The center wavelengths and bandwidths were optimized by the selection of the interference filter to fulfil the three following conditions (see figure 5.4):

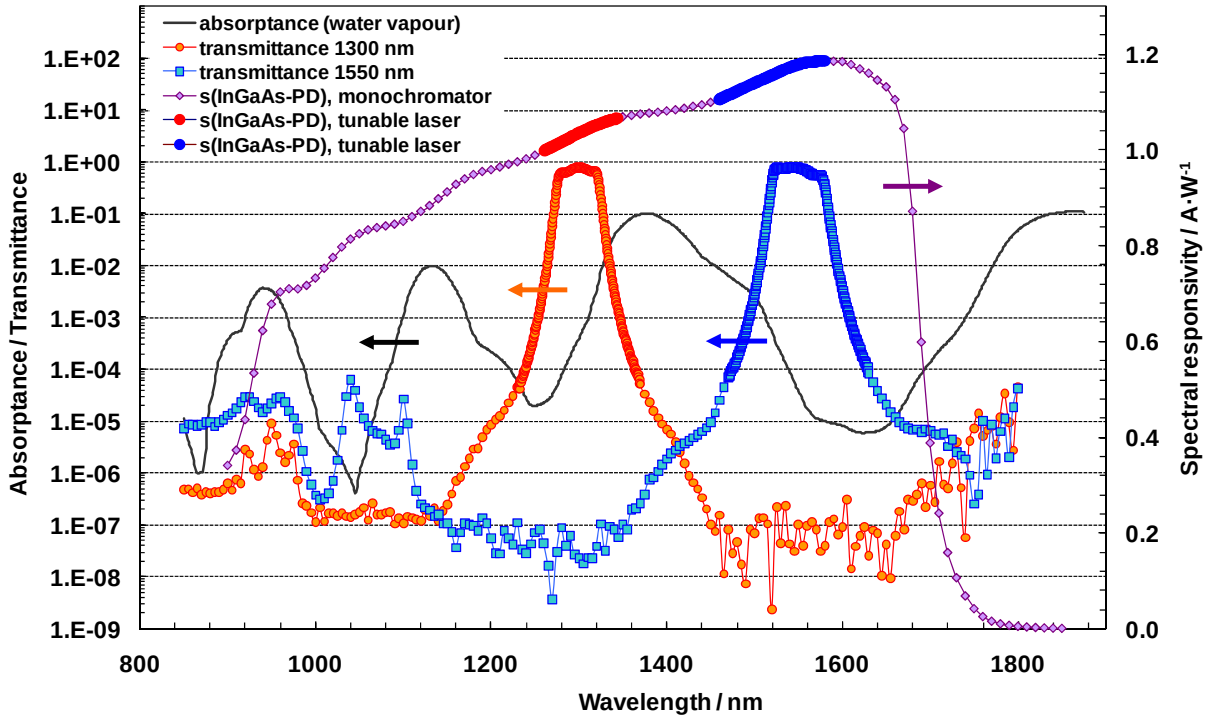

Figure 5.4 : Measured transmittance ("transmittance", left-hand scale) of the interference filters used for the filter radiometers FR1300nm and FR1550nm together with an absorptance curve of a 2m thick layer of air (23 ◦C, 1013hPa, 50% rh) due to water vapor ("absorptance", left-hand scale). The absorptance curve was calculated by convolving the absorption lines in air with a 50 nm normalized bandwidth instrumental function of the filter radiometer. Also shown is the spectral responsivity of an InGaAs photodiode ("spectral responsivity", right-hand scale) used as a transfer standard; the thick regions of the responsivity curve denote the wavelength intervals where tunable lasers were used for its calibration. (The arrows on the curves indicate the position of the corresponding scale of the respective curves)

1. The tuneable laser radiation has to be available in the wavelength region of the filter bandpass for lowest possible calibration uncertainty of the transfer standards.
2. The water vapour absorption when applying these filter radiometers in front of a blackbody has to be minimized.

3. The bandpass of the filter has to be of sufficient distance to the bandgap wavelength of the InGaAs photodiode to minimize the temperature dependence of the spectral responsivity of the filter radiometer.

Custom-made interference filters are used to fulfil these conditions They have a center wavelength of 1300 nm and 1550 nm, respectively. Both of interference filter have a spectral bandwidth of about 50 nm (FWHM) and an out-of-band blocking of more than five orders of magnitude. The correction due to water vapour absorption of these interference filter remains below $4x10^{-4}$ and $4x10^{-5}$ for the interference filter with the center wavelength of 1300 nm and 1550 nm, respectively. Additionally, by avoiding the band gap wavelength range, the effect of a high temperature coefficient [**23,64**] and a possible nonlinearity of the spectral responsivity of the filter radiometer are minimized.

5.1.3 Detector

Suitable detector used for the radiometric temperature measurement below 500 °C are InGaAs photodiodes. The InGaAs photodiodes used as the optical detector for the both of the new filter radiometer were selected from a batch of windowless InGaAs photodiodes with 5 mm diameter of a sensitive area. These InGaAs photodiode were previously characterized with respect to their shunt resistance and the homogeneity of the spectral responsivity at wavelength 1300 nm and 1550 nm (figure 5.5). The shunt resistance of both InGaAs photodiodes is typically more than 10 MΩ. The InGaAs photodiode type GAP5001 (Germanium Power Device) has a homogeneity of the spectral responsivity at wavelength 1300 nm better than 3×10^{-3} (figure 5.5) thus it was used as a detector of the FR1300. As the detector of FR1550 the InGaAs photodiode type FD5000W (Fermionics) was selected through its good homogeneity of the spectral responsivity ($4x10^{-3}$) at the wavelength 1550 nm (figure 5.5).

The InGaAs photodiode is tilted by about 5° with respect to the optical axis in order to avoid inter-reflections between the photodiode and the rear-side of the interference filter. The alignment of the photodiode to the optical axis in the filter radiometer is critical due to the small difference between the diameter of the sensitive area of the tilted photodiode (5 mm) and the diameter of the precision aperture (3 mm). Therefore, to obtain the best concentricity, the photodiode was mounted on a

miniature x-y translation stage and aligned by means of a collimated beam at the spectral comparator facility.

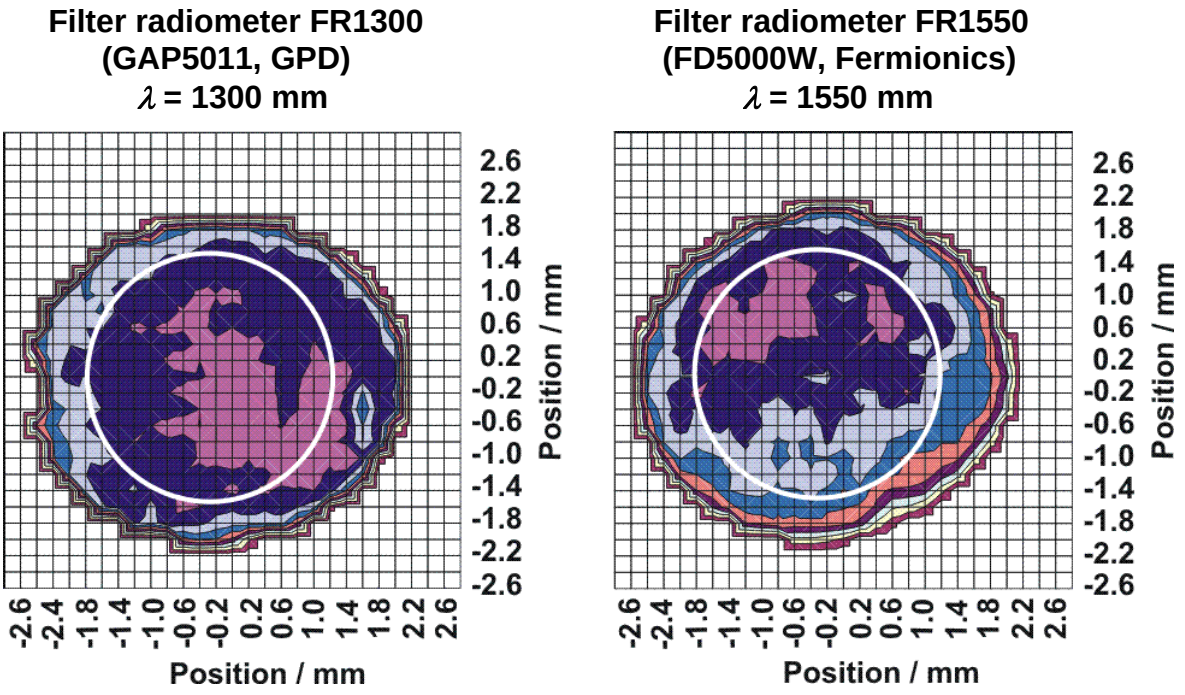

Figure 5.5 : Mapping of the spectral responsivity of the InGaAs photodiodes used for the both new filter radiometers, FR1300 (λ = 1300 nm) and FR1550 (λ = 1550 nm). The measurements were performed with the spectral comparator applying a spot with a diameter of 0.3 mm. One change in color represents a relative change of 1×10^{-3} in spectral responsivity; the white circles denote the area of 3 mm diameter that is used during the filter radiometer calibration and in the application of the filter radiometer.

The temperature controlled housings of the both new filter radiometer are made of brass. A thermostat controls the temperature of the housing of the filter radiometer within ± 50 mK. The temperature is monitored by a Pt100 sensor near the photodiode.

5.2 Calibration of the spectral irradiance responsivity

5.2.1 Principle

The calibration of the filter radiometer at the spectral comparator facility is the transfer of the spectral irradiance responsivity of the absolute calibrated transfer detector (single InGaAs photodiode) on the filter radiometer. By mounting of the precision, diamond-turned aperture with the area A_{transfer} in front of the transfer detector, the spectral responsivity of the transfer detector, which is absolutely

calibrated at the cryogenic radiometer, is transferred into the spectral irradiance responsivity (equation 5.1).

$$s_E(\lambda) = A_{\text{transfer}} \cdot s(\lambda) \qquad 5.1$$

In a radiation field with the spectral irradiance $E(\lambda)$ a detector which has a spectral irradiance responsivity $s_E^{\text{Det}}(\lambda)$, the measured photo current of the detector is equal to:

$$I_{photo}^{\text{Det}}(\lambda) = E(\lambda) \cdot s_E^{\text{Det}}(\lambda) \qquad 5.2$$

When both detectors, the transfer detector and the filter radiometer, are in a radiation field which has the same spectral irradiance, the spectral irradiance responsivity of the filter radiometer, $s_E^{\text{FR}}(\lambda)$, can be calculated according to equation 5.3 with the measured photo current of each detector and the well known spectral irradiance responsivity $s_E^{\text{transfer}}(\lambda)$ of the transfer detector.

$$s_E^{\text{FR}}(\lambda) = \frac{I_{photo}^{\text{FR}}(\lambda)}{I_{photo}^{\text{transfer}}(\lambda)} \cdot s_E^{\text{transfer}}(\lambda) \qquad 5.3$$

The suitable quantity for the characterization of the filter radiometer are the integrated spectral irradiance responsivity (I_s):

$$I_s = \int_{\lambda_{\min}}^{\lambda_{\max}} s_E^{\text{FR}}(\lambda) d\lambda \qquad 5.4$$

and the center wavelength (λ_{CW}):

$$\lambda_{\text{CW}} = \frac{\int_{\lambda_{\min}}^{\lambda_{\max}} s_E^{\text{FR}}(\lambda) \lambda \, d\lambda}{\int_{\lambda_{\min}}^{\lambda_{\max}} s_E^{\text{FR}}(\lambda) d\lambda} \qquad 5.5$$

The shortest wavelength ($\lambda_{\min}$) by of the monochromator used for the calibration of all filter radiometers at the spectral comparator facility is 410 nm. The

calibration at the shorter wavelength is negligible. By the application of all filter radiometers to measure the irradiance of the blackbody at the temperature of 930 K, the contribution of the signal from the wavelength range from 200 nm to 410 nm in comparison to the signal from λ_{min} to λ_{max} is smaller than $5x10^{-7}$ [**65**]. The longest wavelength for the calibration of the InGaAs filter radiometers (λ_{max}) is 1800 nm, which is well beyond the bandgap wavelength region of the InGaAs photodiodes.

5.2.2 Experimental setup

The calibration of the filter radiometers against the transfer detectors has been done at the spectral comparator facility. This facility, which is shown in figure 5.6, has been improved to meet the following requirements :

- For the calibration of the narrow-band detectors e.g. the filter radiometers using in this work with typical spectral bandwidths of the interference filter ranging from 20 nm to 50 nm against broadband detectors e.g. a Si photodiode trap detector or a single InGaAs photodiode, the out-of-band stray light contribution to the signal must be suppressed to 10^{-6}. The values for the stray light contribution of single grating monochromators are typically 10^{-5} [**66**]. A prism (flint or suprasil prism) monochromator (Leiss prism monochromator in figure 5.6) was integrated as a predisperser to achieve the required lower stray light. The combination of a prism monochromator with a grating monochromator to suppress the out-of-band stray light has more advantages than using a double-grating monochromator, in particular the transmitted flux is higher and higher-order suppressing filters are not required.
- For the application of the filter radiometer as a detector to measure the blackbody radiation, it is very important that the filter radiometer is calibrated in the same condition as in the application i.e. with non-polarized light. Because the radiation passing through the monochromator of the spectral comparator facility is polarized [**67,68**], the influence of this polarization on the spectral responsivity of the detectors must be considered in the calibration of the filter radiometer. The effect and the solution of the calibration of the filter radiometer with

the polarized radiation for the application with non-polarized sources i.e. blackbodies are explained in the section 5.2.5.

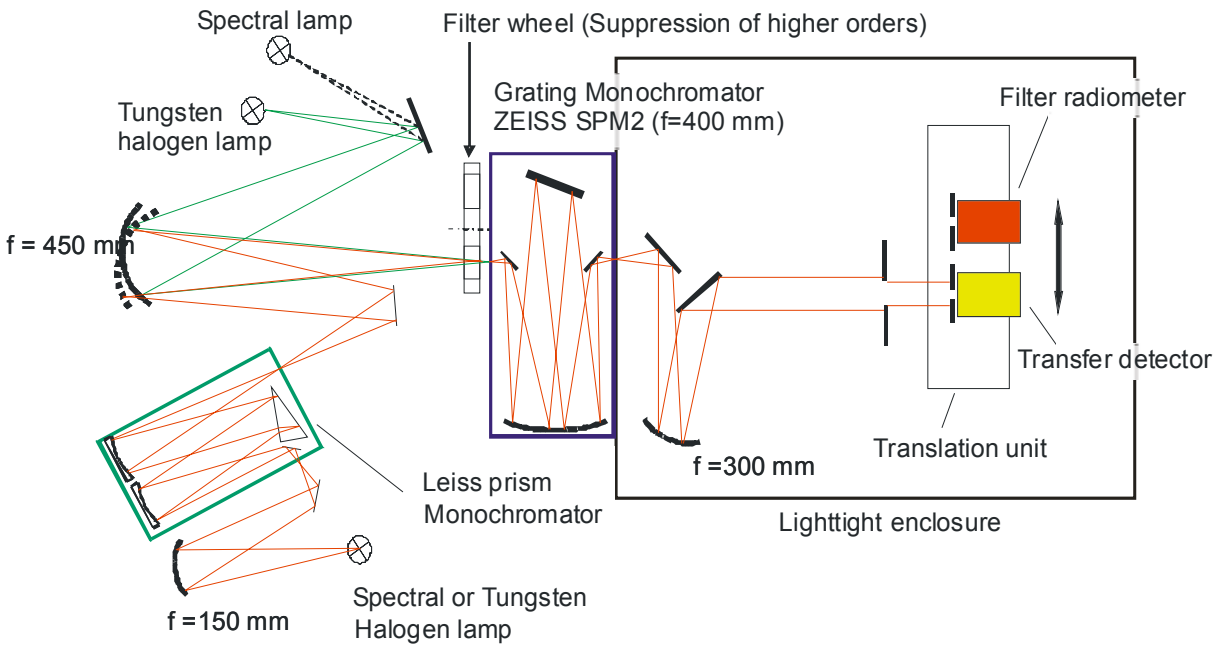

Figure 5.6 : The spectral comparator facility for the calibration of narrow-band filter radiometers against broadband transfer detectors.

A 250-W-Tungsten-Halogen lamp is used as the radiation source for the calibration of the filter radiometer at the spectral comparator facility. The radiation source is imaged with its actual size onto the entrance slit of the prism monochromator. The radiation from the exit silt of the prism monochromator is imaged with its actual size onto the entrance slit of the grating monochromator by a concave mirror (f=450 mm). The calibration of InGaAs filter radiometer is performed by application of gratings with 651 lines·mm^{-1} which provide a spectral dispersion of 4 nm·mm^{-1}. The slit width of the prism monochromator is set in such way that the slit width of the prism monochromator is ten times bigger than the slit width of the grating monochromator. The spectral bandwidth of the monochromator is set to 1 nm for the calibration within the bandpass of the filter radiometer and for the calibration of the out-of-band wavelength region of the filter radiometer the spectral bandwidth is set to 5 nm.

The wavelength setting of both monochromators has been calibrated at about 50 spectral emission lines of different spectral lamps. The grating and the prism are driven synchronously in wavelength by two stepper motors. One step of the stepper motor corresponds to wavelength difference 13 pm for gratings with 651 lines·mm^{-1}.

Behind the exit slit of the grating monochromator the radiation is collimated into a homogenous radiation bundle.

5.2.3 Calibration process

Before the calibration of the filter radiometer, the alignment of both detectors (the transfer detector and the filter radiometer) are done by using the autocollimation method with a laser beam (He-Ne-Laser : 543 nm) which is collinear with the optical axis of the collimation optics behind the monochromator. Then, the position of both detectors in the direction of the optical axis are adjusted in such way that the apertures of both detectors are in the same plane, to ensure that in case of a slight divergence of the radiation bundle (behind the exit slit of the grating monochromator) both detector measure the same irradiance. The accuracy of the positioning of both detector apertures in the same plane is ca. 0.02 mm [**65**]. Finally, both detectors are adjusted in the vertical and horizontal direction to the central position of the radiation bundle. Both detectors are moved reciprocally in the same position within the homogenous radiation bundle, thereby the apertures of both detectors are overfilled. The calibration cycle at each wavelength for each detector comprises 5 measurements of the photo current and 5 measurements of the photo current when the radiation source is shielded by the shutter in front of radiation source (dark measurement). This calibration cycle is typically repeated 3 time.

The characteristic behavior of the spectral responsivity of the filter radiometer used in this work is shown in the figure 5.7. The spectral responsivity can be separated into two wavelength regions: the bandpass and the out-of-band blocking wavelength region. The bandpass is arbitrary defined as the wavelength region in which the spectral responsivity decreases about 4 orders of magnitude with respect to the maximum. Within the bandpass the wavelength increment of the monochromator and the spectral bandwidth is set to 1 nm for the calibration. The calibration of the spectral responsivity in this region is are repeated more than 3 times and the mean value of these calibration values are used as the result. The photo current of the filter radiometer to be calibrated and the transfer detector are measured by a current-to-voltage converter and a digital voltmeter. For the calibration within the bandpass the photo current of both detectors are measured with the same feedback resistor of the current-to-voltage converter (typically 1 GΩ), therefore the absolute resistance value is not critical for the evaluation of the result.

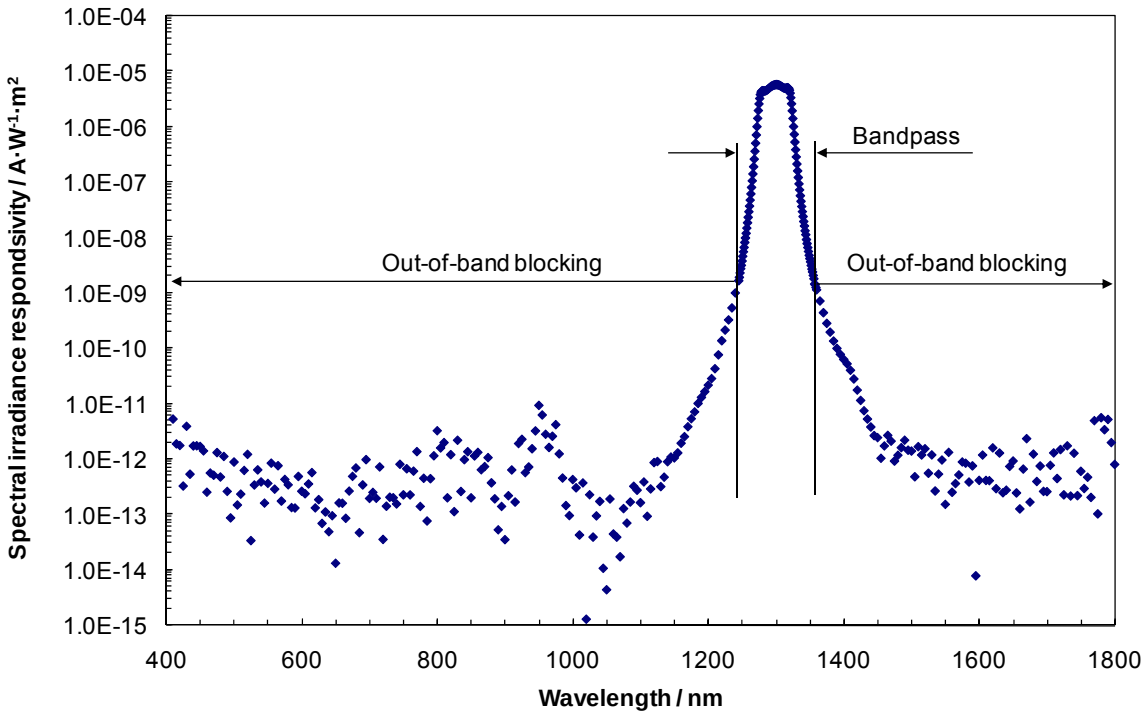

Figure 5.7 : The characteristic behavior of the spectral responsivity of the filter radiometer used in this work with the center wavelength 1300 nm.

Due to the very strong blocking capability of the filter in the out-of-band wavelength region, the photo current contribution from this wavelength region is very small comparative to the integrated signal of the bandpass (ca. $3\text{x}10^{-4}$). Therefore the calibration in this wavelength region was performed only once.

5.2.4 The evaluation of the calibration results

During the calibration process, the photo current of the filter radiometer and the transfer detector is measured and the dark signal correct photo currents of the filter radiometer ($I_{\text{photo}}^{\text{FR,Corr}}$) and of the transfer detector ($I_{\text{photo}}^{\text{transfer,Corr}}$) are equal to :

$$\begin{aligned} I_{\text{photo}}^{\text{FR,Corr}}(\lambda) &= I_{\text{photo}}^{\text{FR}}(\lambda) - I_{\text{photo}}^{\text{FR,Dark}}(\lambda) \\ &= s_E^{\text{FR}}(\lambda) \cdot E_{\text{Mon}}(\lambda) \end{aligned} \qquad 5.6$$

$$\begin{aligned} I_{\text{photo}}^{\text{transfer,Corr}}(\lambda) &= I_{\text{photo}}^{\text{transfer}}(\lambda) - I_{\text{photo}}^{\text{transfer,Dark}}(\lambda) \\ &= s_E^{\text{transfer}}(\lambda) \cdot E_{\text{Mon}}(\lambda) \end{aligned} \qquad 5.7$$

where $I_{\text{photo}}^{\text{FR}}(\lambda)$ is the photo current of the filter radiometer

$I_{\text{photo}}^{\text{FR,Dark}}(\lambda)$ is the photo current of the of the filter radiometer when the radiation source is blocked by a shutter in front of radiation source

$s_E^{\text{FR}}(\lambda)$ is the spectral irradiance responsivity of the filter radiometer

$E_{\text{Mon}}(\lambda)$ is the irradiance from the monochromator at the aperture of the detector

$I_{\text{photo}}^{\text{transfer}}(\lambda)$ is the photo current of the transfer detector

$I_{\text{photo}}^{\text{transfer,Dark}}(\lambda)$ is the photo current of the transfer detector when the radiation source is blocked by a shutter in front of radiation source

$s_E^{\text{transfer}}(\lambda)$ is the spectral irradiance responsivity of the transfer detector

The spectral irradiance responsivity of the filter radiometer (in each polarization direction, 0° and 90°) can be found by dividing equation 5.6 by equation 5.7:

$$s_E^{\text{FR}}(\lambda) = s_E^{\text{transfer}}(\lambda) \cdot \frac{I_{\text{photo}}^{\text{FR,corr}}(\lambda)}{I_{\text{photo}}^{\text{transfer,corr}}(\lambda)} \qquad 5.8$$

The spectral irradiance responsivity of the filter radiometer applied for measurements in the front of non-polarized radiation sources (e.g. blackbody radiation), $s_{E,unpol}^{\text{FR}}(\lambda)$, as explained in section 5.2.5 is the arithmetic mean value of the calibration of the spectral irradiance responsivity in the both direction (0° and 90°) of the polarized radiation source.

$$s_{E,unpol}^{\text{FR}}(\lambda) = \frac{1}{2} \cdot \left[s_{E,0°}^{\text{FR}}(\lambda) + s_{E,90°}^{\text{FR}}(\lambda) \right] \qquad 5.9$$

An overview of the spectral responsivity irradiance of the InGaAs photodiode filter radiometers used in this work is given in figure 5.8.

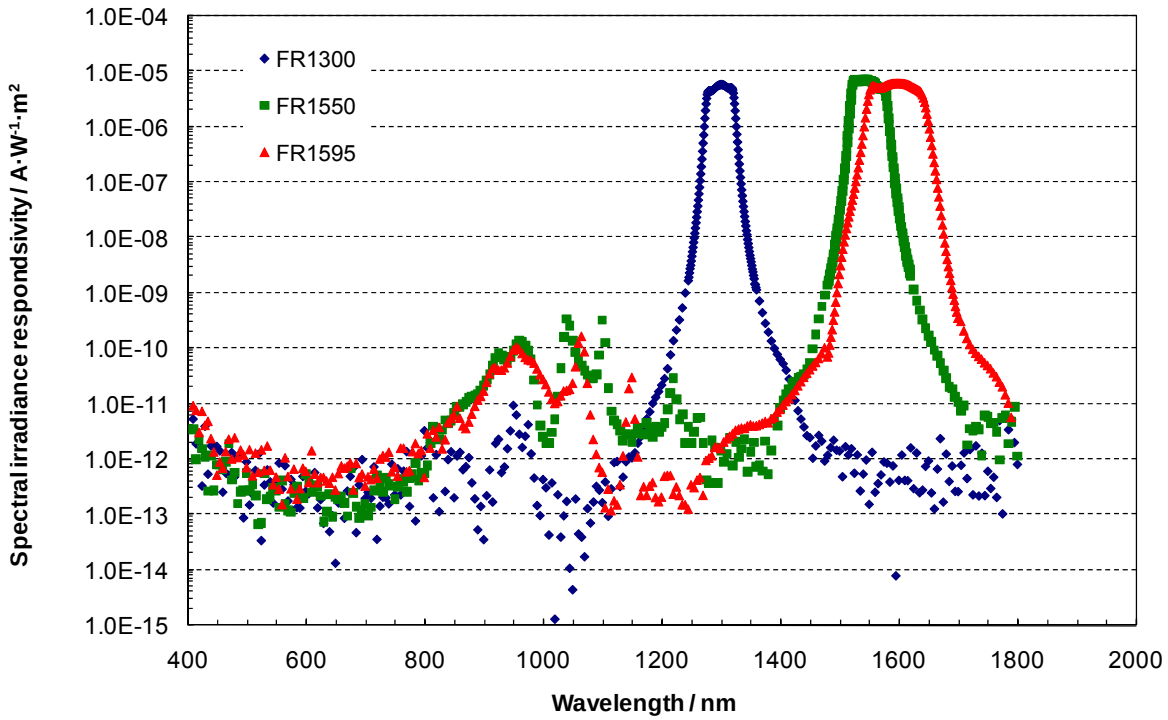

Figure 5.8 :. An overview of the spectral irradiance responsivity of the InGaAs photodiode based filter radiometers used in this work

5.2.5 Polarization effects

Radiation passing through the monochromator of the spectral comparator facility is polarized. The degree of polarization behind the exit slit of the monochromator is a function of wavelength and depends on the applied grating [**67,68**]. On the other hand the spectral responsivity of the photodiode is sensitive to the polarization of the incident radiation.

The polarization state of any radiation source can be written with the Stokes-vector formalism as [**69**]:

$$\vec{S}(\lambda)=\begin{pmatrix} S_0(\lambda) \\ S_1(\lambda) \\ S_2(\lambda) \\ S_3(\lambda) \end{pmatrix} \qquad 5.10$$

The first parameter of the Stokes-vector S_0 is the intensity of the radiation source while the other parameter S_1, S_2 and S_3 are describing the polarization state. As the radiation of the blackbody is unpolarized [**70**], thus by the application of the

filter radiometer at the blackbody, the Stokes-vector of the blackbody radiation is described as :

$$\vec{S}(\lambda)_{\mathrm{BB}} = \begin{pmatrix} E_{\mathrm{BB}}(\lambda) \\ 0 \\ 0 \\ 0 \end{pmatrix} \qquad 5.11$$

The first component in the Stokes-vector, $E_{\mathrm{BB}}(\lambda)$, is the irradiance of the blackbody at the aperture of the filter radiometer. Because the radiation of the blackbody is unpolarized, the other components S_1, S_2 and S_3 are equal zero. The filter radiometer represents a linear polarizer which is characterized by the Müller-matrix, $M_{0°}^{\mathrm{FR}}$ (equation 5.12) [**69**] describing the polarization properties of the interference filter and the photodiode.

$$M_{0°}^{\mathrm{FR}}(\lambda) = \begin{pmatrix} p_x^2(\lambda) + p_y^2(\lambda) & p_x^2(\lambda) - p_y^2(\lambda) & 0 & 0 \\ p_x^2(\lambda) - p_y^2(\lambda) & p_x^2(\lambda) + p_y^2(\lambda) & 0 & 0 \\ 0 & 0 & 2p_x(\lambda)p_y(\lambda) & 0 \\ 0 & 0 & 0 & 2p_x(\lambda)p_y(\lambda) \end{pmatrix} \qquad 5.12$$

Thus the Stokes-vector at the detector $\vec{S}^{\mathrm{FR}}(\lambda)$ can be written as:

$$\vec{S}^{\mathrm{FR}}(\lambda) = M_{0°}^{\mathrm{FR}} \cdot (\lambda) \cdot S_{\mathrm{BB}}(\lambda) = \frac{1}{2} \begin{pmatrix} E_{\mathrm{BB}}(\lambda) \cdot \left(p_x^2(\lambda) + p_y^2(\lambda)\right) \\ E_{\mathrm{BB}}(\lambda) \cdot \left(p_x^2(\lambda) - p_y^2(\lambda)\right) \\ 0 \\ 0 \end{pmatrix} \qquad 5.13$$

The photo current measured by the filter radiometer $I_{\mathrm{photo}}^{\mathrm{FR}}$ of a blackbody with the irradiance $E_{\mathrm{BB}}(\lambda)$ is equal to :

$$I_{\mathrm{photo}}^{\mathrm{FR}}(\lambda) = s_E^{\mathrm{FR}}(\lambda) \cdot E_{BB}(\lambda) \qquad 5.14$$

whereby $s_E^{\mathrm{FR}}(\lambda)$ is the spectral irradiance responsivity of the filter radiometer. The irradiance $E^{\mathrm{FR}}(\lambda)$ for a diode that is polarization insensitive is equal:

$$E^{\mathrm{FR}}(\lambda) = \frac{1}{2}\left(p_x^2(\lambda) + p_y^2(\lambda)\right) \cdot E_{BB}(\lambda) \qquad 5.15$$

The polarization insensitive spectral irradiance responsivity of the photodiode in the filter radiometer is appropriated as $s_{E,\mathrm{Diode}}^{\mathrm{FR}}(\lambda)$. By using equation 5.15 , the photo current of the photo diode can be rewritten as:

$$I_{\mathrm{photo}}^{\mathrm{FR}}(\lambda)=s_{E,\mathrm{Diode}}^{\mathrm{FR}}(\lambda)\cdot E^{\mathrm{FR}}(\lambda)=\frac{1}{2}\cdot s_{E,\mathrm{Diode}}^{\mathrm{FR}}(\lambda)\cdot\left(p_x^2(\lambda)+p_y^2(\lambda)\right)\cdot E_{BB}(\lambda) \qquad 5.16$$

By the comparison of equation 5.14 with equation 5.16 it can be seen that the required spectral irradiance responsivity of the filter radiometer $s_E^{\mathrm{FR}}(\lambda)$, which is polarization sensitive, for the measurement of the non-polarized radiation sources such as blackbody, is combination of two terms :

$$s_E^{\mathrm{FR}}(\lambda)=\frac{1}{2}\cdot s_{E,\mathrm{Diode}}^{\mathrm{FR}}(\lambda)\cdot p_x^2(\lambda)+\frac{1}{2}\cdot s_{E,\mathrm{Diode}}^{\mathrm{FR}}(\lambda)\cdot p_y^2(\lambda) \qquad 5.17$$

At the spectral comparator facility the filter radiometer radiometers were calibrated in two orthogonal positions rotated around the optical axis and denoted as 0°- and 90°-position. During the calibration, the photo currents of the both detectors were measured and were formed in the ratio $Q_I(\lambda)$. When the filter radiometer was is the 0°-potion, the polarization plane was in the x-direction i.e. the term $p_{\mathrm{y}}^2(\lambda)=0$. The ratio of the photo current in this position assign as:

$$Q_I^{0^\circ}(\lambda)=\frac{I_{\mathrm{photo}}^{\mathrm{FR},0^\circ}(\lambda)}{I_{\mathrm{photo}}^{\mathrm{transfer}}(\lambda)}=\frac{p_{x,FR}^2(\lambda)\cdot s_E^{\mathrm{FR,Diode}}(\lambda)}{s_E^{\mathrm{transfer}}(\lambda)} \qquad 5.18$$

After transformation of equation 5.18 results the first term in equation 5.17 of spectral irradiance responsivity :

$$p_{x,\mathrm{FR}}^2(\lambda)\cdot s_E^{\mathrm{FR,Diode}}(\lambda)=Q_I^{0^\circ}(\lambda)\cdot s_E^{\mathrm{transfer}}(\lambda) \qquad 5.19$$

In the next step the filter radiometer was rotated into the 90°-position, in this position a polarization component in y-direction is existing and $p_{\mathrm{x}}^2(\lambda)=0$. Thus the ratio of the photo current can be calculated by:

$$Q_I^{90^\circ}(\lambda)=\frac{I_{\mathrm{photo}}^{\mathrm{FR},90^\circ}(\lambda)}{I_{\mathrm{photo}}^{\mathrm{transfer}}(\lambda)}=\frac{p_{y,FR}^2(\lambda)\cdot s_E^{\mathrm{FR,Diode}}(\lambda)}{s_E^{\mathrm{transfer}}(\lambda)} \qquad 5.20$$

and the second term of the spectral irradiance responsivity in equation 5.17 is given by:

$$p_{y,\mathrm{FR}}^{2}(\lambda)\cdot s_{E}^{\mathrm{FR,Diode}}(\lambda)=Q_{I}^{90°}(\lambda)\cdot s_{E}^{\mathrm{transfer}}(\lambda) \qquad 5.21$$

The spectral irradiance responsivity of the filter radiometer that is sensitive to the polarization of radiation for the application in front of a non-polarization radiation source like blackbody radiation can be found by:

$$s_{E}^{\mathrm{FR}}(\lambda)=\frac{1}{2}\cdot s_{E}^{\mathrm{transfer}}(\lambda)\cdot\left[Q_{I}^{0°}(\lambda)+Q_{I}^{90°}(\lambda)\right] \qquad 5.22$$

To calibrate the spectral irradiance responsivity from equation 5.22 the filter radiometer were calibrated in two orthogonal positions (0° and 90°), while keeping the transfer detector fixed (0° and 90°). The spectral responsivity for unpolarized radiation is the arithmetic mean of the two orthogonal measurements. The calibration results for both new InGaAs-FRs, FR1300 and FR1550 are shown in the table 5.1 respective table 5.2.

Table 5.1: The integral spectral responsivity I_{S}, the center wavelength λ_{CW} and the relative change of the two parameters I_{S} and λ_{CW} with respect to orthogonal rotation of the transfer detector of the filter radiometer FR1300.

	I_{S}	λ_{CW} / pm	$\frac{\Delta I_{\mathrm{S}}}{I_{\mathrm{S}}}$	$\Delta\lambda_{\mathrm{CW}}$ / pm
Mean value: IGA3 0°- FR1300 0°&90°	34.8691	1299.307		
Mean value: IGA3 90°- FR1300 0°&90°	34.8647	1299.296	1.3E-04	0.011
Mean value: IGA3 0°&90°- FR1300 0°&90°	34.8669	1299.301	-	-
			-	-

Table 5.2: The integral spectral responsivity I_S, the center wavelength λ_{CW} and the relative change with table 4.1of the filter radiometer FR1550.

	I_S	λ_{CW} / pm	$\frac{\Delta I_S}{I_S}$	$\Delta\lambda_{CW}$ / pm
Mean value: IGA3 0°-FR1550 0°&90°	45.7072	1547.900		
Mean value: IGA3 90°-FR1550 0°&90°	45.7108	1547.903	7.7E-05	0.003
Mean value: IGA3 0°&90°-FR1550 0°&90°	45.7090	1547.901	-	-
			-	-

Table 5.1 and table 5.2, show that the relative change of the mean value of the spectral responsivity of the filter radiometer (the filter radiometer rotated around the optical axis 0° and 90° but the transfer detector was keep fixed) with two orthogonal measurements (0° and 90°) of the transfer detector (single photodiode: IGA3) is $1.3\text{x}10^{-4}$ resp. $7.7\text{x}10^{-5}$ and the change of the center wavelength is 11 pm resp. 3 pm. The relative difference of the mean value of the spectral responsivity of the filter radiometer in two orthogonal measurements of the transfer detector is also less than $2\text{x}10^{-4}$. These differences are within the repeatability of the calibration ($2\text{x}10^{-4}$ for I_S and 13 pm for λ_{CW}), thus the mean value spectral responsivity of the filter radiometer with one measurement orientation of the transfer detector (0° or 90°) is sufficient for the calibration the spectral responsivity of the filter radiometer.

5.2.6 Stray light

The stray light is referred to as the transmitted radiant flux outside the nominal bandpass of the monochromators. For the calibration of a narrow-band detector e.g. filter radiometer against a broadband detector e.g. single photodiode, the level of stray light has a significant influence on the spectral responsivity which cannot be neglected for high accuracy calibrations.

The transmitted radiant flux of an ideal monochromator with the nominal wavelength λ_c and the same slit width of entrance- and exit slit is a triangle form with the spectral bandwidth of $\Delta\lambda$ (FWHM) and the total bandpass of $2\cdot\Delta\lambda$ (see figure 5.9). However for the non-ideal monochromator the radiant power at wavelength lower than $\lambda_c - \Delta\lambda$ and higher than $\lambda_c + \Delta\lambda$ are not equal to zero.

In the calibration of an arbitrary detector at the spectral comparator, the photocurrent at the nominal wavelength λ_c is the product of three wavelength-dependent factors: the spectral flux of the source $P(\lambda)$, the transfer function of the monochromator $M(\lambda_c,\lambda)$ and the spectral responsivity of the detector $s(\lambda)$ and is given by:

$$I_{photo}(\lambda)=\int_0^{\infty} P(\lambda)M(\lambda_c,\lambda)s(\lambda)d\lambda \qquad 5.23$$

For an ideal monochromator the transfer function is zero outside its bandpass. For a non-ideal monochromator the transfer function decreases to a non-zero value due to the stray light, therefore the photo current can be split into three terms and is given in equation 5.24.

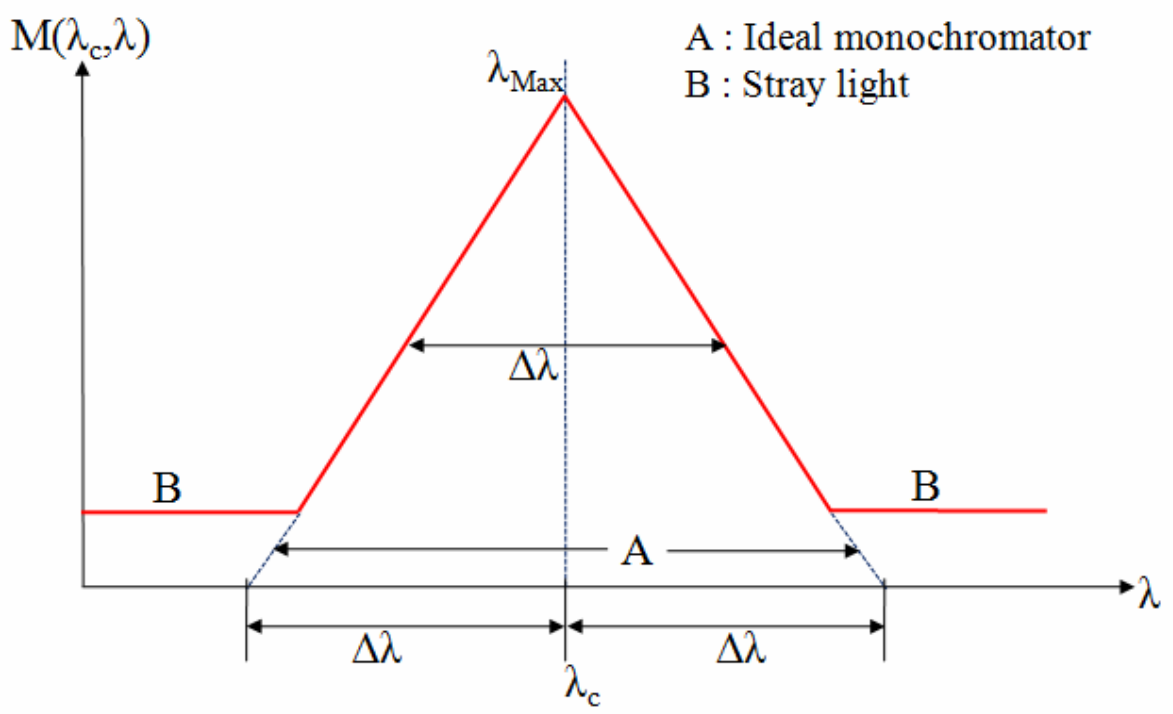

Figure 5.9 : Schematic diagram of the transfer function of the monochromator $M(\lambda_c,\lambda)$ with the same slit width of entrance- and exit slit.

$$I_{photo}(\lambda)=\int_0^{\lambda_0-\Delta\lambda} P(\lambda)M(\lambda_c,\lambda)s(\lambda)d\lambda+\int_{\lambda_0-\Delta\lambda}^{\lambda_0+\Delta\lambda} P(\lambda)M(\lambda_c,\lambda)s(\lambda)d\lambda+\int_{\lambda_0+\Delta\lambda}^{\infty} P(\lambda)M(\lambda_c,\lambda)s(\lambda)d\lambda \qquad 5.24$$

The 2nd term in the equation 5.24 is the part of photocurrent for the assumption of an ideal monochromator. The 1st and 3rd term is the additional contribution to the

photocurrent due to the stray light of the non-ideal monochromator. These two additional contributions to the photocurrent due to the stray light are depending on the characteristic of the spectral responsivity of the detector. For the calibration of filter radiometers two cases can be distinguished:

1. If the nominal wavelength λ_c of the monochromator is set within the bandpass of the filter radiometer, the determined spectral responsivity for the filter radiometer will be too low due to the fact that the broadband transfer detector e.g. the single InGaAs photodiode is sensitive to the stray light contributions of the non-ideal monochromator and the narrowband filter radiometer is mainly insensitive in this wavelength region where the stray light occurs.
2. If the wavelength is set in the out-of-band blocking wavelength region of the filter radiometer, the main contribution to the signal of the filter radiometer will be from the stray light integrated over the bandpass of the filter radiometer. Thus the spectral responsivity of the filter radiometer wavelength region in out-of-band blocking will be too high [**71**].

To resolve the problem due to the stray light contributions, a prism monochromator was integrated in front of the grating monochromator as a predisperser. This combination is equivalent to a limitation of the wavelength interval of the source flux and results in minimized stray light contributions. An experimental proof for this is shown in figure 5.10.

Figure 5.10 is the result of the calibration of the filter radiometer with two methods. First, the filter radiometer was calibrated with the combination of a long pass filter and the grating monochromator. Second, the filter radiometer was calibrated with the combination of the LEISS-prism monochromator as a predisperser and grating monochromator. Figure 5.10 shows that the normalized spectral irradiance responsivity of the filter radiometer in the out-of-band blocking wavelength region is about one order of magnitude lower by using the LEISS-prism monochromator than by using a long pass filter. Therefore for the calibration of the filter radiometer, the prism monochromator has been used to minimize the contributions due to the stray light.

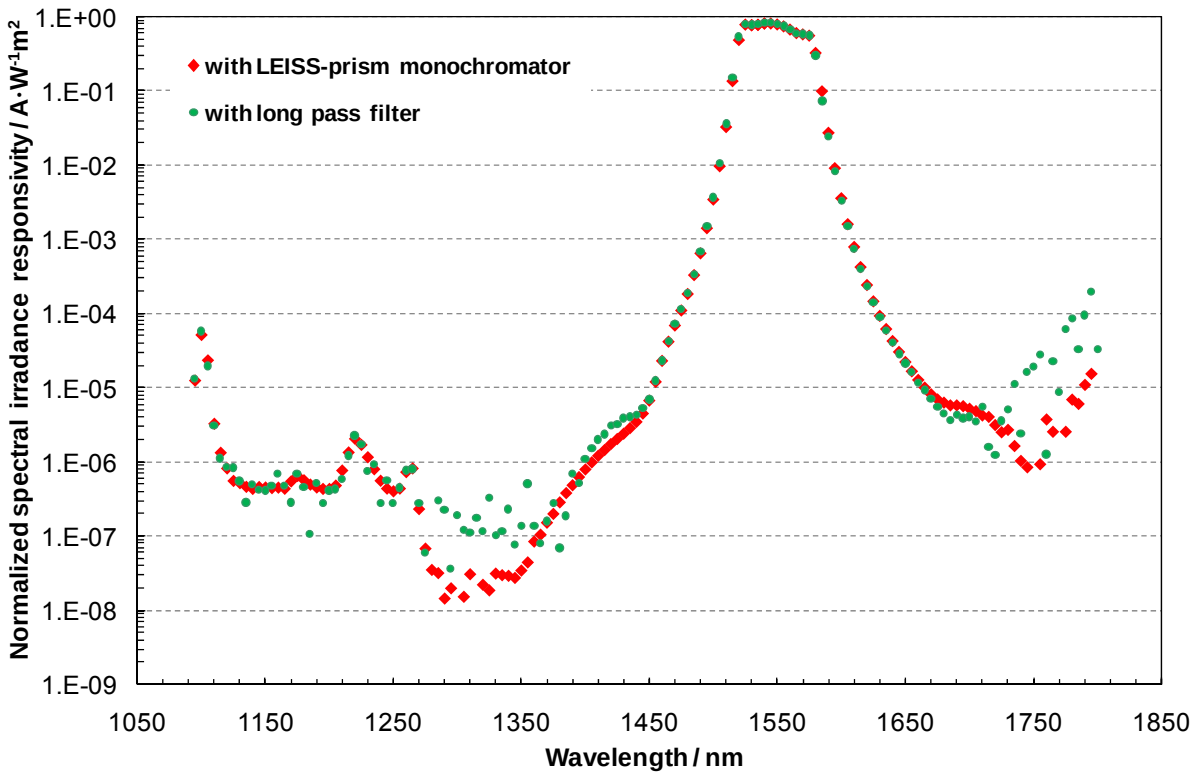

Figure 5.10 : The spectral responsivity of FR1550 with and without prism monochromator as a predisperser

5.2.7 Temperature coefficient

The temperature dependence of the spectral responsivity of the InGaAs photodiode is significantly increasing at the wavelength near the bandgap, e.g. at the wavelength 1595 nm, the relative increasing of the temperature coefficient of the InGaAs photodiode is about 5×10^{-4} K^{-1} [**23**]. Additionally to the detector generated effects, interference filter show a shift of the center wavelength towards longer wavelength with rising of temperature. This effect is due to the enlargement of the optical path length in the interference filter layer due to the temperature expansion [**72,73**]. For the two new InGaAs filter radiometers the band pass of the interference filter was selected at a wavelength which have a sufficient distance to the bandgap wavelength of the InGaAs photodiode to minimize the temperature dependence of the spectral responsivity of the filter radiometer.

The temperature coefficients of the two new InGaAs filter radiometers (the detector and the interference combined in one unit) were determined by measuring the spectral irradiance responsivity ratio between the InGaAs filter radiometers and the transfer detector (single InGaAs photodiode) at the spectral comparator facility.

The temperature of the InGaAs filter radiometers was varied to three different temperatures e.g. 20 °C, 25 °C and 30 °C, while the temperature of the transfer detector was kept at the constant temperature of 25 °C. The relative change of the integrated spectral responsivity with the temperature and the shift of the center wavelength with the temperature are displayed in table 5.3.

Table 5.3: The temperature coefficient of the InGaAs filter radiometers

Center Wavelength (λ_{cw}) / nm	$\frac{\Delta I_S}{I_S} \cdot \frac{1}{\Delta T_{FR}}\,\mathrm{K}^{-1}$ x 10^{-4}	$\frac{\Delta \lambda_{CW}}{\Delta T_{FR}} / \mathrm{pm} \cdot \mathrm{K}^{-1}$
1301	-1.8	+65
1542	-0.4	+80
1595	9.1	+85

The change of the integrated spectral responsivity with temperature is a combined effect of the temperature dependence of the detector and the interference filter. For the first InGaAs filter radiometer designed and constructed at PTB which has a center wavelength of the interference filter at 1595 nm and a bandwidth of 100 nm (FWHM), the temperature coefficient of the detector becomes dominant, resulting in an significant increase of the integrated spectral responsivity with temperature. In contrast to the first InGaAs filter radiometer of PTB, the new InGaAs filter radiometers have the center wavelength of the interference filter at 1300 nm and 1550 nm and a bandwidth of 50 nm (FWHM) which is of sufficient distance from the band gap. By selecting these center wavelengths the temperature coefficient of the detector is very small, the main contribution to the temperature coefficient of the filter radiometer is by the temperature coefficient of the interference filter. Therefore relative change of the integrated spectral responsivity as the function of temperature of the new InGaAs filter radiometers are significantly smaller than from the first InGaAs filter radiometer of PTB. Figure 5.11 and figure 5.12 also show the measured relative change of the integrated spectral irradiance responsivity and the shift of the center wavelength for both new InGaAs filter radiometers, FR1300 and FR1550 respectively. The shift of the center wavelength towards longer wavelength of 65 pm K^{-1} and 80 pm K^{-1} of the FR1300 and FR1550 respectively, can be explained the behaviour of interference filters with increasing temperature [**72**].

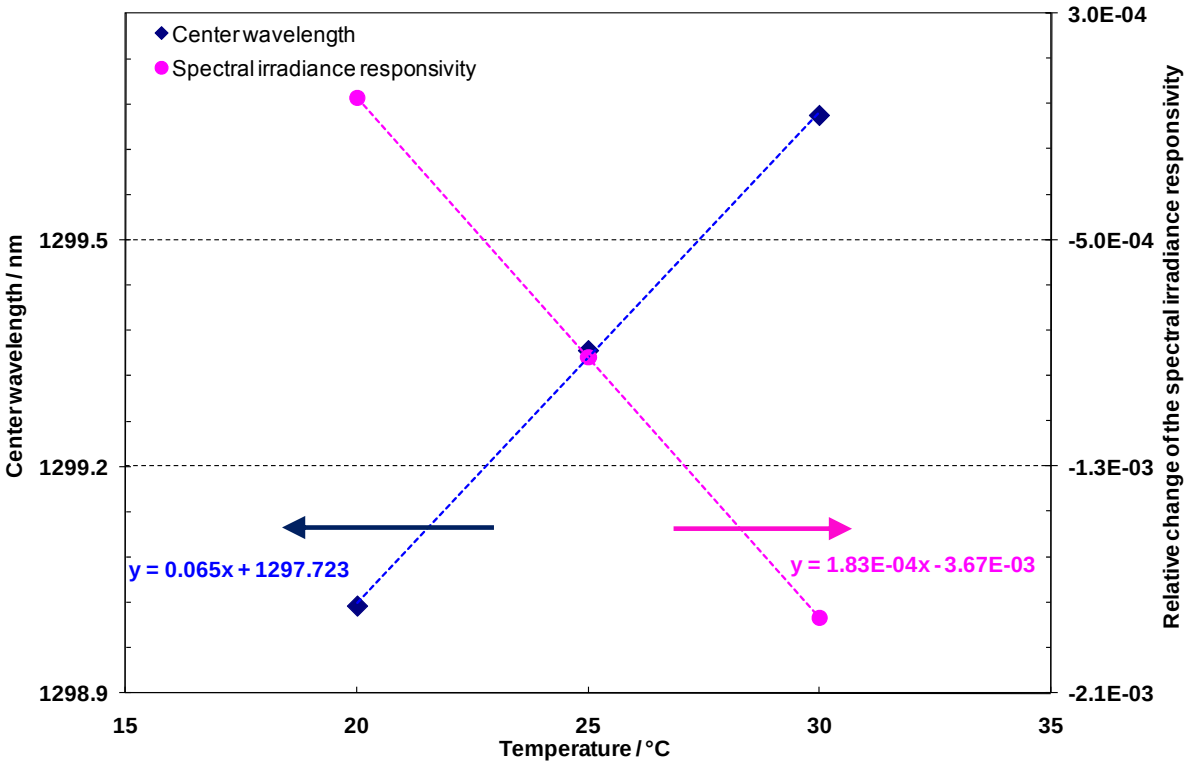

Figure 5.11 : The change of the center wavelength and the integrated spectral irradiance responsivity of the FR1300 as a function of temperature

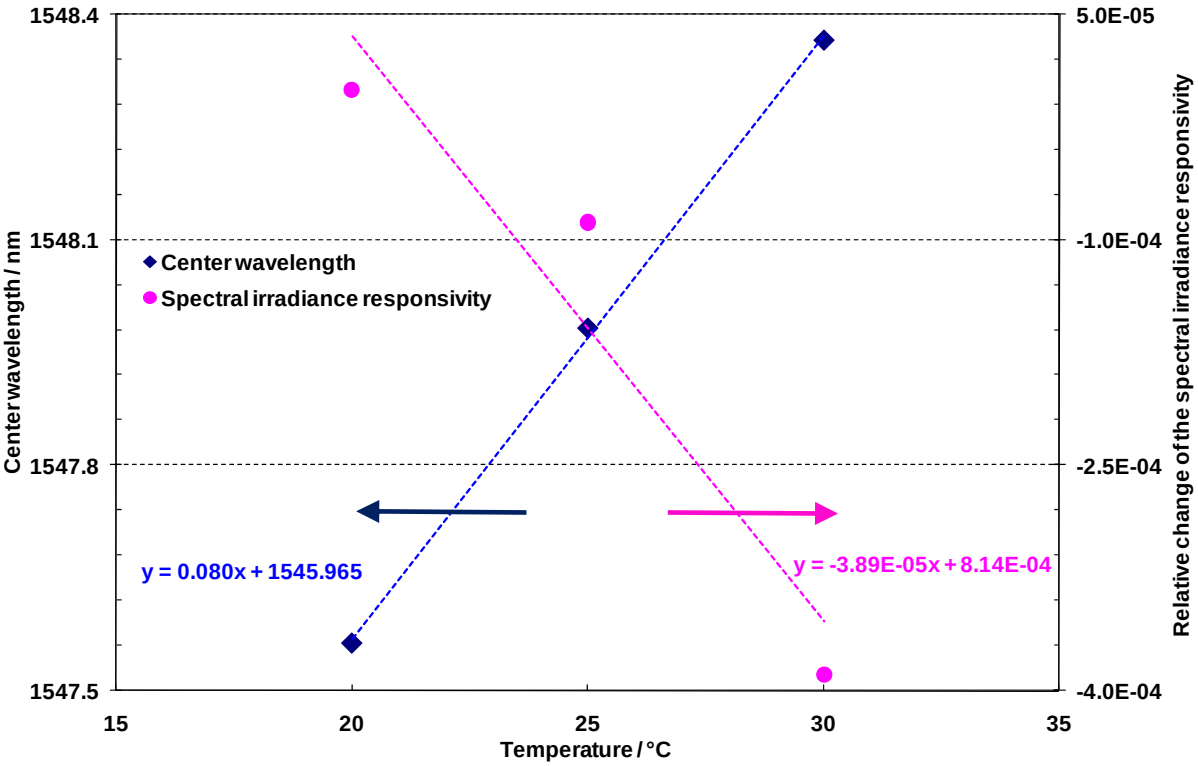

Figure 5.12 : The change of the center wavelength and the integrated spectral irradiance responsivity of the FR1550 as the function of temperature

An approximation can be used to estimate the uncertainty contribution to the photo current due to temperature coefficient for the filter radiometer applied for the irradiance measurement in front of a blackbody. The relative change of the photo current of the filter radiometer due to the temperature coefficient can be calculated by using Taylor-series and the Wien approximation as follows:

$$\frac{\Delta I_{\text{photo}}}{I_{\text{photo}}} = \frac{I_{\text{photo}}\left(T_{\text{FR}} + \Delta T_{\text{FR}}\right) - I_{\text{photo}}\left(T_{\text{FR}}\right)}{I_{\text{photo}}\left(T_{\text{FR}}\right)} = \\ = \left[\left(\frac{c_2}{\lambda_{\text{CW}}^2 T} - \frac{5}{\lambda_{\text{CW}}}\right) \cdot \frac{\Delta\lambda_{\text{CW}}}{\Delta T_{\text{FR}}} + \frac{\Delta I_S}{\Delta T_{\text{FR}}} \cdot \frac{1}{I_S}\right] \cdot \Delta T_{\text{FR}} \qquad 5.25$$

The temperature of the filter radiometers is measured by means of platinum resistance thermometers type Pt100 which are mounted in each filter radiometer and are controlled within ±50 mK during their calibration and application. The resultant relative uncertainty contribution due to the temperature coefficient to the photocurrent are shown in the table 5.4.

Table 5.4: The relative change of the photocurrent with a change of the InGaAs filter radiometers temperature of 50 mK

Center Wavelength (λ_{cw}) / nm	$\frac{\Delta I_{\text{photo}}}{I_{\text{photo}}}$ x 10^{-4}
1301	0.2
1542	0.2
1595	0.3

5.3 Uncertainty of the filter radiometer calibration

The uncertainty budget for the calibration of the two new InGaAs filter radiometers and the first InGaAs filter radiometer of the PTB in terms of the spectral irradiance for the radiometric measurement in front of a blackbody at the temperature of 419 °C are given in the table 5.5. The uncertainty contribution of the spectral responsivity of the transfer detector is already explained in chapter 4. A Monte-Carlo method presented in [**74**] was used for the calculation of the uncertainty component arising from the transfer detectors. This method was applied due to the fact that the

uncertainty of the spectral responsivity over the bandpass wavelength region of the transfer standard is not constant, having its origin in the calibration of the transfer standard against the cryogenic radiometer, which was performed applying both tuneable laser (in two wavelength region: 1260 nm to 1380 nm and 1460 nm to 1580 nm) and monochromator radiation (950 nm to 1650 nm). For FR1300 and FR1550 the uncertainty component from the spectral responsivity of the transfer detector is about three times smaller than for the FR1595 due to the considerably higher uncertainty of the spectral responsivity in the bandpass wavelength range for this filter radiometer. The uncertainty of spectral responsivity of the transfer detector is the largest uncertainty contribution in the calibration of all filter radiometers.

The repeatability of the integrated spectral irradiance responsivity after a complete new alignment of the optical path and the detectors was within $2x10^{-4}$. The new alignment of the detectors amount the uncertainty with respect to a possible tilting of the detector aperture of about 0.15° [**65**] which corresponds to a relative error of the aperture area of the detector of $2x10^{-6}$ and is therefore negligible. It is sufficient to consider only the uncertainty due to the absolute measurement of the transfer detectors aperture area. The area of the apertures of the transfer detector was measured with the procedure outlined in [**75**]. Due to the small sensitive area (3 mm diameter) of the aperture which is used in front of the transfer detector a large uncertainty contribution in the uncertainty budget results. The relative uncertainty of the spectral irradiance responsivity regarding to the measurement of the transfer detector aperture area amounts $2.7x10^{-4}$ [**76**]. The diameter of the transfer detector was measured before and after the period of the measurements in this work in order to determine its long term stability and the result is shown in table 6.2. Since the change of the diameter of this aperture is more than the uncertainty of the aperture diameter measurement, therefore the uncertainty due to the instability of the aperture area about $2x10^{-4}$ is additionally combined into the standard measurement uncertainty of the filter radiometer calibration.

At the spectral comparator facility the apertures of the transfer detectors as well as the aperture of filter radiometer are overfilled and diffraction losses occur, which have to be corrected. The correction of the diffraction is explained in the chapter 6. The relative standard uncertainty due to the correction of the diffraction at the aperture of the transfer detector is about $0.4x10^{-4}$ and the corresponding relative

standard uncertainty regarding the diffraction correction at aperture of the filter radiometer is about $1x10^{-4}$.

The collimated beam behind the exit slit of the grating monochromator is showing a slight divergence of about 0.2˚ due to the finite dimensions of the exit slit of the monochromator. Therefore the spectral irradiance is a function of the distance of the aperture plane from the exit slit. The alignment error of the two aperture planes (transfer detector and filter radiometer) with respect to one common plane is 0.02 mm. This results to an uncertainty contribution in the relative uncertainty of the spectral irradiance responsivity of about $0.2x10^{-4}$. The uncertainty contribution associated with the inhomogeneity of the spectral comparator beam was calculated by convoluting the measured beam inhomogeneity with the measured inhomogeneity of the photodiodes.

The uncertainty resulting from wavelength-dependent effects, e.g. the temperature coefficient of the interference filter, the calibration uncertainty of the monochromator and the reproducibility of the center wavelength after a new alignment, is calculated for the lowest blackbody temperature (419 °C) at which the signal-to-noise ratio of the filter radiometers still can be used. The uncertainty contribution associated with the temperature coefficient of the filter radiometers was calculated by using the measured values of the corresponding temperature coefficients showed in the table 5.4 and from the assumption that the temperature of the filter radiometers during calibration at spectral comparator facility and in the application at the blackbody can be controlled within ± 50 mK.

The uncertainty component due to bandwidth effects of the monochromator was estimated according to [**77**], the resulting relative uncertainty of the spectral irradiance responsivity due to this effect is less than $0.5x10^{-4}$.

The described improved technique for the calibration of filter radiometers in the wavelength range between 400 nm and 1800 nm at the spectral comparator facility minimizes the influence of stray light by complementing the grating monochromator with a prism predisperser. By performing the calibration in two orthogonal positions, filter radiometers can be calibrated for the use with unpolarized sources. The influence of temperature on the interference filters and the photodiodes is considered and reduced by a careful control of the temperature of the detectors during calibration and application of the filter radiometers. With this calibration method, the

two new InGaAs filter radiometers can be calibrated with uncertainties lower than 6.5×10^{-4}, the main contribution resulting from the InGaAs transfer-detector.

Table 5.5 : Contributions to the relative standard uncertainty ($k = 1$) for the measurement of the spectral irradiance in front of a blackbody for the two new InGaAs filter radiometers and the already existent InGaAs filter radiometer of the PTB.

Source of uncertainty	**Filter radiometer $\Delta S_E/S_E$(x10^4)**		
	FR1300	**FR1550**	**FR1595**
Calculated contribution of the uncertainty of the spectral responsivity of the transfer detector	4.1	3.9	13.0
Repeatability	2.0	2.0	2.0
Aperture area of transfer detector	2.7	2.7	2.7
Stability of aperture area of transfer detector	2.0	2.0	2.0
Diffraction correction at transfer detector aperture	1.0	1.0	1.0
Distance from the exit slit monochromator	0.5	0.5	0.5
Temperature coefficient of the filter radiometer	0.2	0.2	0.2
Stability of the tungsten lamp	0.2	0.2	0.2
Monochromator bandwidth effect	0.5	0.5	0.5
Homogeneity of the spectral comparator beam	0.2	0.2	0.2
Uncertainty of the center wavelength (25 pm, 419 °C)	2.1	1.4	1.3
Combined relative standard uncertainty	**6.2**	**5.8**	**13.7**

However for the FR1595 the uncertainty is still more than $1x10^{-3}$ due to the too high uncertainty of the spectral responsivity of the transfer detector in the bandpass wavelength range for this filter radiometer. This uncertainty is still too high for the for the investigation of the deviation of the ITS-90 temperature for the thermodynamic temperature (T-T_{90}). Therefore this filter radiometer is not suitable for the measurement in this work.

Chapter VI

The thermodynamic temperature determination

6.1 Principle

The principle set-up for the radiometric thermodynamic temperature determination by the measurement of the irradiance is shown in the figure 6.1. The source of the irradiance is the blackbody (large aperture area blackbody: LABB), which is a good approximation of an ideal blackbody with the thermodynamic temperature *T*. The spectral radiance of the LABB is given by:

$$L_\lambda(\lambda,T)=\varepsilon(\lambda)\cdot L_{\lambda,\mathrm{BB}}(\lambda,T)=\varepsilon(\lambda)\cdot\frac{2hc^2}{n^2\lambda^5}\cdot\frac{1}{e^{\frac{hc}{n\lambda kT}}-1} \qquad 6.1$$

whereby $\varepsilon(\lambda)$ is the emissivity of the LABB and $L_{\lambda,\mathrm{BB}}(\lambda,T)$ is the spectral radiance of the blackbody radiator according to Planck's law. The area of the radiation source is defined by the precision aperture A_1 with the diameter r_1 . The precision aperture A_2 with the diameter r_2 of the detector (filter radiometer) at the distance d is concentric and parallel to the precision aperture A_1.

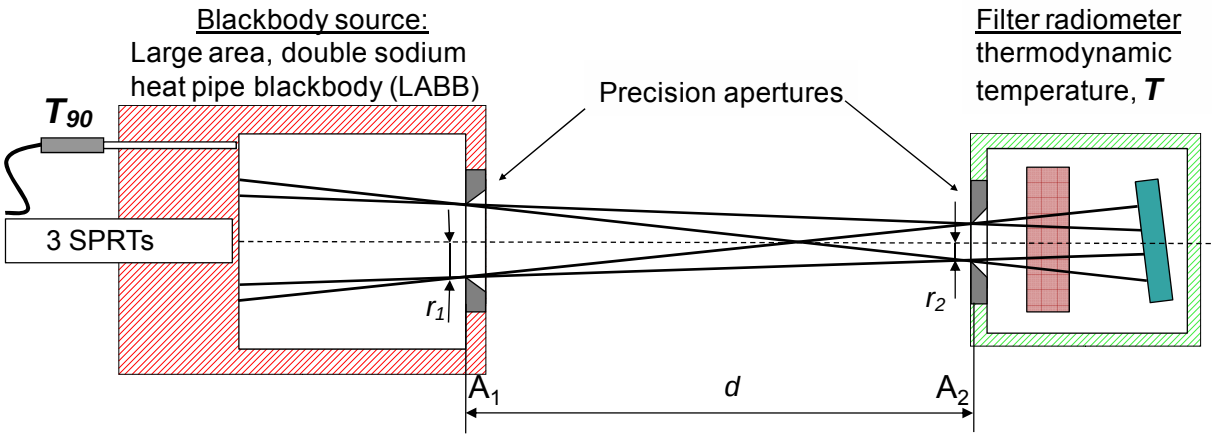

Figure 6.1 : Schematic diagram of experimental arrangement for the simultaneous measurement of the ITS-90 temperature T_{90} (via platinum resistance thermometers) and the thermodynamic temperature T (via filter radiometer) of large area double heat-pipe blackbody (LABB).

The radiant flux from one area element dA_1 of the aperture A_1 to the area element dA_2 of the aperture A_2, $d\Phi_{1\to 2,\lambda}(\lambda,T)$, is given by:

$$d\Phi_{1\to 2,\lambda}(\lambda,T) = L_\lambda(\lambda,T)\cdot\frac{dA_1\cos\theta_1\cdot dA_2\cos\theta_2}{d'^2} \qquad 6.2$$

whereas $L_\lambda(\lambda,T)$ is the spectral radiance of LABB, d' is the distance between two area element and θ_1, θ_2 are respective the angles between the normal vectors of the area elements. The total radiative transfer from the radiation source to the detector can be calculated by:

$$d\Phi_{1\to 2,\lambda}(\lambda,T) = L_\lambda(\lambda,T)\int_{A_1}\int_{A_2}\frac{dA_1\cos\theta_1\cdot dA_2\cos\theta_2}{d'^2} \qquad 6.3$$

For the experimental setup (figure 6.1) used here the analytical solution is calculated by [**78**]

$$d\Phi_{1\to 2,\lambda}(\lambda,T) = L_\lambda(\lambda,T)\frac{2\cdot\pi r_1^2\cdot\pi r_2^2}{r_1^2+r_2^2+d^2+\sqrt{\left(r_1^2+r_2^2+d^2\right)^2-4r_1^2r_2^2}} \qquad 6.4$$

The spectral irradiance at the aperture of the detector is equal to:

$$\begin{aligned} E_\lambda(\lambda,T) &= \frac{d\Phi_{1\to 2,\lambda}(\lambda,T)}{\pi r_2^2} = \\ &= \varepsilon\cdot L_{\lambda,\mathrm{BB}}(\lambda,T)\underbrace{\frac{2\cdot\pi r_1^2\cdot\pi r_2^2}{r_1^2+r_2^2+d^2+\sqrt{\left(r_1^2+r_2^2+d^2\right)^2-4r_1^2r_2^2}}}_{\text{geometry factor G}} \end{aligned} \qquad 6.5$$

The photocurrent of the filter radiometer in the experimental setup as shown in figure 6.1 in term of its spectral irradiance responsivity can be written as:

$$I_{\text{photo, FR}} = \int_{\lambda_{\min}}^{\lambda_{\max}} s_E^{\mathrm{FR}}(\lambda)\cdot E_\lambda(\lambda,T)d\lambda = \varepsilon\cdot G\cdot\int_{\lambda_{\min}}^{\lambda_{\max}} s_E^{\mathrm{FR}}(\lambda)\cdot L_{\lambda,\mathrm{BB}}(\lambda,T)d\lambda \qquad 6.6$$

whereby G is the geometry factor defined in equation 6.5 and $L_{\lambda,\mathrm{BB}}(\lambda,T)$ is the spectral radiance of an ideal blackbody according to Planck's law. According to the equation 6.6, the measurement of the photocurrent $I_{\text{photo,FR}}$ therefore allows to

determine the thermodynamic temperature of the blackbody radiator, if the following parameters are known: the spectral irradiance responsivity of the detector s_E^{FR}, the geometry factor G, i.e. the aperture radii r_1, r_2 and the distance d between the apertures, and the emissivity ε of the blackbody radiator.

6.2 The radiation source

A high-accuracy source of thermal radiation and a calibrated filter radiometer are required for the accurate determination of the thermodynamic temperature in this work. A blackbody radiator is an ideal source of thermal radiation, therefore a blackbody radiator has been chosen as a source for the determination of its thermodynamic temperature by radiometric measurement. However, ideal blackbodies can be approximated only by cavity radiators. There are two technical problems that have to be solved to bring the emissivity of a cavity radiator as close as possible to unity:

- First, a large ratio of the inner surface area to the radiating area must be achieved. This ratio can, in principle, be optimized by increasing the cavity length.
- Second, the problem of the non-temperature homogeneity along the cavity walls due to the increasing geometrical dimensions (cavity length). To ensure sufficient temperature homogeneity along the cavity walls, the cavity radiator has been designed as heat-pipes [**79**].

A heat-pipe has a very high thermal conductance and the thermal conductivity is several hundred times better than that of copper [**49**]. The heat-pipe is constructed as a double-walled hollow tube enclosing an inner cylinder open to one side for cavity radiators. A small amount of a substance serves as the working fluid inside the double-walled tube. Inside the hollow tube there is equilibrium between the liquid and the gaseous phase of the working fluid. At the hotter spots, liquid is evaporated while at the colder spots the gas condenses. The condensate returns to the evaporator by using capillary forces from a wick structure enclosed in the heat-pipe. Because of the high latent evaporation respectively condensation heat, this structure has a high thermal conductance leading to a very good temperature homogeneity. However, every heat-pipe material can be operated only in a limited temperature range [**80**]. For this work (in the temperature range from 419 °C to 660 °C), sodium is the suitable heat-pipe material. The design of the LABB developed at PTB for

thermodynamic temperature determinations [**81**] in this work is shown in figure 6.2. The main feature of the LABB is the radiating inner cavity which is formed by a sodium heat-pipe and is itself enclosed in a second sodium heat-pipe, ensuring an excellent temperature homogeneity. A 1.2 m long standard platinum resistance thermometer (SPRT) was used to determine the temperature distribution close to the cylindrical part of the cavity wall for different cavity temperatures by inserting the SPRT into the cavity and measuring the temperature at different immersion depths. The calculation of the real wall temperature distribution from these measurements by this method is described in [**82**]. Knowing the temperature distribution along the cavity wall and applying a Monte-Carlo simulation program for the calculation of the cavity emissivity described in section 6.2.1, one can calculate the influence of the inhomogeneous temperature distribution on the effective emissivity of the LABB [**82**].

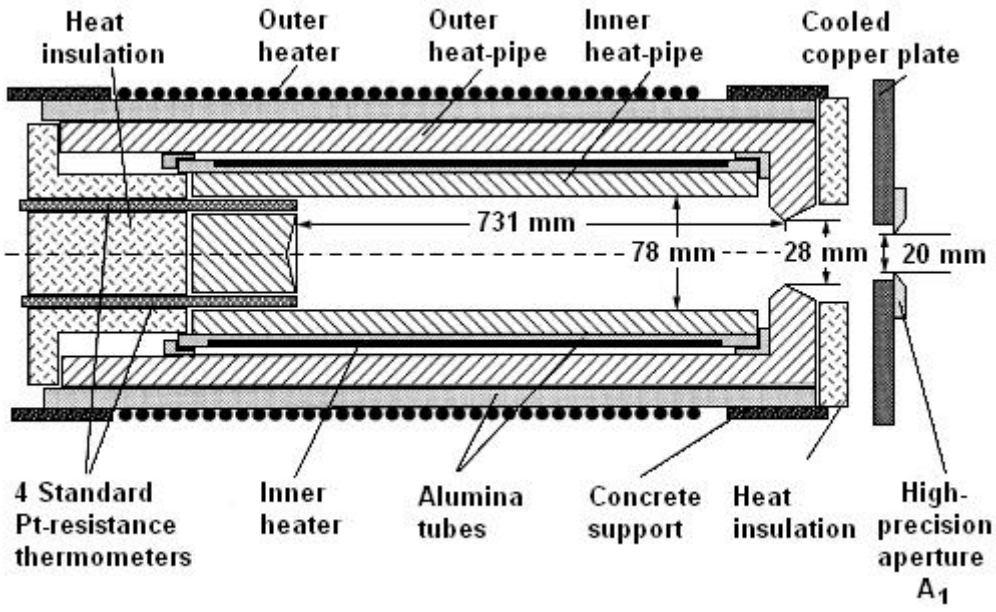

Figure 6.2 : Schematic drawing (not to scale) of the double heat-pipe large area blackbody (LABB) used as the radiation source for the determination of the thermodynamic temperature in this work [**28**].

6.2.1 The emissivity of the radiation source:

In practice the condition of a radiation cavity opening negligible in comparison to the inner surface area at the cavity cannot be adequately fulfilled. Therefore it is necessary to determine experimentally or theoretically the actual emissivity of the cavity. However it is difficult to measure high emissivity of cavity radiators with sufficient accuracy [**49**], thus mathematical models are generally used to calculate the emissivity. The most accurate methods for the calculation is a Monte-Carlo

simulation combined with a ray-tracing technique [**47,83**]. This methods were further developed by the PTB and used to calculate the absorptivity, and consequently the emissivity, of the cavity.

This method uses an inverse ray tracing technique and considers photons which enter the cavity through the aperture instead of photons emitted by the blackbody. A photon is virtually inserted into the cavity at a certain angle and its trace through the cavity is followed by geometrical calculations. The path of this photon is traced inside the cavity as long as it is either absorbed or leaves the cavity [**82**]. A diffuse reflection of this photon on the walls is being assumed. The reflection probability is given by $1-\varepsilon_{\mathrm{w}}(\lambda)$, with $\varepsilon_{\mathrm{w}}(\lambda)$ being the local emissivity of the cavity wall. The isothermal emissivity $\varepsilon_{\mathrm{iso}}$ is the ratio of the absorbed photon to the photons inserted into the cavity. This emissivity, $\varepsilon_{\mathrm{iso}}$, depends only on the geometry of the cavity and the local emissivity $\varepsilon_{\mathrm{w}}(\lambda)$ of the cavity wall.

The non-isothermal temperature distribution along the cavity wall results into a non-isothermal emissivity, $\varepsilon_{noniso}(\lambda)$. For the calculation of this emissivity $\varepsilon_{noniso}(\lambda)$, every absorbed photon is weighted by the spectral radiance according to Planck's law of radiation with the actual temperature T of the location where the photon is absorbed. The spectral radiance $L_{\lambda}(\lambda,T)$ assigned to a single absorbed photon is connected to the spectral radiance $L_{s,\lambda}(\lambda,T)$ of a blackbody at the same temperature by

$$L_{\lambda}(\lambda,T)=\varepsilon_{\mathrm{w}}(\lambda)L_{\lambda,\mathrm{BB}}(\lambda,T) \qquad 6.7$$

The non-isothermal behaviour of the cavity is described by introducing a temperature difference ΔT from the reference temperature T, usually the temperature of the bottom of the cavity. The change in spectral radiance in equation 6.7 can be written in a linear approximation as:

$$\begin{aligned} L_{\lambda}(\lambda,T-\Delta T)&=\varepsilon_{\mathrm{w}}(\lambda)L_{\lambda,\mathrm{BB}}(\lambda,T-\Delta T)= \\ &=\varepsilon_{\mathrm{w}}(\lambda)\left[L_{\lambda,\mathrm{BB}}(\lambda,T)-\frac{\partial L_{\lambda,\mathrm{BB}}(\lambda,T)}{\partial T}\Delta T\right] \end{aligned} \qquad 6.8$$

Using Wien's approximation for Planck's law, equation 6.8 becomes approximately

$$L_\lambda(\lambda, T-\Delta T) = \varepsilon_{\mathrm{w}}(\lambda)\left[1-\frac{c_2}{\lambda T^2}\Delta T\right]L_{\lambda,\mathrm{BB}}(\lambda, T) \qquad 6.9$$

Equation 6.9 can be rewritten as:

$$L_\lambda(\lambda, T-\Delta T) = \varepsilon_{\mathrm{w}}(\lambda)\varepsilon_{\Delta T,\mathrm{w}}(\lambda, \Delta T)L_{\lambda,\mathrm{BB}}(\lambda, T) \qquad 6.10$$

with $\varepsilon_{\Delta T,\mathrm{w}}(\lambda, \Delta T)$ specifying the change in local emissivity due to a temperature difference ΔT.

Equation 6.10 describes the spectral radiance contribution of one photon. In order to calculate the spectral radiance for the whole cavity, the contributions of all photons have to be summed up and the sum has to be divided by the number of contributing photons N. This procedure can be applied for both isothermal and non-isothermal cavities. For the isothermal blackbody, the sum of the spectral radiance is given as:

$$L_{\lambda,\mathrm{BB},iso} = \frac{1}{\mathrm{N}}\sum_n F(\Omega_n)\varepsilon_{\mathrm{w}}(\lambda)L_{\lambda,\mathrm{BB}}(\lambda, T) \qquad 6.11$$

The parameter $F(\Omega_n)$denotes the view factor for the trace of photon n and is implicitly taken into account by the Monte-Carlo simulation. In the case of non-isothermal blackbody, application of equation 6.10 yields

$$L_{\lambda,\mathrm{BB},noniso} = \frac{1}{\mathrm{N}}\sum_n F(\Omega_n)\varepsilon_{\mathrm{w}}(\lambda)\varepsilon_{\Delta T,\mathrm{w}}(\lambda, \Delta T_n)L_{\lambda,\mathrm{BB}}(\lambda, T) \qquad 6.12$$

The emissivity $\varepsilon_{\Delta T}$ describes the transition from a isothermal blackbody to a non-isothermal blackbody which is defined by

$$\varepsilon_{\Delta T} = \frac{L_{\lambda,BB,noniso}}{L_{\lambda,BB,iso}} \qquad 6.13$$

The spectral radiance of the isothermal blackbody can be written as

$$L_{\lambda,BB,iso} = \varepsilon_{iso}L_{\lambda,BB}(\lambda, T) \qquad 6.14$$

For the non-isothermal blackbody the emissivity ε_{noniso} can be written as:

$$\varepsilon_{noniso} = \varepsilon_{iso} \cdot \varepsilon_{\Delta T} = \frac{L_{\lambda,BB,noniso}}{L_{\lambda,BB}(\lambda,T)} = \frac{1}{N}\sum_{n} F(\Omega_n)\varepsilon_w(\lambda)\varepsilon_{\Delta T,w}(\lambda,\Delta T_n) = \frac{1}{N}\sum_{n} F(\Omega_n)\varepsilon_w(\lambda)\left(1-\frac{c_2}{\lambda T^2}\Delta T_n\right) \quad 6.15$$

The application of the above mentioned Monte-Carlo simulation requires knowledge of the temperature distribution along the cavity walls, which has to be measured separately. With the measured temperature distribution along the cavity wall of the LABB from [**82**] and the presented Monte-Carlo simulation, the emissivity of the LABB can be calculated. The obtained values for the emissivity of the LABB are given in table 6.1

Table 6.1: Calculated emissivity for the blackbody LABB at a wavelength λ= 1.6 µm for various blackbody temperatures

LABB temperature / °C	415	450	480	510
Emissivity	0.999588	0.999865	0.999888	0.999664

6.2.2 Description of the radiation source:

The LABB consists of two concentric sodium heat-pipes. The radiating cavity is formed by the inner heat-pipe (figure 6.2). Both heat-pipes can be operated up to 1000 °C and are held in place by alumina tubes supported by concrete rings at each end. In order to fill the field-of-view of a filter radiometer without the use of lens, the blackbody has a very wide aperture of 28 mm diameter. For technical reasons it is formed by the outer heat-pipe. To archive a high emissivity, the cavity dimensions have to be very large: the length is 731 mm and the diameter 78 mm, resulting in an emissivity as shown in table 6.1. The front surface of the outer heat-pipe is covered with heat-insulating fiber. A high-precision aperture, A_1 with an accurately known diameter of 20 mm is mounted on a temperature-controlled copper plate in front of the opening of the blackbody in order to define the effective source area. A resistance heater around the outer heat-pipe is connected to a 10 kW DC power supply and heats the blackbody to a temperature a few degrees below the measurement temperature. The power supply includes a commercially available controller which achieves a temperature stability of ± 0.1 °C. A second heater around the inner heat-pipe is used for fine control of the cavity temperature to within ±2 mK.

It is operated with a 100 W power supply and it can produce an additional temperature rise of the inner heat-pipe by about 10 °C. The bottom of the inner heat-pipe has four bores for standard platinum resistance thermometers which are connected to a type F18 standard automatic thermometry bridge. One of the standard platinum resistance thermometers is used as sensor of the fine-control loop. A computer program converts its resistance to the corresponding temperature. The first order delay time of the inner heat-pipe is about 100 min, and its dead time is 2 min [**84**]. This behavior is taken into account by a PID algorithm and a predictor algorithm which calculates the input signal for the 100 W power supply. The time needed for stabilization after starting the control program is about 1 hour. Each of the standard platinum resistance thermometers is shielded with a thin platinum-tube and a tube of very pure alumina. A voltage of 3.6 V is applied between the inner heat-pipe and the Pt-tubes to prevent positive ions originating from the cavity wall material from poisoning the thermometers. The standard platinum resistance thermometer using for temperature control is always left inside the heat-pipe, whereas the other three calibrated standard platinum resistance thermometers applied for the ITS-90 temperature measurement are inserted before and removed after each measurement.

6.2.3 Temperature stability of the radiation source:

To achieve a relative statistic uncertainty of photo current measured by the filter radiometer during the radiometric temperature determination at the LABB of the order $1x10^{-4}$, the typical measurement periods are about 14 hours at a temperature 419 °C. For this reason it is very important that the temperature t_{90} of the LABB is stable for the measurement period. This was achieved for each temperature of LABB by determination of optimized parameters of the control process in the PID controller (dead time and transition value) with the step-response method described in [**85**] for the inner heat-pipe. Figure 6.3 shows the stability of the LABB for a measurement period more than 17 hours at the temperature 419 °C which is the lowest temperature and 660 °C which is the highest temperature of the LABB investigated in this work.

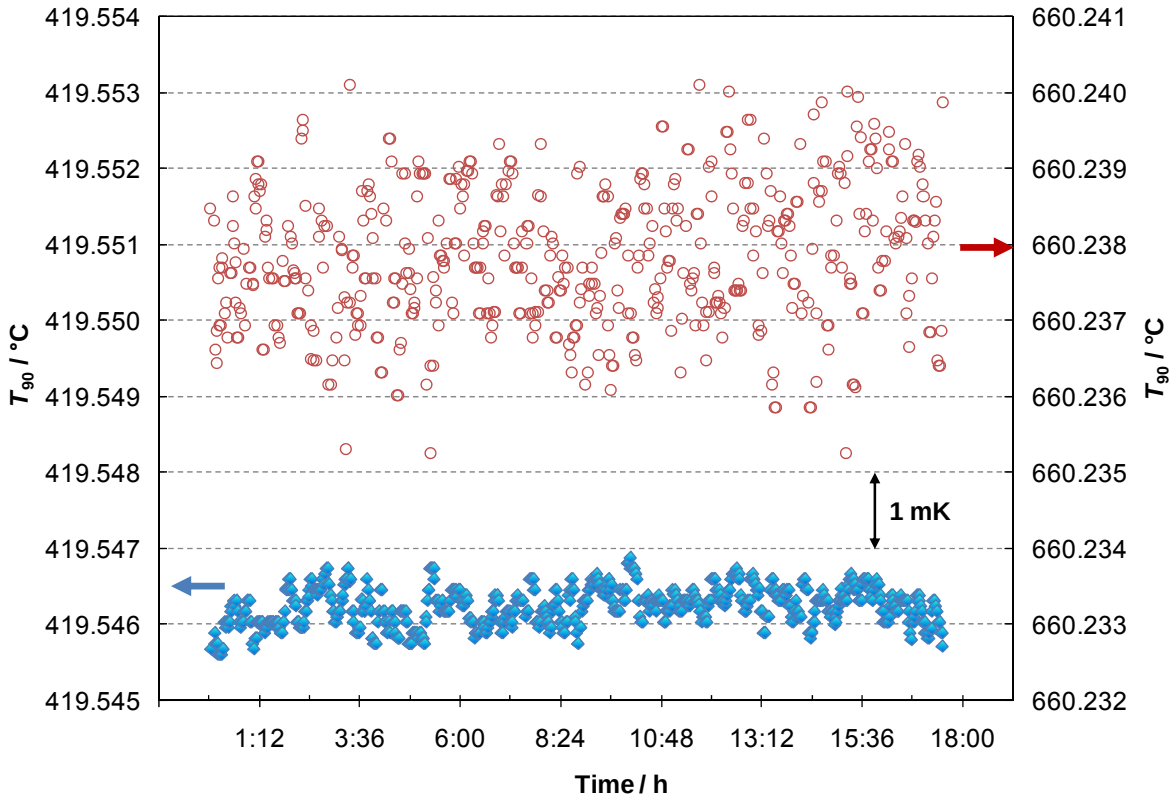

Figure 6.3 : Temperature stability of the LABB at 419 °C (left hand side) and 660 °C (right hand side) measured with a standard platinum resistance thermometer over a period of more than 17 hours

The temperature stability at the LABB at the temperature of 419 °C is ±0.5 mK for a measurement period longer than 17 hour. At the temperature of 660 °C the duration of a measurement period with filter radiometers at the LABB is shorter than 6 hours to achieve a relative statistic uncertainty of the measured photo current during the radiometric temperature determination at the LABB smaller than $1x10^{-4}$. However the temperature stability of the LABB at this temperature is about ±2 mK for the measurement period longer than 17 hour. The uncertainty contribution of the temperature stability is equivalent to a relative uncertainty of the spectral radiance at a wavelength of 1300 nm of $\pm 1.2x10^{-5}$ at the temperature of 419 °C and $\pm 2.5x10^{-5}$ at the temperature of 660 °C.

6.3 Experimental setup

The two basic elements of the experimental setup for the thermodynamic temperature determination are the LABB as a high-accuracy source of spectral irradiance and the filter radiometer as the detector. The accepted solid angle of the filter radiometer is defined by the diameter of the apertures A_1 and A_2 at a distance d between both apertures (figure 6.1). A detailed description of the LABB is already given in section 6.2, the filter radiometers and their calibration can be found in chapter 5. The experimental setup is shown in the figures 6.1 and 6.4.

The filter radiometer with the aperture A_2 (radiometer aperture) and the radiator aperture A_1 are aligned on a 2 m long optical bench made of granite. The optical axis z of this experiment is defined by the center of the radiator aperture A_1 and center of the filter radiometer aperture A_2 . The radiator aperture A_1 is fixed in the direction of z-axis on the optical bench and serves as the reference point for the measurement of the distance between both apertures. The radiometer aperture A_2, the radiator aperture A_1 and the LABB can be adjusted by the justified elements in the x-, y- and z-direction.

The filter radiometer are mounted on an insulated plate on an adjusting element unit (see figure 6.4). This unit is fixed on a slider on the granite bench, which is used for rough adjustment of the distance between both apertures by means of a scale on the granite bench. The fine adjustment of the aperture distance is done interferometricaly by DC electric servo-motors and a translation stage. After the adjustment of the filter radiometer and the aperture distance, both apertures are masked with black caps in order to prevent the inter-reflection between the apertures.

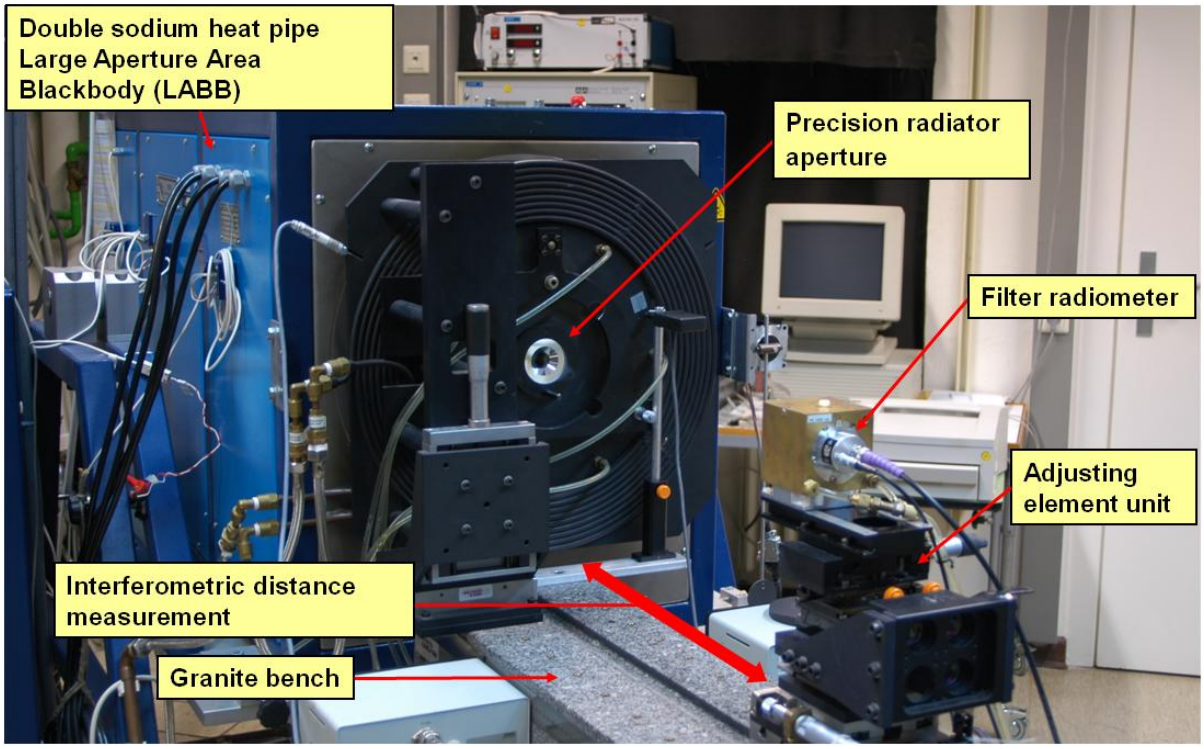

Figure 6.4 : A photography of experimental setup for the determination of a possible deviation between the thermodynamic temperature and the ITS-90 temperature (T-T_{90}). The LABB radiates through the cooled precision radiator aperture onto the precision aperture of the filter radiometer. The distance between both apertures is set by a laser interferometer.

The temperature of the filter radiometer is measured by a Pt100-type the platinum resistance thermometer, the temperature of the filter radiometer is controlled by means of a thermostat at 25.0±0.5 °C, which is the same temperature during the calibration of the filter radiometer at the spectral comparator facility.

The photo current of the filter radiometer was measured at the BNC connector of the filter radiometer with a low-noise coaxial cable by a current-to-voltage converter with calibrated feedback resistors and a calibrated digital voltmeter. Additionally during the spectral irradiance measurement at the LABB, the ambient temperature, the atmospheric pressure and the relative humidity are recorded for the evaluation of the measurement results (ex. the calculation of the refractive index of air and the correction due to the water vapour absorption).

Analyzing the dependence of the parameters r_1 , r_2 and d from the geometrical factor G in the equation 6.5, it can be shown that for the apertures and the distances between both apertures used in this experiment (r_1 = 10 mm, r_2 = 1.5 mm and, typical, d = 750 mm) the geometrical factor G is only dependent

on the diameter r_1 of the radiator aperture A_1 and the distance d between both apertures. Therefore the diameter of the radiator aperture and the distance between both apertures have to be precisely measured.

6.3.1 The precision apertures:

For this work, the radiator aperture used for the measurement of the spectral irradiance at the LABB and the aperture of the transfer detector applied during the calibration of the filter radiometer at the spectral comparator facility, have to be precisely characterized with respect to their surface areas. The radiator aperture and the filter radiometer apertures used in this work are diamond turned aluminium apertures with a knife edge. The aperture of the transfer detector is a diamond turned copper aperture with a knife edge. The land of these aperture are very thin (ca. 15 µm). The nominal value of the diameter of the radiator aperture is 20 mm, the filter radiometer apertures and transfer detector aperture have a nominal diameter of 3 mm. The diameter of these apertures are measured with the non-contact laser stylus method described in [**75**]. The absolute standard uncertainty of this method for apertures with diameters up to 20 mm is 0.4 µm. The diameter of the radiator aperture (aperture Nr. 5) has been re-measured after the spectral irradiance measurements in this work in order to determine the long term stability of the diameter. The results given in table 6.2 show that the change of the diameter of the aperture is within the measurement uncertainty. The thermal expansion effect on the diameter of the radiator aperture during the spectral irradiance measurements is minimized by the mounting this aperture on a temperature controlled copper plate with a temperature controlled to 25.0±0.5 °C (see figure 6.2).

Table 6.2: The diameter of the radiator aperture (Nr. 5) and its change between 2001 to 2009 and the diameter of the aperture of the transfer detector (Nr. Cu1)

	Radiator Aperture (Nr. 5)	**Transfer detector aperture (Nr. Cu1)**
Diameter (2001) / mm	20.0191	
Diameter (2005) / mm		3.0244
Diameter (2009) / mm	20.0192	3.0253
Change of the diameter / µm	0.1	0.9

6.3.2 The alignment:

All of the components of the experimental setup was carefully aligned before the performance of the irradiance measurements at the LABB. Before the beginning of the alignment procedure a diode laser was used as the alignment instrument and was aligned parallel to the optical bench by means of a pinhole. In a first step, the non-operated LABB has been aligned in such way that the laser beam passes through the center of the cavity aperture to the center of the cavity bottom. After that, the radiator aperture was aligned perpendicular to the optical axis using the returned reflex of the laser beam and a pinhole. The maximum deviation of the radiator aperture from the perpendicular plane is about ±3° [**65**]. This deviation results in a relative error of the radiator aperture area of maximum 2×10^{-5}. In a next step the filter radiometer is aligned perpendicular to the laser beam with the same principle as that of the radiation aperture. The uncertainty of this alignment is ±4° which corresponds to a relative error of the filter radiometer aperture area of 2.5×10^{-5} [**65**]. Finally, both apertures are positioned concentric to the laser beam with an uncertainty of about ±1 mm. This uncertainty is equivalent to a relative error of the distance between both apertures during the spectral irradiance measurements of less than 2×10^{-6}, which is negligible.

6.3.3 The aperture distance:

In the first step of the adjustment of the distance between aperture A_1 and A_2, the distance is roughly set by manually sliding the unit consisting of the adjusting elements and the filter radiometer to the desired position within ±1 mm. After this the fine positioning is interferometricaly arranged within ±1 µm. The interferometric distance measurement has to be corrected with actual the wavelength in air of the He-Ne-Laser used by the interferometers. The refractive index n in the distance evaluation unit of the interferometers is updated for every aperture distance setting. This correction is calculated according to Edlen's formulae [**86**] with the current values of the ambient temperature, the atmospheric pressure and the relative humidity. The filter radiometer is translated by a DC electric servo-motor in the optical axis direction during the fine positioning process. During the control loop of the fine positioning, the actual position of the filter radiometer measured by the interferometer is compared to the set position and then used to regulate the DC electric servo-motor

in the moving direction. However the interferometer can only measure the relative distances. Thus for the absolute measurement of the distance between the apertures A_1 and A_2, both apertures have to be located in the same reference plane (zero-point). Thereto the aperture of the filter radiometer with an outer diameter of 18 mm is moved carefully into the radiator aperture which has an inner diameter of 20 mm until an incremental length gauge (resolution: 0.5 µm) shows that both apertures are located in the same plane. However this process can only be done as long as the LABB is not operating. Therefore a second reference point is additionally defined as the zero-point for the determination of the aperture distance during the spectral irradiance measurement at the LABB. This second reference point is defined by a 40 mm long pin, parallel to the optical axis, which is fixed on the temperature controlled copper plate in front of the LABB, and is used for the determination of the aperture distance during the spectral irradiance measurement. With the aid of the incremental length gauge it can be detected when the filter radiometer just touches the parallel pin. After the determination of the distance between zero-point and the second reference point, the absolute aperture distances can be calculated. The relative uncertainty component arising from the aperture distance determination is calculated assuming an absolute uncertainty of 50 µm for a distance of 1 m.

6.4 Radiometric measurement of thermodynamic temperature

For this work the thermodynamic temperature *T* in the temperature range from 419 °C to 660 °C at the LABB was determined applying the absolutely calibrated, new InGaAs filter radiometers. Furthermore the thermodynamic temperature was also measured by using two absolutely calibrated silicon photodiode-based filter radiometers (Si-FRs) in order to underpin the results of the thermodynamic temperature determination with the new improved, InGaAs filter radiometers. The measurement setup is shown in the figure 6.1 and figure 6.4.

6.4.1 Measurement process:

The determination of the thermodynamic temperature *T* of the LABB via the spectral irradiance measurement was performed for several temperatures in the interval between 419 °C to 660 °C, namely, at 419 °C (Zn-FP), 457 °C (gas thermometry reference value), 500 °C, 550 °C, 600 °C and 660 °C (Al-FP). Two absolutely calibrated, new InGaAs filter radiometers with the center wavelengths of

1300 nm (FR1300) and 1550 nm (FR1550) and two Si-FRs with the center wavelength of 800 nm (FR800) and 900 nm (FR900) are applied as detectors for the thermodynamic temperature determination. However due to the low signal-to-noise ratio of the Si-FRs if applied for the measurement of temperatures below 500 °C, the Si-FRs are applied for the temperature determination only in the temperature range between 550 °C and 660 °C.

In order to prove the accuracy of the diffraction correction and to identify additional systematic effects (e.g. the angular dependence of the interference filter transmission), the aperture distance d between the radiator aperture in front of the LABB and the filter radiometer aperture was varied from 750 mm up to 1750 mm with a 250 mm steps interval for the measurement with InGaAs filter radiometers and from 500 mm to 1750 mm for the measurement with Si-FRs.

To verify the reproducibility of the thermodynamic temperature determination, the measurements were performed in 2 periods. In the first period from 2006 to 2007 the measurement at 660 °C was repeated twice with the InGaAs filter radiometers including a complete shutdown of the furnace in between. The second measurement period was partly repeated after 8 months.

6.4.2 The corrections:

6.4.2.1 Atmospheric absorption:

For the absolute radiometric measurement at the LABB with InGaAs filter radiometers which have center wavelengths in the near infrared wavelength range the consideration of the atmospheric absorption effects are required. The largest effect is the absorption due to water-vapour. The calculated absorption due to water-vapour in the wavelength interval from 800 nm to 1900 nm, assuming a 2 m thick layer of air with a temperature of 23 °C, an atmospheric pressure of 1013 hPa and 50% relative humidity is shown in figure 6.5. The calculation of the absorption was performed applying the AIRSENTRY software [**87**] by convolving the line absorption spectra of air with a 50 nm normalized bandwidth instrumental function of both new InGaAs filter radiometers. The center wavelength of the InGaAs filter radiometers are highlighted in figure 6.5. It can be seen that the correction due to the water-vapour absorption is necessary only for the FR1300, and is of the order of some 10^{-4}, the correction for FR1550 being negligible. The correction due to the

water-vapour for FR900 is in same order as that of FR1300, for FR800 this correction is negligible [**21**].

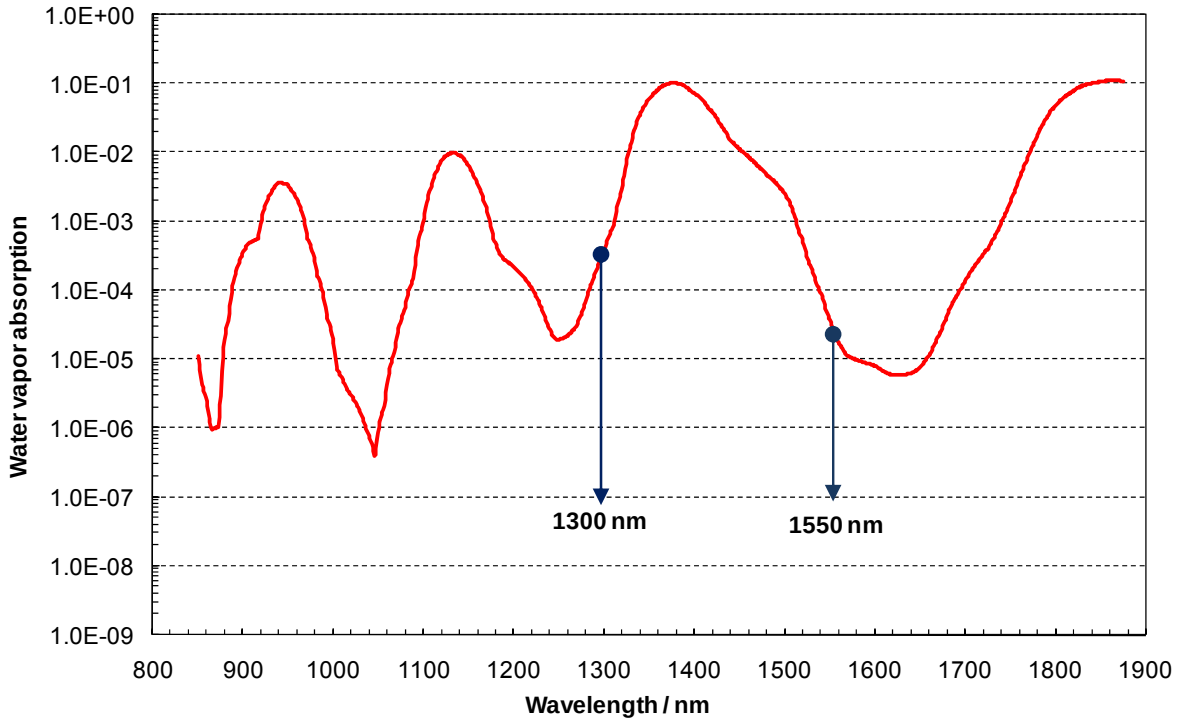

Figure 6.5 : Absorption curve due to water-vapour for a 2 m thick layer of air with 23 °C, 1013hPa, and 50% relative humidity as the atmospheric condition. The highlighted wavelengths denote the center wavelengths of the InGaAs filter radiometers used for thermodynamic temperature measurement.

6.4.2.2 Diffraction at apertures:

At the LABB and the spectral comparator facility precision apertures are used to limit the optical beam diameter and to define the optical beam geometry. Diffraction effects η at these apertures lead to a deviation between the measured radiation flux Φ and the flux calculated by means of geometrical optics Φ_0 :

$$\Phi = (1+\eta)\Phi_0 \qquad 6.16$$

In general, the diffraction contribution η is small for a large ratio between the aperture diameter and the wavelength but can have a positive or a negative sign [**88**]. In the case that the detector is underfilled, η becomes negative, but in the case that the radiation overfills the detector aperture, which is the typical experiment setup in this work, η becomes positive and is generally <<1. However for precision measurements η can not neglected.

For irradiance measurements at the LABB, diffraction occurs at both apertures (A_1 and A_2) that define the optical geometry (figure 6.6A). Since both effects are small, they can be treated independently and the two corrections add to:

$$\eta\left(A_1 + A_2\right) \approx \eta\left(A_1\right) + \eta\left(A_2\right) \qquad 6.17$$

For the calculation of the diffraction correction at the filter radiometer aperture, the furnace aperture acts as a source and the photo diode as an underfilled detector (figure 6.6C). By using the reciprocity theorem of Kirchhoff [**89**], the deviation due to diffraction does not change even when source and detector are exchanged. Consequently the diffraction at the furnace aperture can be calculated with the filter radiometer aperture acting as a source and the opening of the blackbody radiator LABB acting as an underfilled detector (figure 6.6B). Therefore both diffraction correction can be treated physical and mathematical as equivalent.

According to [**90**], exact solutions and approximations for this diffraction problem are available. A simple approximation is given below:

$$\eta\left(u,w,w'\right) \approx -\frac{1}{2\pi w}\ln\frac{\left(w'+w\right)^2 - u^2}{\left(w'-w\right)^2 - u^2} \qquad 6.18$$

whereas

$$\left.\begin{aligned} u &= \frac{2\pi}{\lambda} r^2 \left(\frac{1}{s} + \frac{1}{s'}\right) \\ w &= \frac{2\pi}{\lambda} r \frac{a}{s} \\ w' &= \frac{2\pi}{\lambda} r \frac{a'}{s'} \end{aligned}\right\} \qquad 6.19$$

Thereby a denotes the source radius, a' the detector radius, and r the aperture radius. The deviation of this approximation from the exact solution is less than $3\text{x}10^{-5}$ when $\left(w+w'\right)^2 - u^2 > 6000$. For the measurement setup in this work, for the diffraction at the filter radiometer aperture, $\left(w+w'\right)^2 - u^2$ amounts in order of some 10^5 and for the diffraction that occurs at furnace aperture, $\left(w+w'\right)^2 - u^2$ is more than $1\text{x}10^7$. Therefore the approximation with the equation 6.18 can be used for the diffraction correction calculation.

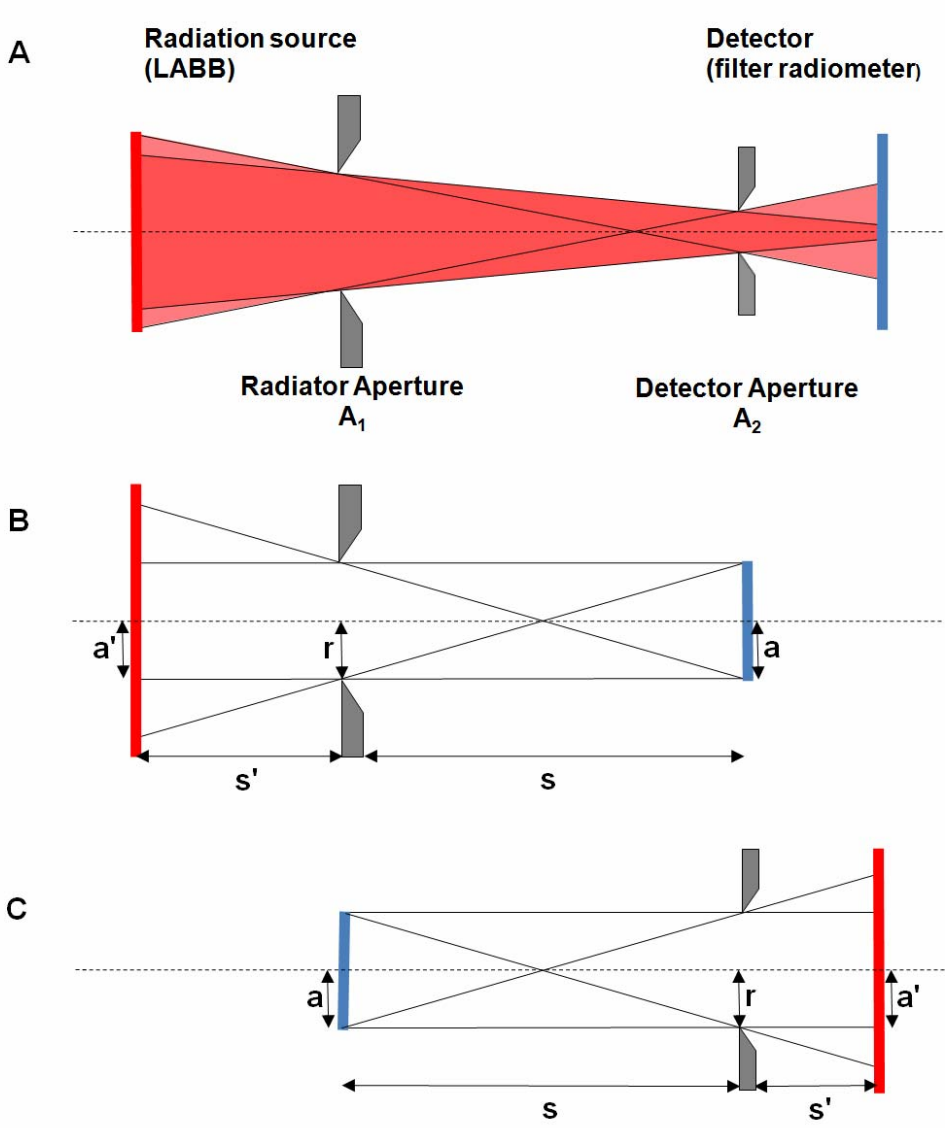

Figure 6.6 : A) Diffraction occurs at both apertures during the irradiance measurements at LABB. B) Calculation of the diffraction correction occurring at the furnace aperture. C) Calculation of the diffraction correction occurring at the filter radiometer aperture. While a denotes as source radius, a' as detector radius, and r as aperture radius.

During the calibration of the filter radiometer at the spectral comparator facility, diffraction occurs at the aperture of filter radiometer and at the aperture in front of the transfer detector. The radiation source at the spectral comparator facility can be considered as punctiform. Thus a and w are close to zero and the approximation in equation 6.18 can be given as:

$$\eta(w') \approx \frac{2}{\pi w'} = \frac{\lambda s'}{\pi^2 r a'} \qquad 6.20$$

For the measurements with sources which have a broad spectral characteristic like the LABB, the diffraction correction has to be calculated for all wavelengths measured. The applied filter radiometer have only a narrow bandpass of about 20 nm to 50 nm. On the other hand the diffraction correction η is proportional to the wavelength and varies little across the bandpass. Thence, for simplification, only the center wavelength of the interference filters is used for the calculation of the correction. The total diffraction correction η_{total} at the spectral comparator facility and at the LABB is given as equation 6.21 [**65**]:

$$\eta_{total} = \eta_{LABB,RA} + \eta_{LABB,FR} - \eta_{SP,FR} + \eta_{SP,TD} \qquad 6.21$$

With $\eta_{LABB,RA}$ as the diffraction correction of the radiator aperture at the LABB, $\eta_{LABB,FR}$ as the diffraction correction of filter radiometer aperture at the LABB, $\eta_{SP,FR}$ as the diffraction correction of the filter radiometer aperture at the spectral comparator facility and $\eta_{SP,TD}$ as the diffraction correction of the transfer detector aperture at the spectral comparator facility. The results of the calculation of the diffraction correction for each filter radiometer are shown in figure 6.7.

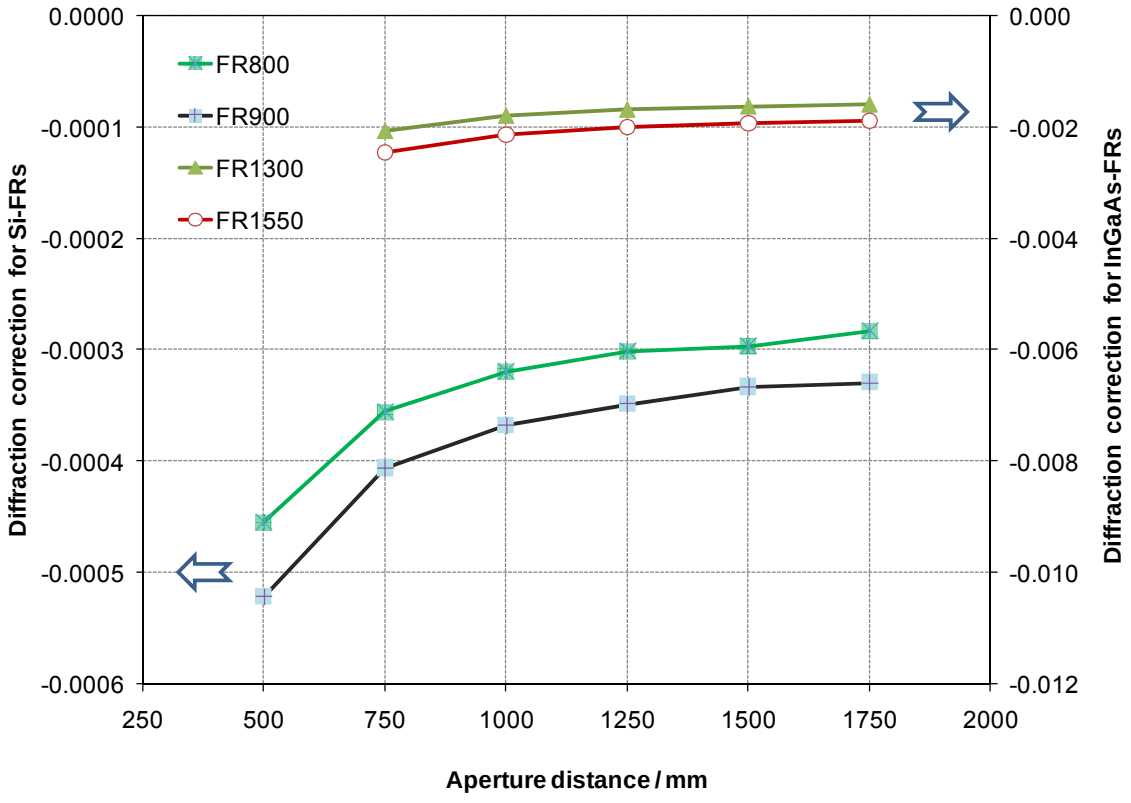

Figure 6.7 : The total diffraction correction for the Si-FRs (left-hand scale) and for the InGaAs filter radiometers (right-hand scale)

6.5 Measurement of the ITS-90 temperature T_{90}

For the determination of the deviation of the thermodynamic temperature T from the ITS-90 temperature T_{90}, the temperature T_{90} of the blackbody (LABB) was simultaneously measured with the radiometric measurement of T with three standard platinum resistance thermometer (SPRTs) of 0.25 Ω type. They are connected to an F18 resistance bridge together with a calibrated 1 Ω standard resistance, controlled at 20 °C, via an automatic switch box. The reading and the calculation of the measured resistance ratio into an ITS-90 temperature T_{90} were done automatically by a computer. The T_{90} value of the LABB is the mean value of the temperature measured from the three SPRTs. The SPRTs have been calibrated according to the ITS-90 at the defining fixed points before and after the radiometric measurements.

6.5.1 The stability of the SPRTs

The stability of the SPRTs were verified before and after the radiometric measurements. For this, the resistance of the SPRTs were measured at the triple point of water (TPW) with a precisely resistance bridge and a calibrated standard resistance. The TPW is realized by a water triple point cell.

The relative change of the resistance of the three SPRTs at TPW converted into an ITS-90 temperature equivalent during the measurement of the ITS-90 temperature performed at the LABB is illustrated in the figure 6.7. The periods of each measurement temperature are shown in the table 6.3.

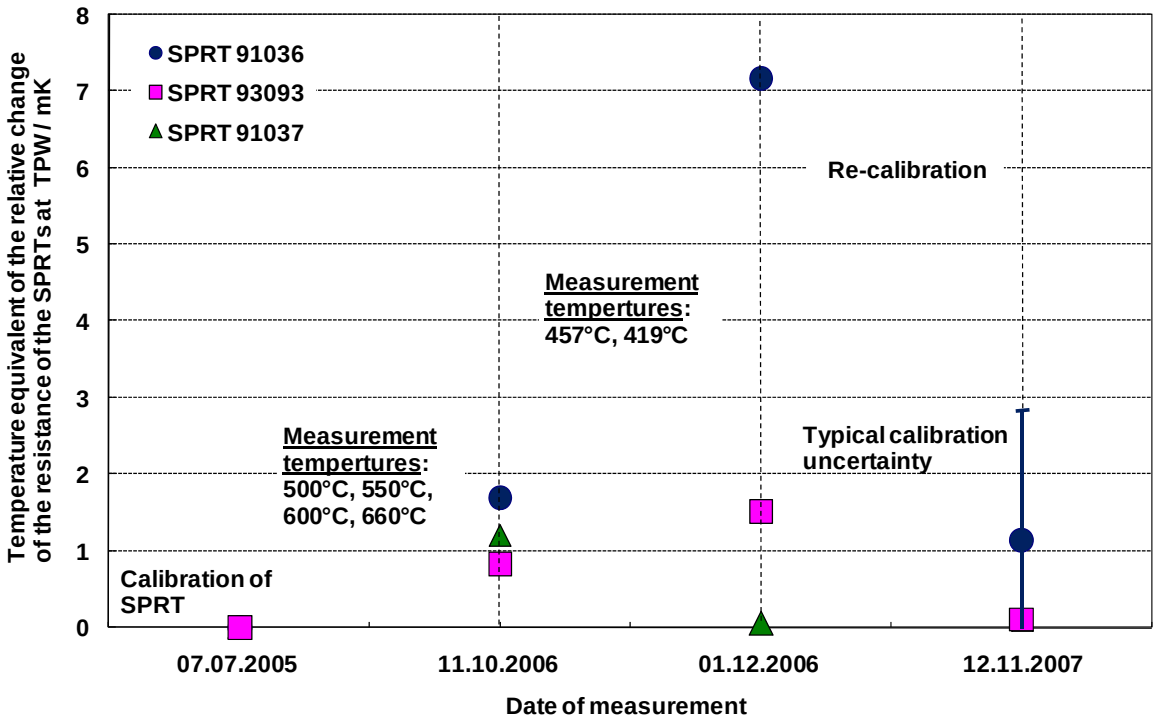

Figure 6.7 : The temperature equivalent of the change of the resistance of the SPRTs at TPW during the measurement of the ITS-90 temperature at LABB, relative to last calibration of SPRTs before the measurement at 07.07.2005

Table 6.3: Dwelling time of the SPRTs in the cavity bottom of the LABB as function of the cavity temperature.

	$t_{90,\mathrm{LABB}}$ / °C	Duration / days
Measurement period I	500	17
	550	15
	600	9
	660	9
	457	10
	419	10
	660	7
	600	7
	550	7
Measurement period II	660	16
	550	21
	457	6
	419	5

After the measurements of the ITS-90 temperature at the temperatures of 500 °C, 550 °C, 600 °C and 660 °C, the change of the resistance at the TPW of all SPRTs were less than 2 mK, which is still within their calibration uncertainty.

However after the measurements of the ITS-90 temperature at 457 °C and 419 °C, the resistance at the TPW of the SPRT 91036 has significantly changed to more than 7 mK. In order to localize the changing time of this SPRT, all measurements of the ITS-90 temperature of this period for all radiometric measurement have been analyzed. Since the resistance of the SPRT 91037 at the TPW after this measurement period has minimally changed, this SPRT has been used as the reference SPRT in order to monitor the drift of the other SPRTs. For the measurement of the ITS-90 temperature from 660 °C down to 500 °C, the temperature deviation of each SPRT agree within their calibration uncertainties.

Figure 6.8 shows the temperature in the cavity bottom of LABB measured with three SPRTs at the temperatures 457 °C and 419 °C. At the temperature of 457 °C, the SPRT 91036 has a small drift towards higher temperatures, however the observed deviation between all SPRTs is still within the calibration uncertainty of 3 mK at the Zn-FP (k=1). At the temperature of 419 °C the SPRT 91036 shows a significant drift towards higher temperatures. This drift can be considered as the result of the change of the SPRT due to its instability during the application at the temperature of 419 °C and has been confirmed by the measured change of the resistance at the TPW after the measurements at 419 °C. The enclosed volume of the sensor in all SPRTs is filled with a mixture of 90% Ar and 10% O_2 by the manufacturer [**91**]. Therefore the cause of the change of the SPRTs, applied in the temperature range below 500 °C, can be traced back onto the formation of an oxide layer on the platinum sensor of the SPRTs [**92**]. Therefore all SPRTs were annealed in a vertical position at a temperature of 675 °C in a heat-pipe over several hours before the re-calibration in order to dissociate the oxide layer formed during their application in the temperature range from 450 °C to 520 °C [**65**]. As shown in figure 6.7, the change of all of the SPRT resistances at the TPW after re-calibration and used during the measurement period II (table 6.3), agree within the calibration uncertainty again.

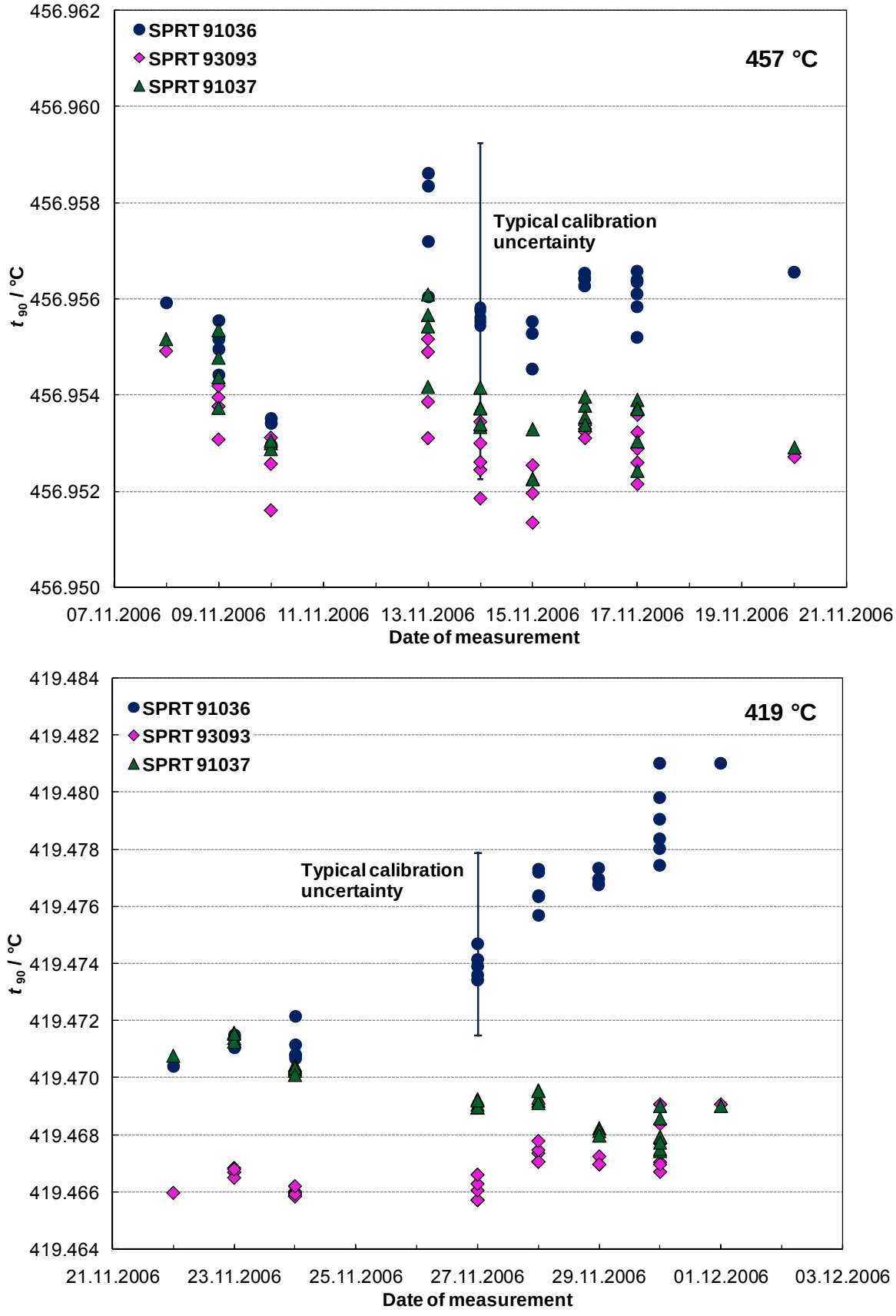

Figure 6.8 : The temperature of the cavity bottom of LABB using three SPRTs during the radiometric measurement at the temperature of 457 °C and 419 °C. At 457 °C the temperature measured by three SPRTs are agree within their calibration uncertainty (3 mK). At 419 °C a drift the SPRT 91036 due to its instability can be observed.

The application of the SPRTs for the determination of T_{90} at the temperatures of 457 °C and 419 °C were performed at the end of each measurement period (see table 6.3) in order to keep the SPRTs as stable as possible for the T-T_{90} measurement in the temperature interval from 660 °C down to 457 °C. Due to the instability of the SPRT 91036, only the T_{90} temperature of the SPRT 93093 and 91037 are used for the evaluation of the measurements performed at 419 °C.

6.5.2 Correction and the Uncertainty of the T_{90}-temperature

A temperature gradient ΔT_{B} between the temperature of the cavity bottom and the temperature measured by SPRTs in the heat-pipe occurs due to radiation losses through the cavity aperture. ΔT_{B} can be calculated in equation 6.22 from the equilibrium between the radiation loss and the heat supply via heat conduction [**16**].

$$\Delta T_{\mathrm{B}} \approx \varepsilon \cdot \sigma \cdot T^4 \cdot \frac{d}{\lambda_b} \cdot \left(\frac{r}{l}\right)^2 \qquad 6.22$$

whereby ε is the local emissivity (0.75), σ is the Stefan-Boltzmann constant ($5{,}67 \cdot 10^{-8}$ W·m^{-2}·K^{-4}), λ_b is the thermal conductivity of Inconel (15 W·m^{-1}·K^{-1}), d is the wall thickness (3.35 mm), r is the radius of the cavity aperture (14 mm) and l is the length of the cavity (731 mm). The correction values applied in the temperature range from 419 °C to 660 °C showed in table 6.4 are based on the numerical values given in the brackets for the variables in equation 6.22.

Table 6.4: The correction for the temperature drop at the bottom of the LABB due to the radiation losses through the cavity aperture

$t_{90,\mathrm{LABB}}$ / °C	419	457	500	550	600	660
ΔT_{B} / mK	0.8	0.9	1.2	1.6	2.0	2.5

The measurement current of the resistance bridge of 10 mA leads to a self-heating of the sensors of the platinum resistance in the SPRTs and thereby to a too high measured T_{90} temperature. The self-heating of the SPRTs was determined at the Zn-FP and at the Al-FP via the measurement at 10 mA and at $10 \cdot \sqrt{2}$ mA. The correction due to the self-heating amounts 1.6 mK at the Zn-FP and 1.5 mK at the Al-FP. Since the difference between both corrections is very small, the correction for the

self-heating in the temperature range from 419 °C to 660 °C was estimated to 1.6 mK with an uncertainty of 0.5 mK.

The uncertainty of the ITS-90 realization via the SPRTs in the blackbody results from the calibration of the SPRTs, the uncertainty of the determination of the SPRTs resistance ratio with the resistance bridge and the uncertainty of the standard resistance. The uncertainty at the Zn-FP amounts 3.2 mK and 4.9 mK at the Al-FP. The uncertainty for the other temperature values between this two fixed points were linearly interpolated.

The stability of the measurement of ITS-90 temperature during the radiometric measurement of the thermodynamic temperature at the LABB was better than ±1.5 mK.

The maximum change of the resistance at the TPW of the SPRT 93093 and SPRT 91037 which were used in the evaluation of the ITS-90 temperature during the measurement of thermodynamic temperature amounts 2 mK. Since the moment of this change could not be determined, this change was added into the uncertainty of the calibration of the SPRT. For this reason the uncertainty at the Zn-FP amounts to 5.4 mK and to 8.4 mK at the Al-FP. The combined uncertainty and the correction of the measurement of the ITS-90 temperature are shown in table 6.5.

Table 6.5: The measurement uncertainty and the correction of the T_{90} temperature determination of the LABB during the irradiance measurement

Source	419 °C		660 °C	
	Correction	Uncertainty	Correction	Uncertainty
Realization of ITS-90	-	3.2 mK	-	4.9 mK
Gradient at the cavity bottom	-0.8 mK	0.2 mK	-3.2 mK	0.8 mK
Stability of the LABB	-	1.5 mK	-	1.5 mK
Stability of the SPRT	-	5.9 mK	-	8.4 mK
Self-heating of the SPRT	-1.6 mK	0.5 mK	-1.6 mK	0.5 mK
Combined (*k*=1)	-2.4 mK	6.9 mK	-4.8 mK	9.9 mK

6.6 The deviation of T_{90} from the thermodynamic temperature

The determination of the deviation of the ITS-90 temperature from the thermodynamic temperature (T-T_{90}) was done at the LABB. The thermodynamic temperature T was determined by an iterative numerical calculation according to equation 6.6 with the measured photocurrent of the filter radiometers during the radiometric measurement. These measurements were done directly after the calibration of the filter radiometers. The ITS-90 temperature T_{90} of the LABB was sensed simultaneously with the radiometric measurements by the SPRTs. The diffraction index of air has been calculated from the average of the measured values of the atmospheric pressure, the atmospheric temperature and the relative humidity. The numerical value from CODATA(2002) has been used for the Boltzmann constant : k = 1.3806505·10^{-23} J·K^{-1} with a relative uncertainty of 1.8x10^{-6} [**93**].

6.6.1 The uncertainty of the T-T_{90} determination

The equation for the measured photo-current of the filter radiometer together with the applied corrections can be taken as the basis for the uncertainty evaluation:

$$I_{\text{photo}} = \varepsilon \cdot G(r_1, r_2, d) \cdot \left(1 + \underbrace{\eta_{\text{LABB,RA}} + \eta_{\text{LABB,FR}}}_{\text{Diffraction at the LABB}} - \overbrace{\eta_{\text{SP,FR}} + \eta_{\text{SP,TD}}}^{\text{Diffraction at the spectral comparator facility}} \right) \cdot \int_{\lambda_{\min}}^{\lambda_{\max}} s_E^{\text{FR}}(\lambda) \cdot L_{\lambda,BB}(\lambda, T) d\lambda \qquad 6.23$$

The measured photo-current in the equation 6.6 can be approximated as [**65**]:

$$\begin{aligned} I_{\text{photo}} &\approx \varepsilon \cdot G(r_1, r_2, d) \cdot L_{\lambda,BB}(\lambda_{cw}, T) \cdot \int_{\lambda_{\min}}^{\lambda_{\max}} s_E^{FR}(\lambda) \cdot d\lambda \\ &= \varepsilon \cdot G(r_1, r_2, d) \cdot L_{\lambda,BB}(\lambda_{cw}, T) \cdot I_s \end{aligned} \qquad 6.24$$

with I_s and λ_{cw} as defined by equation 5.4 respective equation 5.5. With the aid of the equation 6.24, equation 6.23 can be converted to:

$$L_{\lambda,BB}(\lambda_{cw}, T) = \frac{U_{photo}}{R_F \cdot G(r_1, r_2, d) \cdot \varepsilon \cdot I_s} \cdot \frac{1}{1 + \eta_{\text{LABB,RA}} + \eta_{\text{LABB,FR}} - \eta_{\text{SP,FR}} + \eta_{\text{SP,TD}}} \qquad 5.25$$

whereby U_{photo} is the converted voltage from the measured photo-current via a current-to-voltage converter and R_F is the feedback resistor of the current-to-voltage converter.

The uncertainty contribution from the geometry of the experiment setup results from the contribution of each variable in the geometry factor $G(r_1, r_2, d)$ in equation 6.5 whereby for a first order uncertainty evaluation only the radiator aperture (A_1 resp. r_1) and the aperture distance d has been considered. The value for the diameter for the aperture A_1 is given in table 6.2, the absolute uncertainty for the measurement of the diameter of this aperture amounts 0.40 µm which corresponds to a relative standard uncertainty of the aperture area of 4×10^{-5} (for the 20 mm aperture diameter). The radiator aperture is mounted on a temperature controlled copper plate (see figure 6.2) with a controlled temperature of 25 °C in order to minimize the aperture heating through the absorption of radiation power from the blackbody. The inner diameter of this temperature controlled copper plate is only slightly bigger than the outer diameter of the radiation aperture (24 mm). Thus, on the one hand a large-area heat contact between the radiator aperture and the temperature controlled copper plate is achieved and on the other hand the ratio of the radiator aperture area which is directly exposed to the radiation power of the LABB is as small as possible. In [**10**] it was shown that at a blackbody temperature of 962 °C, the relative influence on the aperture area via the absorption from the radiation power is smaller than 3×10^{-5}. Since the total radiation power is proportional to T^4, hence for this work (maximum blackbody temperature is 660 °C) the influence from this effect can be considered as negligible. The temperature of the radiator aperture was measured indirectly by a temperature sensor (Pt 100) in the temperature controlled copper plate near the radiation aperture. Therefore exists the uncertainty due to the temperature measurement from 0.5 °C. With the thermal expansion coefficient of aluminum of 23.8×10^{-6} K^{-1}, this uncertainty corresponds to a relative uncertainty of the radiator aperture area of 3×10^{-5}.

An aperture distance of 1000 mm was assumed for the calculation of the uncertainty contribution due to the determination of the aperture distance. This contribution is the combined uncertainty from the uncertainty of the interferometic distance measurement (1.5 µm), the second reference point (2 µm) and the adjustment inaccuracies (15 µm). The uncertainty contribution from the aperture

distance determination has an additional contribution from the thickness of the aperture land which amounts ca.15 µm for the radiator aperture and the filter radiometer aperture with the 5 mm diameter and ca. 60 µm for the 3 mm diameter filter radiometer aperture. Additionally, the uncertainty of the total diffraction correction is combined into the measurement uncertainty.

The measurement of the photo-current is performed indirect via a current-to-voltage converter through the measurement of a voltage, U_{photo}, with the aid of a digital-voltmeter (DVM). The switchable feedback resistors, R_F, of the current-to-voltage converter (1 kΩ - 10GΩ) have been calibrated using a constant-current source and a calibrated 1 kΩ-standard resistance traceable to the SI-unit (ampere) via ratio measurement. The traceability of the voltage measurement has been ensured through the calibration of the DVM at a calibrator.

The atmospheric pressure, the atmospheric temperature and the relative humidity have been measured during the radiometric irradiance measurement. Hence each actual value was used for the calculation of the refractive index n with an absolute uncertainty of $3\text{x}10^{-6}$ which corresponds to a relative uncertainty contribution of the irradiance measurements of $3\text{x}10^{-5}$. The calculation of the thermodynamic temperature *T* by iteration has been done numerically with a computer program with a relative uncertainty smaller than $5\text{x}10^{-5}$. The uncertainty contribution from the emissivity of the LABB amounts $8\text{x}10^{-5}$ [**65**].

The uncertainty from the spectral irradiance responsivity and the center wavelength in the calibration of the filter radiometer contribute to the measurement of the thermodynamic temperature at the LABB. The uncertainty contribution of the spectral irradiance responsivity is shown in the table 5.5. The uncertainty of the center wavelength of the filter radiometer (10 pm for the Si-FRs and 25 pm for the InGaAs filter radiometers) has been calculate in a relative radiance- resp. irradiance uncertainty with equation 6.26:

$$\frac{E_\lambda(\lambda+\Delta\lambda,T)-E_\lambda(\lambda,T)}{E_\lambda(\lambda,T)}=\frac{L_{\lambda,BB}(\lambda+\Delta\lambda,T)-L_{\lambda,BB}(\lambda,T)}{L_{\lambda,BB}(\lambda,T)}=\left(\frac{c_2}{\lambda^2 T}-\frac{5}{\lambda}\right)\cdot\Delta\lambda \qquad 6.26$$

The combined relative standard uncertainty from the spectral radiometric determination of the thermodynamic temperature *T* at the blackbody LABB are shown in table 6.5 for the filter radiometers FR1300 and FR1550 and in table 6.6 for the filter

radiometers FR900 and FR800. The relative uncertainty of the spectral irradiance measurement has been converted into a temperature equivalent by:

$$\frac{E_\lambda(\lambda,T+\Delta T)-E_\lambda(\lambda,T)}{E_\lambda(\lambda,T)}=\frac{L_{\lambda,BB}(\lambda,T+\Delta T)-L_{\lambda,BB}(\lambda,T)}{L_{\lambda,BB}(\lambda,T)}=\frac{c_2}{\lambda T^2}\cdot\Delta T \qquad 6.27$$

The combined uncertainty for the thermodynamic temperature measurement and the uncertainty of the ITS-90 temperature measurement results in the uncertainty for the T-T_{90} and is shown in table 6.7.

Table 6.5: The standard uncertainty contribution (k=1) for the determination of the thermodynamic temperature through the irradiance measurement with the filter radiometers FR1300 and FR1550 at the blackbody LABB.

Source of uncertainty	**Filter radiometer $\Delta S_E/S_E$(x10^4)**											
	FR1300						**FR1550**					
Geometry												
Aperture area	0.4						0.4					
Thermal expansion aperture	0.3						0.3					
Distance of apertures	1.0						1.0					
Diffraction correction blackbody (LABB) aperture	1.0						1.0					
Measurement of *T*												
photo current noise	0.5						0.5					
Calibration feedback resistors	1.0						1.0					
Calibration DVM	0.2						0.2					
Refractive index n	0.3						0.3					
Boltzmann constant k	0.2						0.2					
Numerical integration	0.5						0.5					
Emissivity LABB	0.8						0.8					
Homogeneity LABB	2.0						2.0					
Filter radiometer calibration												
Calibration spectral comparator	6.2						5.8					
Diffraction correction filter radiometer aperture	1.0						1.0					
Combined relative standard uncertainty	6.9						6.6					
	t_{90} of LABB / °C						**t_{90} of LABB / °C**					
	419	457	500	550	600	660	419	457	500	550	600	660
Temperature equivalent / mK	30	33	37	42	48	54	34	38	43	48	54	62

Table 6.6: The standard uncertainty contribution (k=1) for the determination of the thermodynamic temperature through the irradiance measurement with the filter radiometers FR800 and FR900 at the blackbody LABB

Source of uncertainty	**Filter radiometer $\Delta S_E/S_E(x10^4)$**				
	FR800		**FR900**		
Geometry					
Aperture area	0.4		0.4		
Thermal expansion aperture	0.3		0.3		
Distance of apertures	0.5		0.5		
Diffraction correction blackbody (LABB) aperture	1.6		1.8		
Measurement of *T*					
photo current noise	0.5		0.5		
Calibration feedback resistors	1.0		1.0		
Calibration DVM	0.2		0.2		
Refractive index n	0.3		0.3		
Boltzmann constant k	0.2		0.2		
Numerical integration	0.5		0.5		
Emissivity LABB	0.8		0.8		
Homogeneity LABB	2.0		2.0		
Filter radiometer calibration					
Calibration spectral comparator	4.2		4.0		
Diffraction correction filter radiometer aperture	0.5		0.5		
Combined relative standard uncertainty	5.2		5.0		
	t_{90} of LABB / °C		**t_{90} of LABB / °C**		
	550	660	550	600	660
Temperature equivalent / mK	19	25	21	24	27

Table 6.7: The standard uncertainty (k=1) for the determination of the deviation of ITS-90 temperature form the thermodynamic temperature $u(T\text{-}T_{90})$ represented in mK as the function of the investigated blackbody LABB temperature and the applied filter radiometer

Filter radiometer	t_{90},LABB					
	419°C	457°C	500°C	550°C	600°C	660°C
	u (T-T_{90}) / mK					
FR800	-	-	-	21	-	27
FR900	-	-	-	22	25	29
FR1300	31	34	38	43	48	55
FR1550	35	39	43	49	55	63

6.6.2 Measurement results from each filter radiometer

The compilation of the results of the radiometric measurement for the determination of the thermodynamic temperature T of LABB respective the deviation of this temperature from the simultaneous measurement T_{90} of the LABB is shown in this section. For the identification of the systematic effects that possibly occur during the radiometric measurement, the results of T-T_{90} of each filter radiometer is represented as a function of the aperture distance. The represented uncertainty contains the uncertainty due to the aperture distance measurement, the diffraction correction and the correction of the atmospheric absorption (for FR900 and FR1300).

The uncertainty of the T-T_{90} determination has been calculated from the uncertainty of the filter radiometer calibration (from chapter 5), the uncertainty of the measurement of the thermodynamic temperature and the uncertainty of the ITS-90 temperature measurement.

6.6.2.1 1300-nm-Filter radiometer (FR1300)

FR1300 has been applied for the following radiometric measurements at the LABB (measurement period and ITS-90 temperature of the LABB

temperature): 3 to 9 August 2006 : 500 °C, 7 to 11 September 2006 : 550 °C, 14 to 18 September 2006 : 600 °C, 27 to 29 September 2006 : 660 °C, 15 to 20 November 2006 : 457 °C, 24 to 29 November 2006 : 419 °C, 13 to 15 December 2006 : 660 °C, 14 to 15 February 2007 : 660 °C, 6 to 7 December 2007 : 660 °C, 11 to 15 January 2008 : 550 °C, 1 to 3 February 2008 : 457 °C and 7 to 9 February 2008 : 419 °C.

The results for T-T_{90} as a function of the aperture distance at the various LABB temperature are illustrated in the figures 5.9(A) (419 °C), 5.9(B) (457 °C), 5.9(C) (500 °C), 5.10(A) (550 °C), 5.10(B) (600 °C) and 5.10(C) (660 °C). The aperture distance dependence, the absorption and the diffraction correction are already calculated and the uncertainty due to these factors are represented in the error bars. It can be seen from the measurement results, within the uncertainty no other additional systematic effect according to the aperture distance are identifiable. Therefore the result of the T-T_{90} has been calculated from the mean value of all measurements.

For the 1st measurement period (in year 2006) the measurement were considered in the evaluation only for the aperture distance of 1250 mm and up due to a slight misalignment of photo diode in the filter radiometer. The photo diode in the FR1300 was re-aligned and the filter radiometer recalibrated after the 1st measurement period and it shows a good result (the results at all aperture distance at each temperature are deviated within the error bars) in the 2nd measurement period.

The results for T-T_{90} from both measurement periods for each investigated ITS-90 temperature are summarized and shown in table 6.8. The repeatability of the results from both measurement periods agree within the uncertainty of the T-T_{90} determination.

Table 6.8: The deviation of the ITS-90 temperature from the thermodynamic temperature (T-T_{90}) determined with the FR1300 and the corresponding standard uncertainty (k=1)

t_{90}	Measurement period		Mean Value	$u(T\text{-}T_{90})$ / mK
	3.08.2006-15.02.2007	6.12.2007-9.02.2008		
	T-T_{90} / mK	T-T_{90} / mK	T-T_{90} / mK	
419 °C	28	26	27	31
457 °C	22	32	27	34
500 °C	2	-	2	38
550 °C	10	35	22	43
600 °C	32	-	32	48
660 °C	29	42	39	55
660 °C 12.2006	36	-		
660 °C 2.2007	42	-		

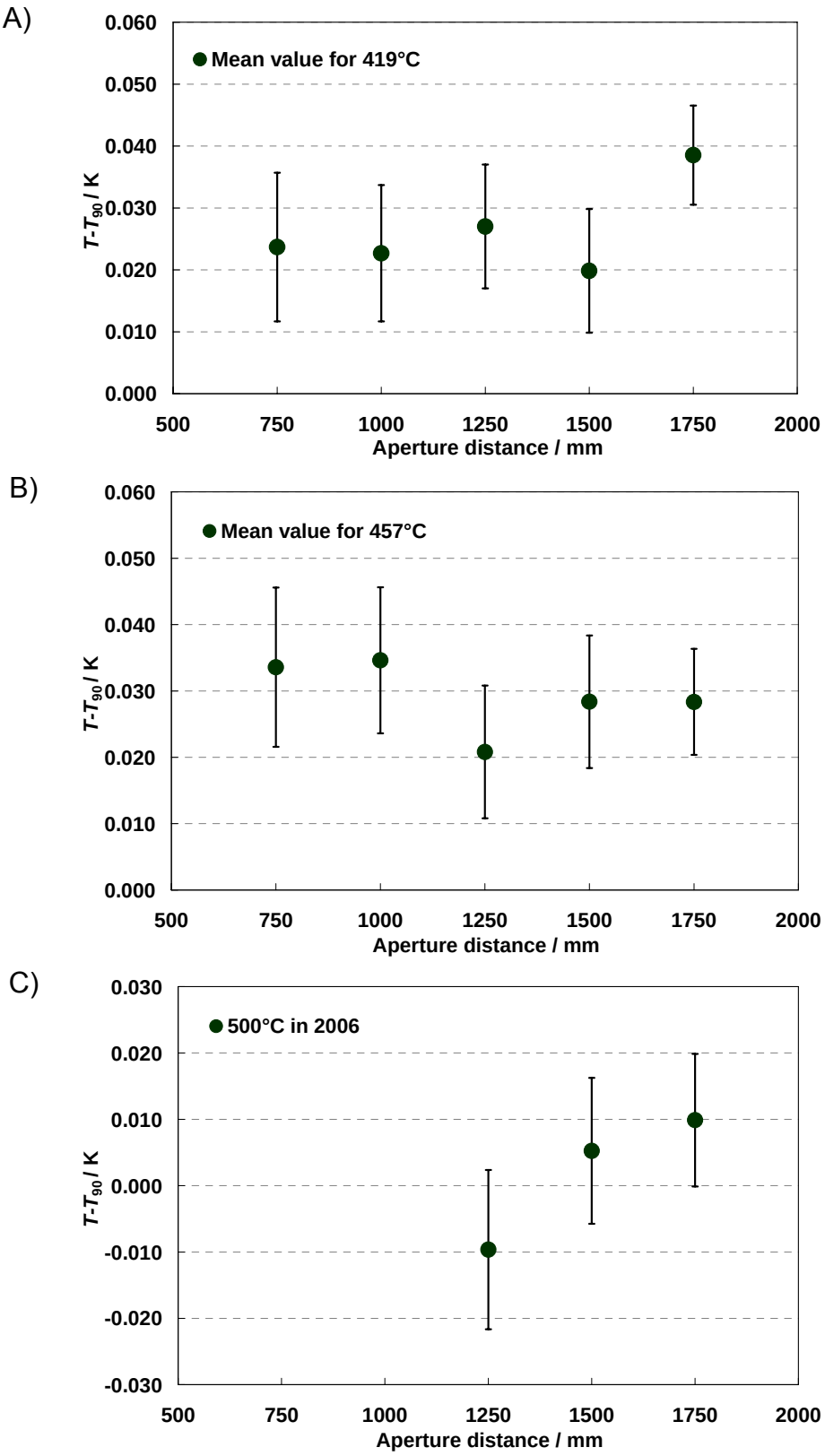

Figure 6.9 : The results for T-T_{90} as a function of the aperture distance for the ITS-90Temperatures of: A) 419 °C (mean value from the measurement in 2006 and 2008), B) 457 °C (mean value from the measurement in 2006 and 2008) and C) 500 °C determined with FR1300. The displayed error bars include the uncertainty from the diffraction correction, the aperture distance determination and the absorption correction.

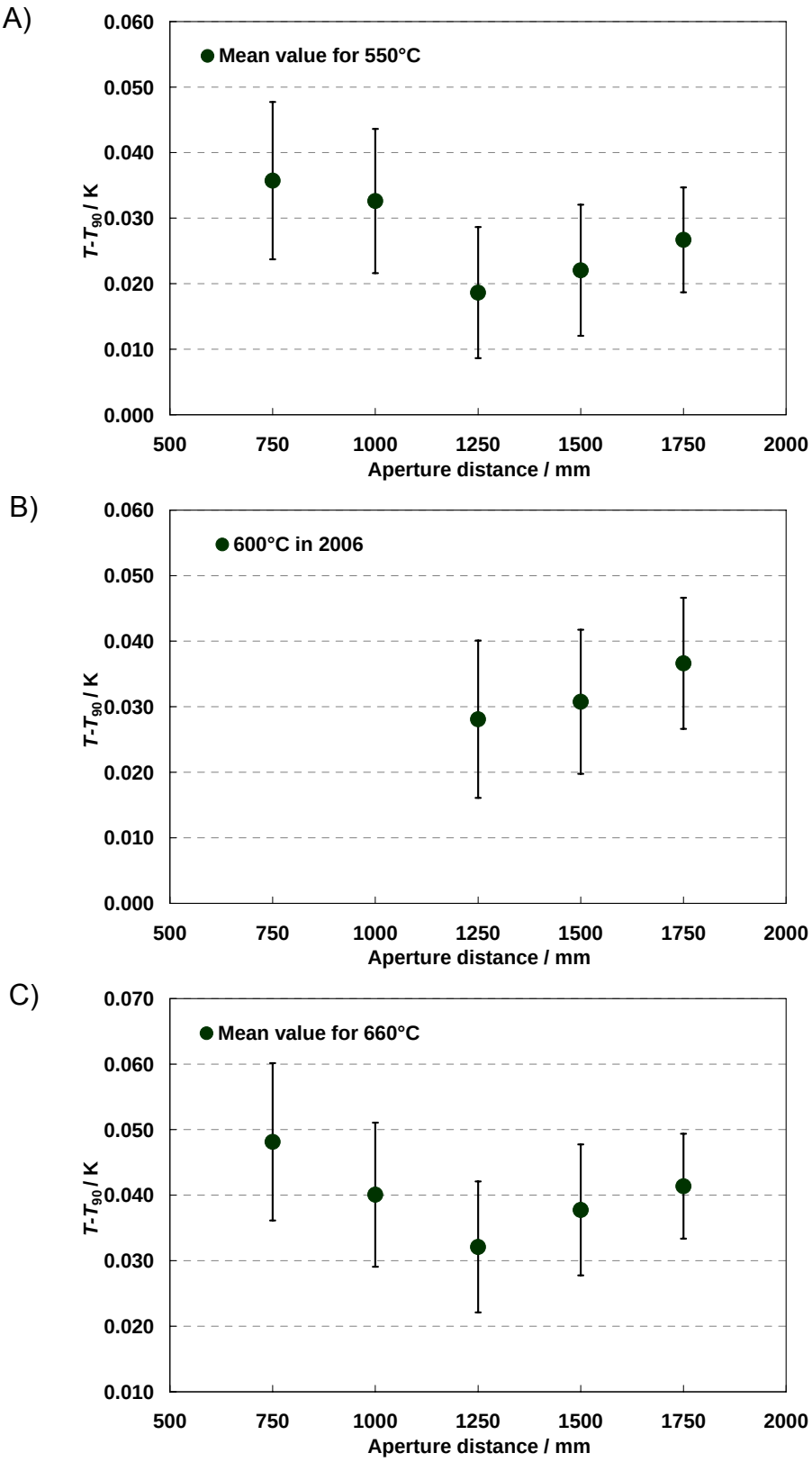

Figure 6.10 : The results for T-T_{90} as a function of the aperture distance for the ITS-90Temperatures of: A) 550 °C (mean value from the measurement in 2006 and 2008), B) 600 °C and C) 660 °C (mean value from the measurement in 2006 and 2008) determined with FR1300. The displayed error bars include the uncertainty from the diffraction correction, the aperture distance determination and the absorption correction.

6.6.2.2 1550-nm-Filter radiometer (FR1550)

The radiometric measurements of the thermodynamic temperature at the LABB by using FR1550 have been done in these following period (measurement period : ITS-90 temperature of the LABB temperature); 14 to 17 August 2006 : 500 °C, 4 to 6 September 2006 : 550 °C, 12 to 13 September 2006 : 600 °C, 25 to 27 September 2006 : 660 °C, 13 to 15 November 2006 : 457 °C, 29 November to 1 December 2006 : 419 °C, 11 to 12 December 2006 : 660 °C, 3 to 5 December 2007 : 660 °C, 8 to 11 January 2008 : 550 °C, 30 January to 1 February 2008 : 457 °C and 5 to 7 February 2008 : 419 °C.

The results for T-T_{90} as a function of the aperture distance at the various LABB temperatures are illustrated in the figures 5.11(A) (419 °C), 5.9(B) (457 °C), 5.9(C) (500 °C), 5.12(A) (550 °C), 5.12(B) (600 °C) and 5.12(C) (660 °C). The error bars are represent the uncertainty due to the aperture distance determination, the absorption correction and the diffraction correction. No additional systematic effects are identifiable within the uncertainty. Therefore, for the calculation of T-T_{90} the mean value from the results of both measurement periods was taken.

The result for T-T_{90} from both measurement periods at each investigated ITS-90 temperature are summarized in table 6.9. The results from both measurement periods agree within the uncertainty of the T-T_{90} determination.

Table 6.9: The deviation of the ITS-90 temperature from the thermodynamic temperature (T-T_{90}) determined with the FR1550 and the corresponding standard uncertainty (k=1)

t_{90}	Measurement period		Mean Value	$u(T\text{-}T_{90})$ / mK
	14.08.2006-12.12.2007	3.12.2007-7.02.2008		
	T-T_{90} / mK	T-T_{90} / mK	T-T_{90} / mK	
419 °C	10	32	21	35
457 °C	10	23	16	39
500 °C	15	-	15	43
550 °C	7	41	24	49
600 °C	22	-	22	55
660 °C	16	67	44	63
660 °C 12.2006	16	-		

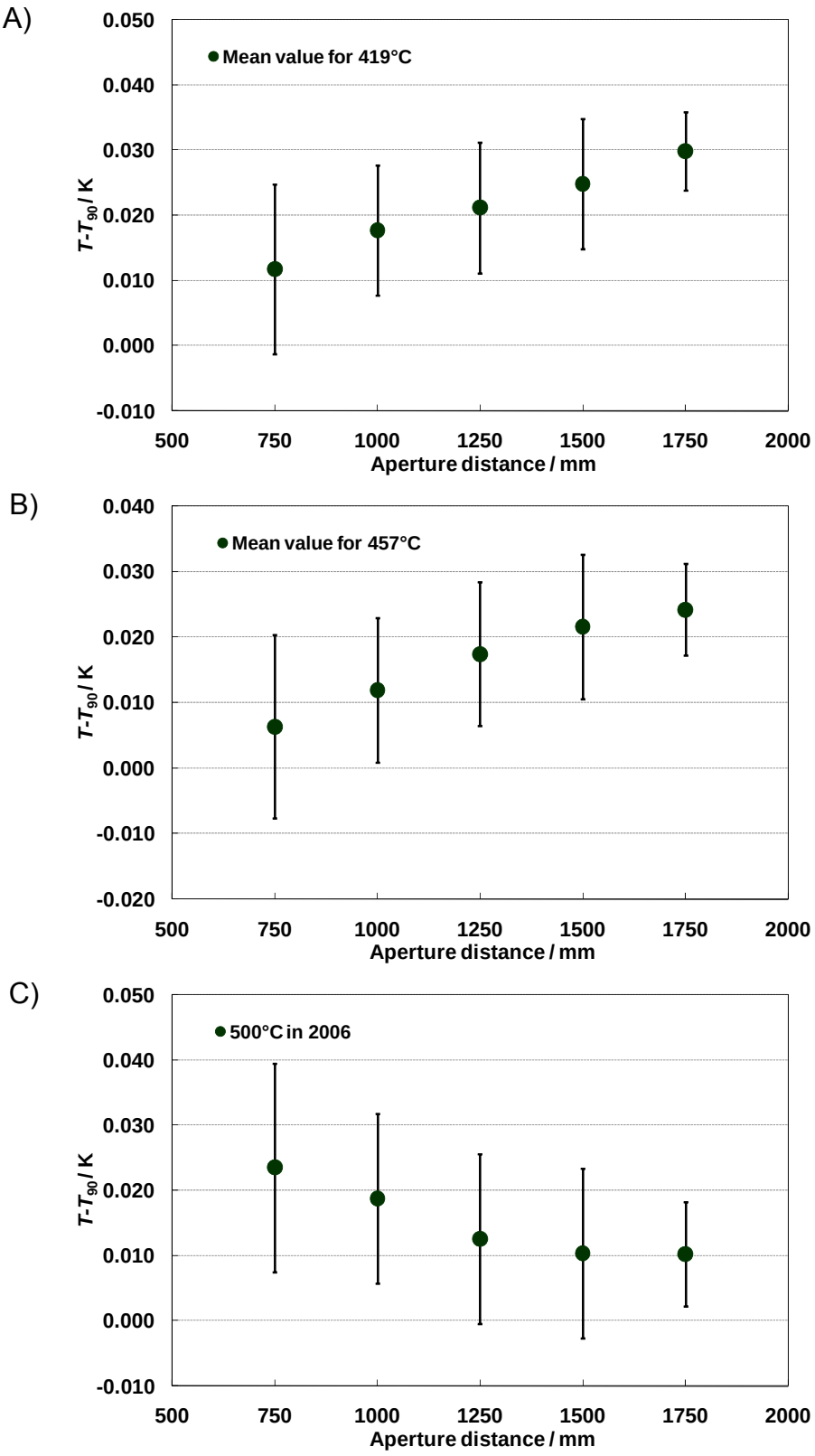

Figure 6.11 : The results for T-T_{90} as a function of the aperture distance for the ITS-90Temperatures of: A) 419 °C (mean value from the measurement in 2006 and 2008), B) 457 °C (mean value from the measurement in 2006 and 2008) and C) 500 °C determined with FR1550. The displayed error bars include the uncertainty from the diffraction correction, the aperture distance determination and the absorption correction.

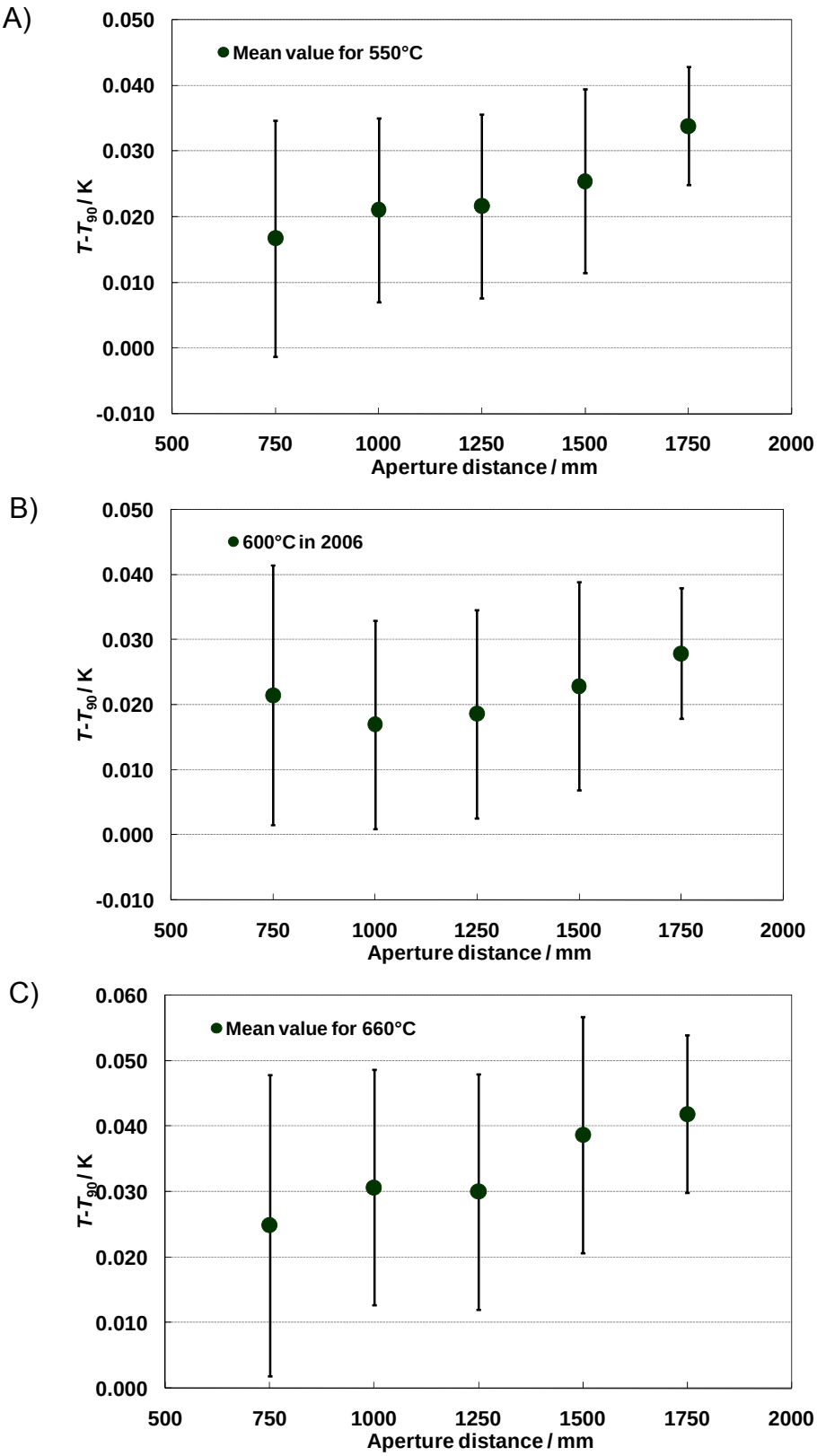

Figure 6.12 : The results for T-T_{90} as a function of the aperture distance for the ITS-90Temperatures of: A) 550 °C (mean value from the measurement in 2006 and 2008), B) 600 °C and C) 660 °C (mean value from the measurement in 2006 and 2008) determined with FR1550. The displayed error bars include the uncertainty from the diffraction correction, the aperture distance determination and the absorption correction.

6.6.2.3 900-nm-Filter radiometer (FR900)

In order to underpin the accuracy of the results for T-T_{90} from measured with the InGaAs filter radiometers, an independent measurement of the thermodynamic temperature was performed with a Si photodiode based filter radiometer with a center wavelength of 900 nm (FR900). Since this filter radiometer has a different geometric construction in comparison to the InGaAs filter radiometers, the measurement of the thermodynamic temperature could be performed for aperture distances beginning from 500 mm. Due to the low signal-to-noise ratio when this filter radiometer is applied for the thermodynamic temperature determination below 500 °C, thus it was used only for the thermodynamic temperature measurement at the temperatures of 550 °C, 600 °C and 660 °C.

The radiometric measurement of the thermodynamic temperature at the LABB using the FR900 have been done in these following periods (measurement period : ITS-90 temperature of the LABB temperature); 16 to 27 February 2007 : 660 °C, 6 to 13 March 2007 : 600 °C and 15 to 20 March 2007 : 550 °C, 14 to 20 December 2007 : 660 °C, and 15 to 18 January 2008 : 550 °C.

The results for the determination of T-T_{90} with this filter radiometer as a function of the aperture distance at the various LABB temperatures are shown in figures 6.13(A) (550 °C), 6.13(B) (600 °C) and 6.13(C) (660 °C). The aperture distance dependence, the absorption correction and the diffraction correction are already considered in the shown results and the uncertainty due to these factors are represented in the error bars. Form the measurement results with this filter radiometer, it can be see that no additional systematic effects are identifiable within the uncertainty. Therefore, for the calculation of T-T_{90} the mean value from the results of both measurement periods was taken

The results for the T-T_{90} from both measurement periods at each investigated ITS-90 temperature are summarized and shown in table 6.10. The good repeatability of the results from both measurement periods can be seen from the fact that they agree within the uncertainty of the T-T_{90} determination.

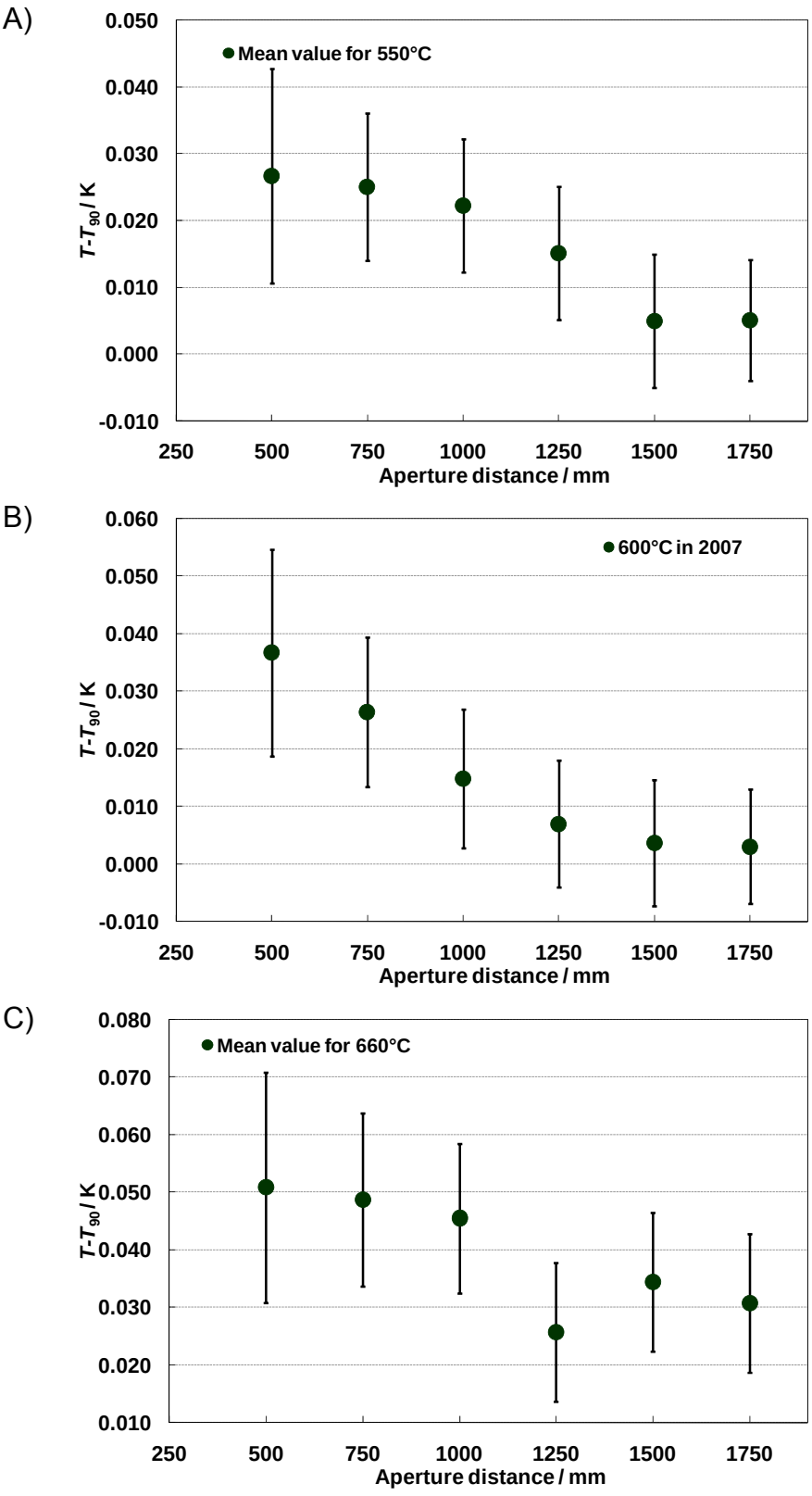

Figure 6.13 : The results for T-T_{90} as a function of the aperture distance for the ITS-90Temperatures of: A) 550 °C (mean value from the measurement in 2007 and 2008), B) 600 °C and C) 660 °C (mean value from the measurement in 2007 and 2008) determined with FR900. The displayed error bars include the uncertainty from the diffraction correction, the aperture distance determination and the absorption correction.

Table 6.10: The deviation of ITS-90 temperature from the thermodynamic temperature (T-T_{90}) determinated with the FR900 with and the corresponding standard uncertainty (k=1)

t_{90}	Measurement period		Mean Value	$u(T\text{-}T_{90})$ / mK
	16.02.2007-07.05.2007	14.12.2007-18.01.2008		
	T-T_{90} / mK	T-T_{90} / mK	T-T_{90} / mK	
550 °C	17	20	19	22
600 °C	11	-	11	25
660 °C	42	37	39	29

6.6.2.4 800-nm-Filter radiometer (FR800)

The FR800 is an additional Si-FR applied in order to corroborate the accuracy of the T-T_{90} determination. This filter radiometer was applied for the determination of the thermodynamic temperature at 550 °C and 660 °C. The radiometric measurements of the thermodynamic temperature at the LABB use of FR800 have been determined in these following periods (measurement period : ITS-90 temperature of the LABB temperature); 10 to 13 December 2007 : 660 °C and 21 to 28 January 2008 : 550 °C.

The results for$T$-T_{90} as the function of the aperture distance at the LABB temperatures of 550 °C and 600 °C are illustrated in figure 6.14(A) respective figure 6.14(B). The aperture distance dependence and the diffraction correction are already considered and the uncertainty due to these factors are represented in the error bars. In the frame of these uncertainties no other additional systematic effect are identifiable. Therefore the result for T-T_{90} determined with the FR800 has been calculated as the mean value of all measurements.

The result for T-T_{90} for both investigated ITS-90 temperatures and their uncertainties are summarized in table 6.11.

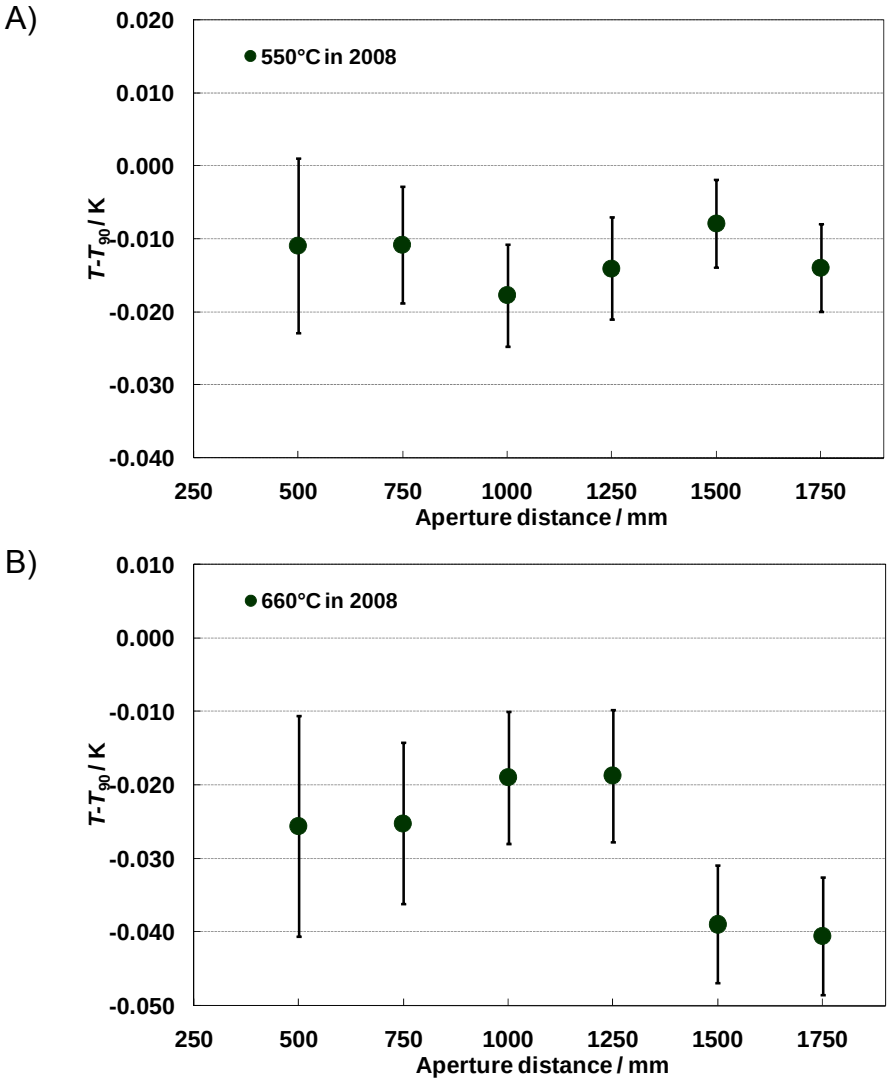

Figure 6.14 : The results for T-T_{90} as a function of the aperture distance for the ITS-90Temperatures of: A) 550 °C, and B) 660 °C determined with FR800. The displayed error bars include the uncertainty from the diffraction correction and the aperture distance determination.

Table 6.11: The deviation of the ITS-90 temperature from the thermodynamic temperature (T-T_{90}) determinated with the FR800 with the corresponding standard uncertainty (k=1)

t_{90}	Measurement period 10.12.2007 - 28.01.2008	$u(T\text{-}T_{90})$ / mK
	T-T_{90} / mK	
550 °C	-13	21
660 °C	-18	27

6.6.3 The thermodynamic uncertainty of the ITS-90

The assigned temperature values of the of the high temperature fixed-points of the ITS-90, namely aluminum (Al), silver (Ag), gold (Au) and copper (Cu), are based on ratio measurements of the radiances between a reference blackbody (variable temperature blackbody) at the temperature of 730 K and each of the fixed-point blackbodies above. The reference temperature of 730 K has its origin in the preparation of the primary thermometric measurements for the introduction of a new and improved temperature scale as the follow-up scale for the IPTS-68 from 1968. In two experiments for the determination of the deviation between the thermodynamic temperature T and the practical temperature T_{68}, T-T_{68} was firstly measured with a constant volume gas thermometer in 1976 in the temperature range from 273.16 K to 730 K and later in 1989 with a minimal modified apparatus in the temperature range from 503 K to 933 K. The difference for T-T_{68} between these two measurements at the highest common temperature (730 K) amounted 30 mK. At that time, in this temperature range, no other kind of primary thermometer which was independent from the gas thermometry was available. Therefore the CCT applied the average value between these two measurements with an uncertainty of 15 mK as the reference temperature for the new temperature scale (ITS-90) for the temperature of 730 K [**14**]. This thermodynamic uncertainty ΔT_{ref} is passed up by the pyrometric ratio measurement of temperature to the thermodynamic temperature determination of the higher fixed-points, Al, Ag, Au and Cu according to the equation :

$$\Delta T(T) = \left(\frac{T}{T_{\mathrm{ref}}} \right)^2 \Delta T_{\mathrm{ref}} \qquad 6.28$$

Therefore the thermodynamic temperature of the high temperature fixed-points e.g. the Ag-fixed-point has an uncertainty of the thermodynamic temperature of 40 mK. The result for T-T_{90} in this work, which are independent from gas thermometry, can be used for the identification the correct value of this reference temperature in order to improve the accuracy of the ITS-90. This can be done either by fitting the results for T-T_{90} with equation 6.28 and using ΔT_{ref} as the fit parameter or the direct measurement of ΔT_{ref} at the reference temperature of 730 K.

6.6.4 Discussion of results for T-T_{90}

All results for the absolute radiometric determination of the deviation between the ITS-90 temperature and the thermodynamic temperature (T-T_{90}) at the blackbody LABB with all filter radiometers applied in this work are summarized and illustrated in figure 6.15.

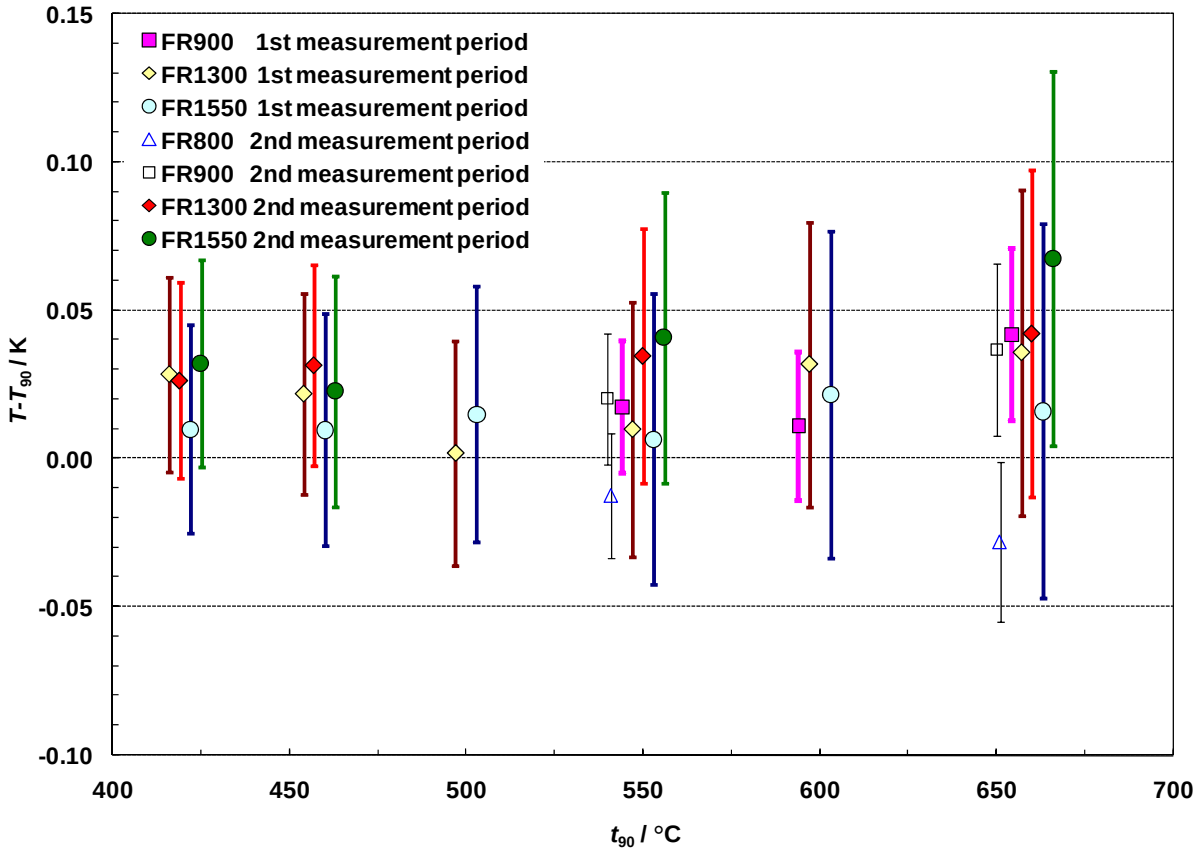

Figure 6.15 : The results for the determination of the deviation between the thermodynamic temperature and the ITS-90 temperature (T-T_{90}) in the temperature range from 419 °C (zinc fixed-point) to 660 °C (aluminum fixed-point). The figure shows the results of the absolute radiometric measurements at the blackbody LABB with two new InGaAs filter radiometers (FR1300 and FR1550) and two Si-FRs (FR800 and FR900). The error bars showed in this figure represent the standard uncertainty (k=1) of these determinations

From figure 6.15, it can be seen that the results of the determination of T-T_{90} for all applied filter radiometer and at all investigated blackbody temperatures agree within their standard uncertainty. The measurement results of T-T_{90} performed with the two new InGaAs filter radiometers, their spectral irradiance responsivity being traceable to the spectral responsivity scale in NIR wavelength range (950 nm to 1650 nm) disseminated on a single InGaAs photodiode, are consistent with the independent measurements results from the Si-FRs, their spectral irradiance

responsivity being traceable to the spectral responsivity scale in wavelength range from 500 nm to 900 nm disseminated on a Si-trap detector.

In order to be able to make a statement which of the selected gas thermometric reference temperatures should have been used for the construction of the ITS-90, the measurement results for T-T_{90} from the FR1300, the FR1550 and the mean vale of all filter radiometers applied in this work have been fitted with equation 6.28 using ΔT_{ref} as the fit parameter. The results for the obtained fit parameter ΔT_{ref} are shown in table 6.12 and the associated polynomial fit function together with the results for T-T_{90} are illustrated in figure 6.16 (for FR1300), figure 6.17 (for FR1550) and figure 6.18 (for all filter radiometers applied in this work).

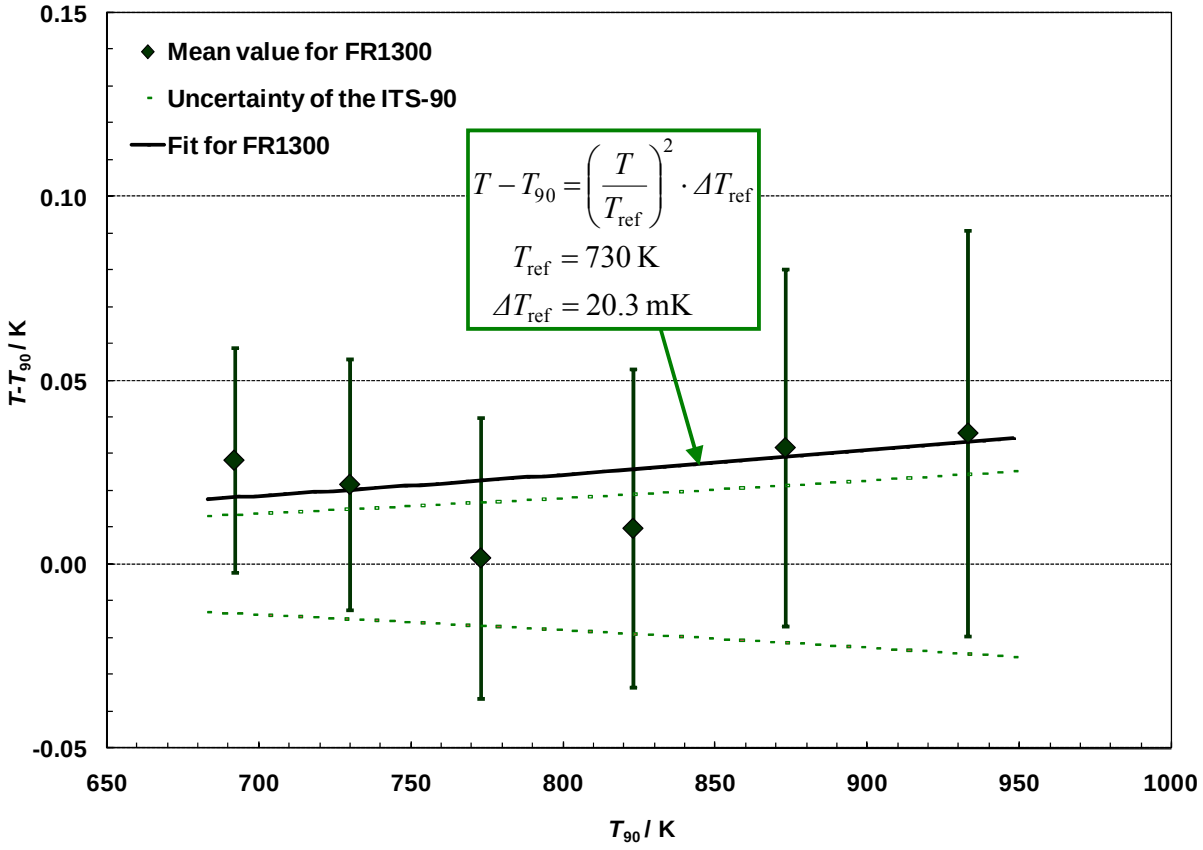

Figure 6.16 : The deviation between the thermodynamic temperature and the ITS-90 temperature, T-T_{90}, measured with the filter radiometer FR1300. The thick plotted line is the fit curve with the equation 6.28 with ΔT_{ref} as the fit parameter. The thermodynamic uncertainty of the ITS-90 is represented as the dotted line.

As showing in figure 6.16, the results of T-T_{90} from the FR1300 are located above the upper boundary of the uncertainty range of the ITS-90, however in the

temperature range between 692 K to 933 K the error bars of these results (T-T_{90}) are still enclosed in the boundary of the uncertainty range of ITS-90.

Table 6.12: The results of the fitted deviation ΔT_{ref} between the reference temperature defined by the ITS-90 and the thermodynamic temperature at T_{90} = 730 K, calculated by fitting of the equation 6.28 to the experimental results for T-T_{90} from both new InGaAs filter radiometers resp. all filter radiometers applied in this work.

Filter radiometer	ΔT_{ref}	$u(\Delta T_{\mathrm{ref}})$, k=1
FR1300	20.3 mK	6.4 mK
FR1550	19.3 mK	3.1 mK
Mean value of all filter radiometers	13.9 mK	8.1 mK

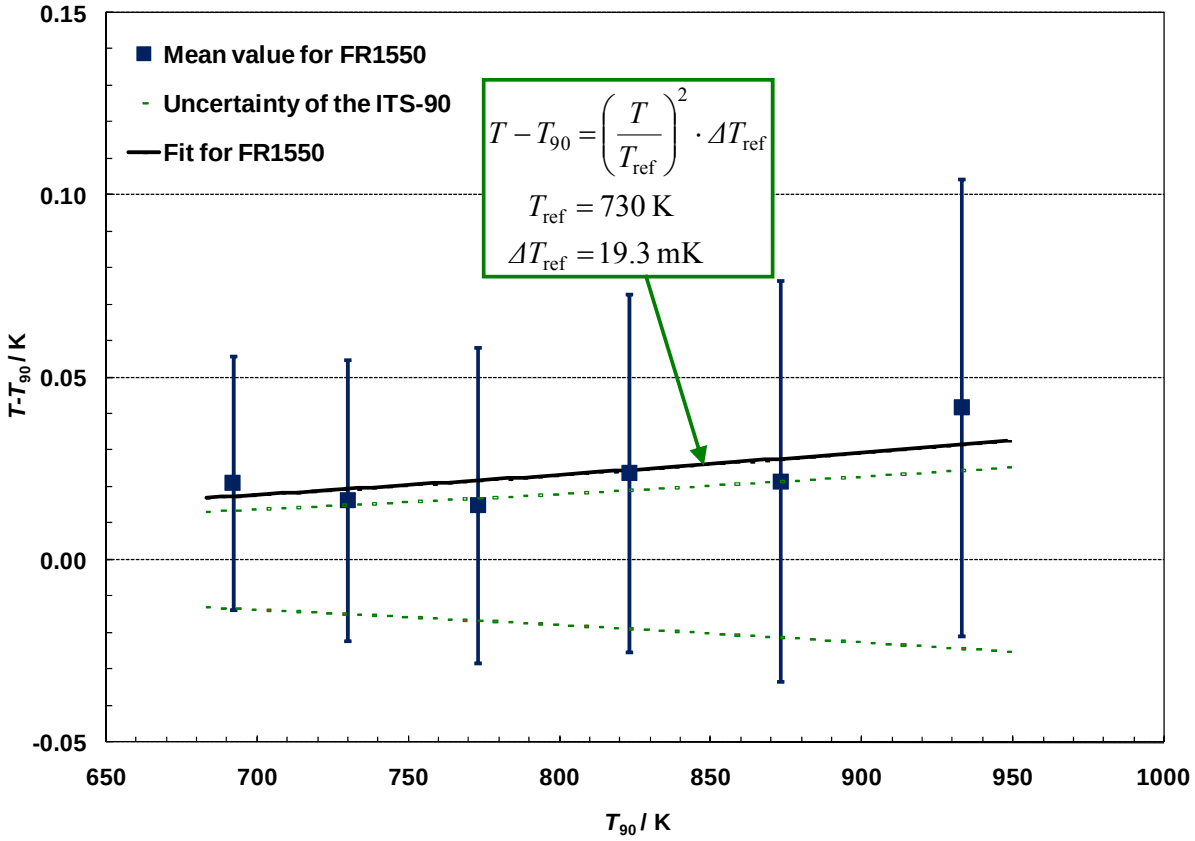

Figure 6.17 : The deviation between the thermodynamic temperature and the ITS-90 temperature, T-T_{90}, measured with the filter radiometer FR1550. The thick plotted line is the fit curve with the equation 6.28 and ΔT_{ref} as the fit parameter. The thermodynamic uncertainty of the ITS-90 is represented as the dotted line.

From the fit curve according to equation 6.28 showed in figure 6.17, the fit parameter ΔT_{ref} amounts 20.3 K with an uncertainty of 6.4 mK (see table 6.12).

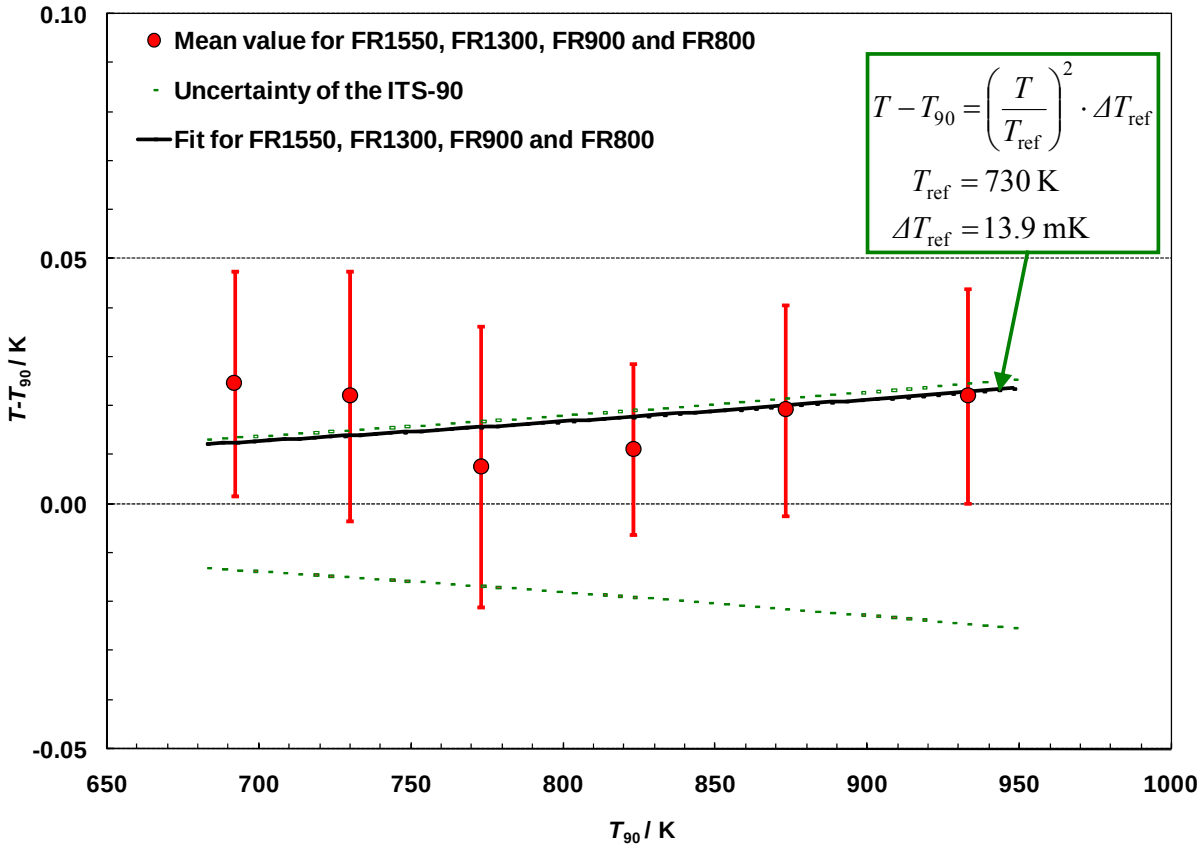

Figure 6.18 : The mean value of the results of T-T_{90} measured with all filter radiometers applied in this work (FR1300, FR1550,FR900 and FR800). The thick plotted line is the fit curve with the equation 6.28 and ΔT_{ref} as the fit parameter. The thermodynamic uncertainty of the ITS-90 is represented as the dotted line.

The results for T-T_{90} from the filter radiometer FR1550, shown in figure 6.17 are also located above the upper boundary of the thermodynamic uncertainty of the ITS-90 but the error bar of the results of T-T_{90} from this filter radiometer still count in the uncertainty boundary of this uncertainty of ITS-90. The result for the fit parameter ΔT_{ref} from the fit curve with the equation 6.28 for the filter radiometer FR1550 amounts 19.3 mK and the uncertainty of ΔT_{ref} from the fit curve is 3.1 mK (k=1).

As shown in figure 6.15, the results for T-T_{90} from all filter radiometers applied in this work agree very well within their standard measurement uncertainty. Therefore the mean value of all filter radiometer can be used for the determination of the reference temperature of the ITS-90. The standard uncertainty of the mean value

from all filter radiometer is reduced due to the more available information from the measurement results. From figure 6.18 it can be seen that the results for T-T_{90} from all filter radiometer applied in this work are also located above the upper boundary resp. inside the boundary of the thermodynamic uncertainty of ITS-90. In the temperature range from 773 K to 933 K the results for T-T_{90} are located inside the boundary of the thermodynamic uncertainty of ITS-90 and at the temperature of 730 K the error bar of the result is enclosed with the boundary of this uncertainty. The fit curve according to the equation 6.28 for these results gave the fit parameter ΔT_{ref} of 13.9 mK with an uncertainty of 8.1 mK.

The results for ΔT_{ref} from these three fit curves agree very well with the obtained values for ΔT_{ref} from fit curves in the previous investigations of T-T_{90} with the absolute spectral radiometric method in [**10**] and [**65**]. T-T_{90} in the previous investigations was determined with silicon photodiode based filter radiometer (Si-FRs). The fit pararmeter for ΔT_{ref} of the fit curves from these investigations amounted 15 mK ± 8 mK for the fit for the results from a Si-FR with the center wavelength at 676 nm (FR676), 16.5 mK ± 6 mK for the fit of the results from a Si-FR with the center wavelength at 801 nm (FR800) and 16.4 mK ± 8.1 mK for the fit of the results from a Si-FR with the center wavelength at 903 nm (FR900).

Furthermore the thermodynamic temperature at the reference temperature at 730 K were directly measured with the new InGaAs-FRs (and the results of the determination of the T-T_{90} at 730 K have been presented in this work). The result for T-T_{90} at the temperature of 730 K in this work amounts 22 mK ± 24 mK and agrees well within the measurement uncertainty with the result for T-T_{90} at this reference temperature from the previous investigation in [**65**], which was the first time that the thermodynamic temperature at temperature of 730 K was measured directly with the FR900 and the result for T-T_{90} amounted 13 mK ± 15 mK.

Therefore, the results of all filter radiometers applied in this work have been confirm the assumption that the selection of the value of the reference temperature, originating from the gas thermometry, at 730 K was around 15 mK too low and indicated the fact that the reference temperature of gas thermometry from the measurement by Edsinger et al. in year 1989 [**5**] as the thermodynamic basis of the ITS-90 above 730 K is more physically plausible. For a better visualization of this conclusion figure 6.19 shows the deviation between the thermodynamic temperature,

T, and the ITS-90 temperature, T_{90}, with two assumption: T_{90} corresponding to the ITS-90 on the basis of the reference temperature form Edsinger et al. [**5**] and T_{90} corresponding to the ITS-90 on the basis of Guildner et al. [**13**].

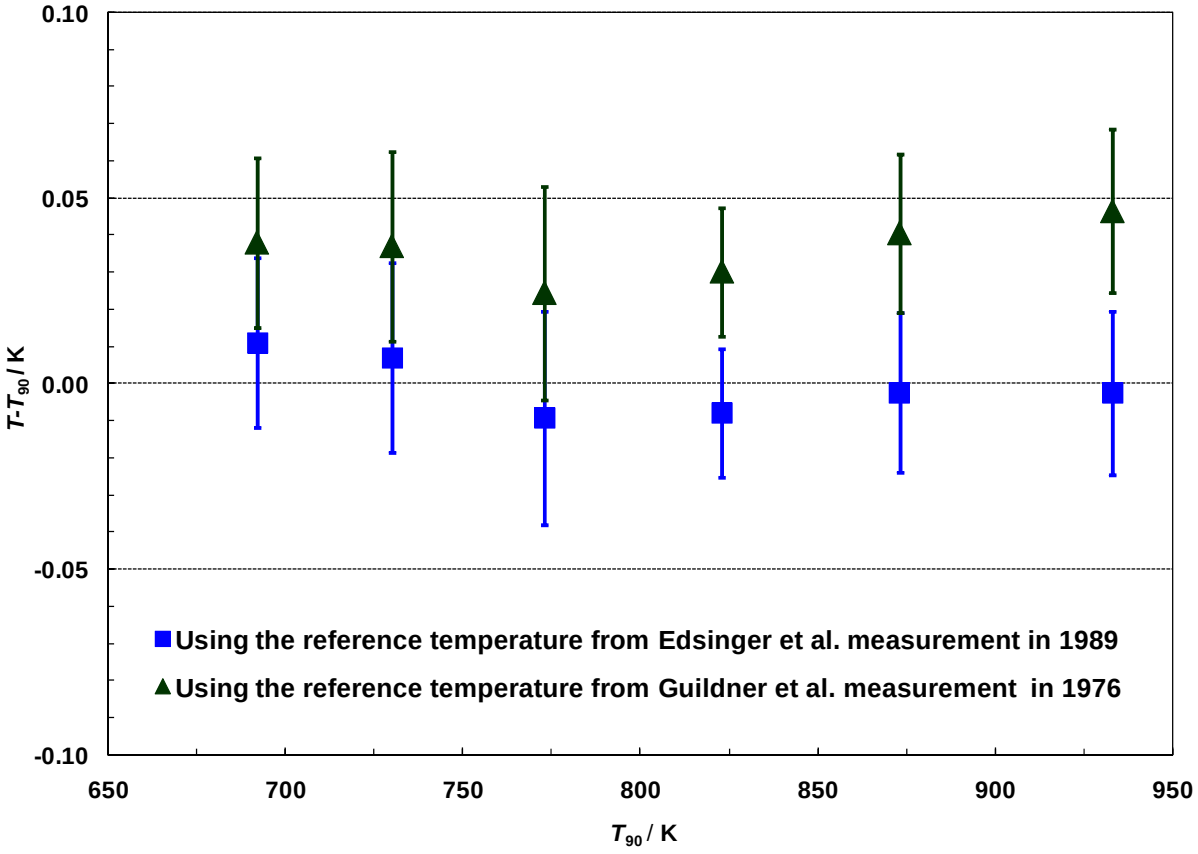

Figure 6.19 : The results for T-T_{90} as the function of T_{90} corresponding to the ITS-90 on the basis of the reference temperature (730 K) measured by Edsinger et al. in 1989 respective T_{90} corresponding to the ITS-90 on the basis of the reference temperature measured by Guildner et al in 1976.

Figure 6.19 shows that the results for T-T_{90} as the function of T_{90} corresponding to the ITS-90 on the basis of the reference temperature (730 K) measured by Edsinger et al in 1989 are located closely to the zero value which confirm that the thermodynamic temperature and T_{90} are close to the same value in contrast to the results for T-T_{90} as the function of T_{90} corresponding to the ITS-90 on the basis of the reference temperature measured by Guilder et al in 1976 which show a significant deviation above zero which lead to the conclusion that the numerical values for T_{90} are significantly less correct with respect to the thermodynamic temperature.

An overview of the classification of the results for T-T_{90} in this work with the previous investigations of thermodynamic temperature by spectral radiometric measurements and by the gas thermometry are illustrated in figure 6.20. The illustration of the previous investigations of the deviation between thermodynamic temperature and the International Temperature Scale shows the results for T-T_{90} in the temperature range between Al-fixed-point and Ag-fixed point from [**10**] as well as the results for T-T_{90} in the temperature range between the reference temperature at 730 K to Al-fixed point from [**65**]. Also presented in this figure are the results of the both gas thermometric measurements [**5,13**], which were used as the thermodynamic basis for the ITS-90 up to the temperature of 730 K. The results of the T-T_{90} in this work confirm in the scale of their standard measurement uncertainty the trend of the spectral radiometric measurement from [**65**] and agree very well with the result from the gas thermometry measurements performed by Edsinger et al in 1989.

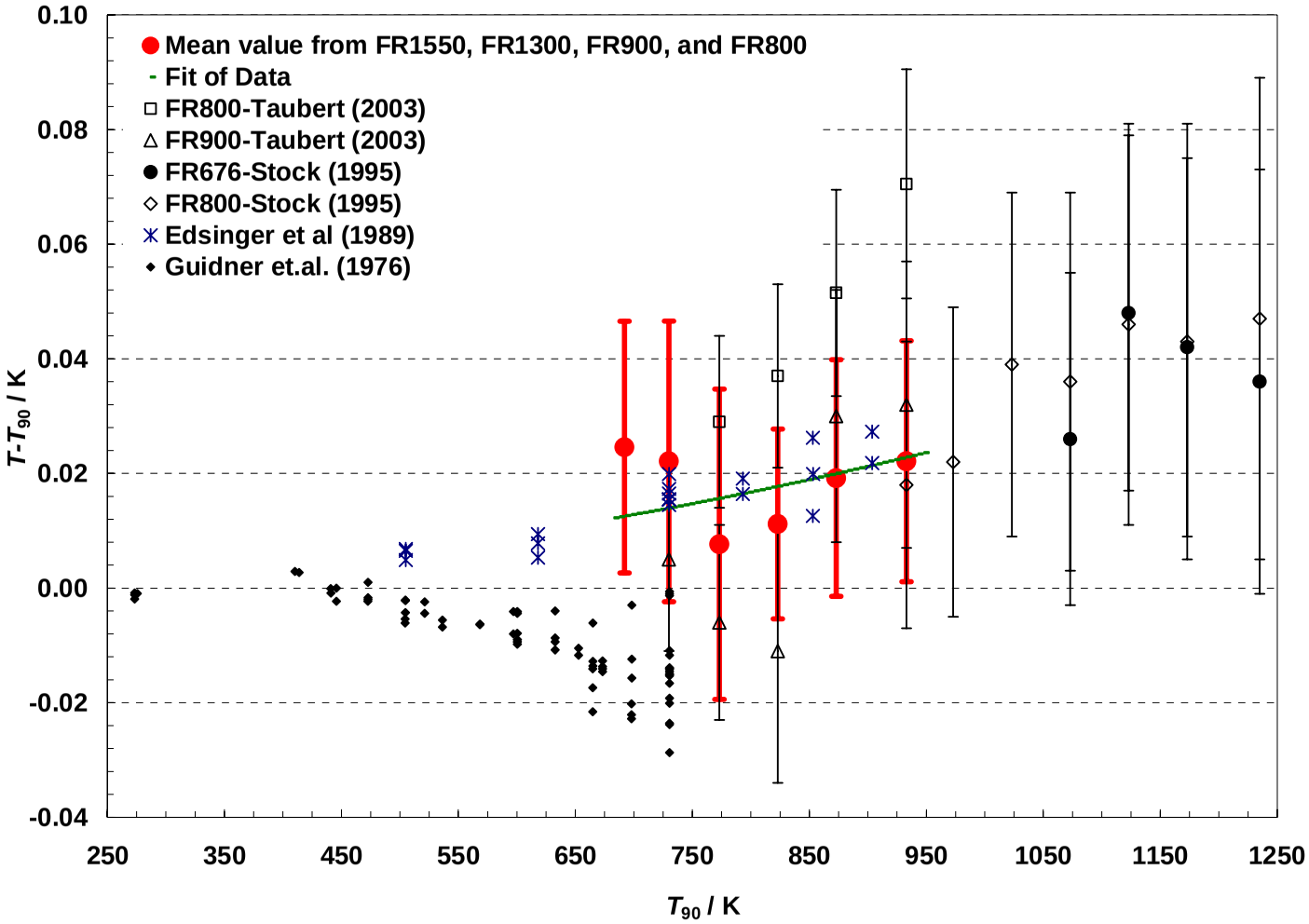

Figure 6.20 : The classification of the result for T-T_{90} in this work with the previous investigation of thermodynamic temperature by the spectral radiometric measurement in the temperature range between Al-fixed-point and Ag-fixed point from [**10**] as well as in the temperature range between 730 K to Al-fixed point from [**65**] and the results of the both gas thermometric measurements from [**5**] and [**13**] up to the temperature of 730 K. The error bars represent the measurement uncertainty with k = 1.

Chapter VII

Summary

In this work, the thermodynamic temperature in the temperature range from 692 K to 933 K is determined by the measurement of the spectral irradiance of a blackbody with absolute calibrated filter radiometers. Thereby the deviations of the fixed-point temperatures of the ITS-90 from the thermodynamic temperature (T-T_{90}) are investigated. The investigation was performed for several temperatures in the interval between the zinc-fixed-point (692.677 K) and the aluminum-fixed-point (933.473 K), namely at 419 °C, 457 °C, 500 °C, 550 °C, 600 °C and 660 °C.

The large area, double sodium heat-pipe blackbody (LABB) was used as a high-accuracy source of spectral irradiance. The emissivity of the LABB was calculated by a Monte-Carlo simulation and resulted 0.9996 at the temperature of 457 °C and 0.9999 for the temperature above 450 °C. The temperature stability of the LABB at the temperature of 419 °C is ±0.5 mK and ±2 mK at the temperature of 660 °C.

Filter radiometers are used as the detectors for the measurement of the spectral irradiance of a blackbody. Two new InGaAs filter radiometers were built in order to take advantage from the new and improved NIR spectral responsivity scale. These two new InGaAs filter radiometers were optimized with respect to their center wavelength at 1300 nm and 1550 nm and bandwidth (FWHM) of 50 nm for a calibration with the lowest possible uncertainties, which is mandatory for high-accuracy radiometric temperature measurements.

The InGaAs filter radiometers were calibrated in terms of their spectral irradiance responsivity against a transfer detector, a single InGaAs photodiode, at the spectral comparator facility of PTB. The transfer detector was previously calibrated in terms of spectral responsivity against primary detector standard, a cryogenic electrical substitution radiometer in the NIR wavelength range from 950 nm to 1650 nm.

A tuneable laser- and monochromator based cryogenic radiometer facility has been newly developed in this work in order to improve the spectral responsivity scale of transfer detectors in NIR spectral range. By using the monochromatized radiation from a tungsten halogen lamp, the calibration of the InGaAs transfer-detector can be performed in the entire NIR spectral range from 950 nm to 1650 nm. Thereby the uncertainty of the calibration has been reduced from 0.17% to about 0.10%. The uncertainty of this calibration is dominated by the cryogenic radiometer instability due to a drift and noise. This contribution to the overall relative uncertainty can be decreased by increasing the radiant power. The second largest contribution is the uncertainty associated with the window transmittance correction, which is measured at each wavelength before, during and after each calibration. Furthermore, the uncertainty of the wavelength of the monochromatized radiation gives a significant contribution. These uncertainty contribution can be reduce by the application of tuneable diode lasers as radiation sources. With the tuneable diode lasers the InGaAs transfer-detector can be calibrated throughout two limited wavelength ranges i.e. 1260 nm to 1370 nm and 1460 nm to 1580 nm. With the much higher radiation power and the narrow bandwidth of the tuneable diode lasers, the uncertainty of the calibration of the spectral responsivity was significantly reduced to 0.02%-0.03%. The uncertainty of the spectral responsivity scale of the InGaAs transfer-detector has been reduced by about a factor of six and is now in the same order of magnitude as the spectral responsivity scale maintained in the visible spectral range on Si trap detectors.

For the calibration at the spectral comparator facility, the sensitive area of the transfer standards for spectral power responsivity is limited with a precision, diamond-turned aperture with a nominal diameter of about 3 mm. By this means, the InGaAs transfer-detector was transferred into a transfer standard of spectral irradiance responsivity. Thereby the filter radiometers can be calibrated in terms of their spectral irradiance responsivity against this transfer-detector. The influence of stray light was minimized by complementing the grating monochromator with a prism predisperser. In order to calibrate the filter radiometer for the use with unpolarized sources i.e. blackbody radiation, the calibration was performed in two orthogonal positions (0° and 90°). The influence of temperature on the interference filters and the photodiodes is considered and reduced by a careful control of the temperature of the both detectors (transfer-detector and filter radiometer) within ±50 mK during

calibration. With this calibration method, the two new InGaAs filter radiometers have been calibrated with uncertainties of about 0.06%.

The calibrated InGaAs filter radiometers have been used directly after their calibration for the absolute radiometric determination of the deviation between the thermodynamic temperature and the ITS-90 temperature (T-T_{90}) at the blackbody LABB in the temperature range between the zinc-fixed-point and aluminum-fixed-point. The radiometric determination of thermodynamic temperature of the blackbody T is higher than the ITS-90 temperature T_{90}. The results of the determination of T-T_{90} for both applied filter radiometer and at all investigated blackbody temperatures agree within their standard uncertainty. The uncertainties of the direct determination of T-T_{90} at the gas thermometry reference temperature of 730 mK by using FR1300 and FR1550 are 34 mK and 39 mK respectively. These uncertainties are too high for a final decision between the two conflicting gas thermometry measurements at NIST. However this decision can be done by fitting the results for T-T_{90}. The fit curves of the results for T-T_{90} from FR1300 and FR1550 result in a deviation between the thermodynamic temperature and the ITS-90 temperature at the reference temperature 730 K of 20.3 mK $\pm$ 6.4 mK (k=1) and 19.3 mK $\pm$ 3.1 mK (k=1) respectively.

Furthermore, measurements of the thermodynamic temperature independent from the NIR spectral responsivity scale were performed with Si photodiode based filter radiometer with a center wavelength of 900 nm (FR900) and 800 nm (FR800) in the temperature range from 550 °C to 660 °C in order to underpin the accuracy of the results for T-T_{90} measured with the InGaAs filter radiometers. The results from these Si filter radiometers are consistent with the results of both InGaAs filter radiometers.

Within the standard uncertainty (k=1) the results of T-T_{90} in this work clearly agrees with the set of gas thermometry measurements by Edsinger and Schooley at NIST in 1989. The gas thermometry results by Guildner und Edsinger in 1979 show a significant deviation from these results. With this absolute radiometric measurement method for the thermodynamic temperature which is independent from the gas thermometry, it was successfully verified that for the construction of ITS-90, the value of the selected reference temperature at 730 K was too low. Therefore the measurement results from this work constitute an important contribution for the improvement of the thermodynamic accuracy of the ITS-90.

Bibliography

1. Messtechnik für die Industrie, Physikalische-Technische Bundesanstalt, Braunschweig und Berlin, 1995

2. Climate change science - Some recent results from the Hadley Centre, The Hadley Centre for Climate Prediction and Research, UK Met Office, 2001

3. Kyoto protocol to the united nations framework convention on climate change, Kyoto, 1997

4. T. J. Quinn, News from the BIPM, Metrologia, 37, 87-98, 2000

5. R. E. Edsinger, J. F. Schooley, Differences between the Thermodynamic Temperature and t(IPTS-68) in the Range 230 °C to 660 °C, Metrologia, 26, 95-106, 1989

6. M. R. Moldover, S. J. Boyes, C. W. Meyer, A. R. H. Goodwin, Primary Acoustic Thermometry from 217 K to 303 K, aus Proceedings of TEMPMEKO ’99, ed. by J. F. Dubbeldam and M. J. de Groot, IMEKO, Delft, 412-417, 1999

7. H. Luther, K. Grohmann, B. Fellmuth, Determination of thermodynamic temperature and ^{4}He virial coefficients between 4,2 K and 27,0 K by dielectric constant gas thermometry, Metrologia, 33, 342-352, 1996

8. D. R. White, R. Galleano, A. Actis, H. Brixy, M. de Groot, J. Dubbeldam, A. L. Reesink, F. Edler, H. Sakurai, R. L. Shepard, J. C. Gallop, The status of Johnson noise thermometry, Metrologia, 33, 325-335,1996

9. T. J. Quinn, J. E. Martin, Total radiation measurements of thermodynamic temperature, Metrologia, 33, 375-381, 1996

10. M. Stock, Realisierung und Vergleich von drei radiometrischen Primärnormalen im sichtbaren Spektralbereich: Kryoradiometer, Elektronenspeichering BESSY I und Hohlraumstrahler, Dissertation, PhD thesis, TU Berlin, Berlin, 1995

11. C. R. 7^{e} Conf. Gén. Poids et Mes., Annexe IV-V, 94-101, 1927

12. H. Preston-Thomas, The International Temperature Scale of 1990 (ITS-90), Metrologia, 27, 3-10, 1990

13. L. A. Guildner, R. E. Edsinger, Deviation of International Practical temperatures from Thermodynamic Temperatures in the Temperature Range from 273.16 K to 730 K, J. Res. Nat. Bur. Stand., 80A, 703-738, 1976

14. R. L Rusby., R. P Hudson., M Durieux., J F Schooley, P. P. M Steur., C. A Swenson, Thermodynamic Basis of the ITS-90., Metrologia, 28, 9-18, 1991

15. P. B. Coates, J. W. Andrews, A precise determination of the freezing point of copper, J. Phys. F.: Metal Phys., 8(2), 277-285, 1977

16. J. Fischer, H. J. Jung, Determination of the Thermodynamic Temperatures of the Freezing Points of Silver and Gold by Near-Infrared Pyrometry, Metrologia, 26, 245-252, 1989

17. H. J. Jung, A Measurement of Thermodynamic Temperatures Between 683 K and 933 K by an Infrared Pyrometer, Metrologia, 23, 19-31, 1986

18. T. Ricolfi, F. Lanza, The silver and copper freezing points as accurate reference standards for radiation pyrometry, High Temperatures- High Pressures, 9, 483-487, 1977

19. V. I. Sapritsky, Black-body radiometry, Metrologia, 32, 411-417, 1995/96

20. A.C. Parr, R.U. Datla, J.L. Gardner, Optical radiometry, Experimental Methods in the physical sciences, vol.41, 231-290, Elsevier Inc, ISSN 1079-4042, 2005

21. D. R. Taubert, J. Hartmann, J. Hollandt, J. Fischer, Investigation of the Accuracy of the ITS-90 with Reference to Thermodynamic Temperature in the Range from 400 °C up to 660 °C, in Temperature: Its Measurement and Control in Science and Industry, Volume 7, ed. Dean C. Ripple, 7-12, AIP, 2003

22. T. J. Quinn, J. E. Martin, A radiometric determination of the Stefan- Boltzmann constant and thermodynamic temperatures between -40 °C and +100 °C, Phil. Trans. Roy. Soc. London, 316, 85-189, 1985

23. L. Werner, R. Friedrich, U. Johannsen, A. Steiger, Precise scale of spectral responsivity for InGaAs detectors based on a cryogenic radiometer and several laser sources, Metrologia, 37, 523-526, 2000

24. L. Werner, J. Fischer, U. Johannsen, J. Hartmann, Accurate determination of the spectral responsivity of silicon trap detectors between 238 nm and 1015 nm using a laser-based cryogenic radiometer, Metrologia, 37, 279-284, 2000

25. D. C. Ripple, D. R. Defibaugh, M.R. Moldover, and G.F. Strouse, Techniques for Primary Acoustic Thermometry to 800 K, Temperature: Its Measurement and Control in Science and Industry, Vol. 7, Proc. AIP Conf. 684, 25-30, 2003

26. S. German, P. Drath, Handbuch der SI-Einheiten, Friedr. Vieweg & Sohn, Braunschweig/Wiesbaden, S. 161ff, 1979

27. R. L. Rusby, R. P. Hudson, M. Durieux, K. Grohmann, H.-J. Jung, P. P. M. Steur, and J. V. Nicholas, "The status of thermodynamic thermometry", Metrologia, 33, 409-414, 1996

28. J. Fischer, B. Fellmuth, Temperature metrology, Rep. Prog. Phys. 68, 1043–1094, 2005

29. D. C. Ripple, D. R. Defibaugh, K. A. Gillis, M. R. Moldover, Primary Acoustic Thermometer for use up to 800 K, from Proceedings of TEMPMEKO ’99, ed. by J. F. Dubbeldam and M. J. de Groot, IMEKO, Delft, 418-423, 1999

30. M. B. Ewing, J. P. M. Trusler, Primary acoustic thermometry between T=90 K and T=300 K, J Chem. Thermodynamics, Vol: 32, 1229-1255, 2000

31. H. Nyquist, Thermal Agitation of Electric Charge in Conductors, Phys. Rev. 32, 110–113, 1928

32. N. P. Fox, J. E. Martin, D. H. Nettleton, Absolute Spectral Radiometric Determination of the Thermodynamic Temperatures of the Melting/ Freezing Points of Gold, Silver and Aluminium, Metrologia, 28, 357-374, 1991

33. J. E. Martin, T. J. Quinn and B. Chu, Further Measurements of Thermodynamic Temperature Using a Total Radiation Thermometer: the Range –130 °C to +60 °C, Metrologia, 25, 107–12, 1988

34. J. E. Martin and P. R. Haycocks, Design considerations for the construction of an absolute radiation detector at the NPL, Metrologia, 35, 229–33, 1998

35. G. K. Burgess, The International Temperature Scale, Bur.Stand. J. Res., 1, 635-640, 1928

36. H. F. Stimson, The International Temperature Scale of 1948, J. Res. Natl. Bur. Stand. (U.S.), 42, 209-217, 1949

37. F. G. Brickwedde, H. van Dijk, M. Durieux, J. R. Clement, and J.K. Logan, The 1958 ^{4}He Scale of Temperature, J. Res. Natl. Bur. Stand. (U.S.), 64A, 1-17, 1960

38. H. F. Stimson, The International Practical Temperature Scale of 1948. Text Revision of 1960, NBS Monograph 37, issued September 8, 7p, 1961

39. R. H. Sherman, S. G. Sydoriak, and T. R. Roberts, The 1962 Scale of Temperatures, IV. Tables, J. Res. Natl. Bur. Stand. (U.S.) 68A, 579-588, 1964

40. The International Practical Temperature Scale of 1968, Metrologia, 5, 35-44, 1969

41. The International Practical Temperature Scale of 1968, Amended Edition of 1975, Metrologia, 12, 7-17, 1976

42. The 1976 Provisional 0.5 K to 30 K Temperature Scale, Metrologia, 15, 65-68, 1979

43. T. J. Quinn, Temperature, 2nd edn. Monographs in Physical Measurement (Academic Press, London), 175–182, 1990

44. G. Kirchhoff, Über das Verhältnis zwischen dem Emissionsvermögen und dem Absorptionsvermögen der Körper für Wärme und Licht, Ann. Phys. Chem. 109, 275-301, 1860

45. M. Planck, Über das Gesetz der Energieverteilung im Normalspectrum, Ann. Phys. 4, 553-563, 1901

46. R. E. Bedford and C. K. Ma, Emissivities of diffuse cavities: Isothermal and nonisothermal cones and cylinders, Journal of the Optical Society of America, (64 (3)):339–349, 1974

47. A. V. Prokhorov, Monte-Carlo method in optical radiometry, Metrologia, 35, 465-471, 1998

48. J. Hartmann and D. R. Taubert, Assessing blackbody emissivity by monte carlo simulation, Proc. of the Int. Conference of Infrared Sensors and Systems, Erfurt, Germany, 133–138, 2002

49. J. Hollandt, R. Friedrich, B. Gutschwager, D.R. Taubert and J. Hartmann, High-accuracy radiation thermometry at the National Metrology Institute of Germany, the PTB, High Temperatures-High Pressures, volume 35/36, 379-415, 2003/2004

50. W. Wien, Sitzungsber. d. Preuss. Akad. Wiss. Berlin, Math-Phys. Kl., 6, 55-62, 1893

51. L Boltzmann, Ableitung des Stefanschen Gesetzes, betreffend die Abhängigkeit der Wärmestrahlung von der Temperatur aus der elektromagnetischen Lichttheorie. Ann. Phys. Ser. 2, 22Ann., 291-294, 1884

52. J. Stefan, Über die Beziehung zwischen der Wärmestrahlung und der Temperatur. Sitzungsber. Akad. Wiss. Wien 79 Teil 2, 391-428, 1879

53. A. E. Klinkmüller, P. Meindl, U. Johannsen, N. Noulkhow, and L. Werner, Improved NIR spectral responsivity scale of the PTB and implications for radiation thermometry, Proceedings of the 9th international conference on new developments and applications in optical radiometry NEWRAD2005, 115, 2005

54. P. Meindl, N. Noulkhow, A.E. Klinkmüller, U. Johannsen, and L. Werner, "New PTB detector calibration capability for spectral responsivity in the NIR range", Proceedings of the 9th international conference on infrared sensors & systems, IRS^2 2006, 213-215, 2006

55. M. López, H. Hofer, S. Kück, High accuracy measurement of the absolute spectral responsivity of Ge and InGaAs trap detectors by direct calibration against an electrically calibrated cryogenic radiometer in the near-infrared, Metrologia, 43, 508-514, 2006

56. D. R. Taubert, R. Friedrich, J. Hartmann, J. Hollandt, „Improved calibration of the spectral responsivity of interference filter radiometers in the visible and near infrared spectral range at PTB", Metrologia, 40, 35-38, 2003

57. N. P. Fox, Primary radiometric quantities and units, Metrologia, 37(5), 507-513, 2000

58. Manual of cryogenic radiometer from Cambridge Research & Instrumentation, Inc. (CRI).

59. P. Meindl, A. E. Klinkmüller, L. Werner, U. Johannsen, K.Grützmacher, New UV spectral responsivity scale of the PTB based on a cryogenic radiometer and an argon plasma arc radiation source, Metrologia, 43, 72-77, 2006

60. P. Meindl, Realisierung der Skala der spektralen Empfindlichkeit von Strahlungsempfängern im UV mit einem Kryoradiometer und spektral zerlegter Strahlung eines Hochstrom-Bogenplasmas, report of the research project, working group 7.21, PTB, 2005

61. N. Noulkhow, R. D. Taubert, P. Meindl and J. Hollandt, Infrared Filter Radiometers for Thermodynamic Temperature Determination below 660 °C, International Journal of Thermophysics, vol. 30, pp.131-143, 2009

62. N. P. Fox, T. R. Prior, E. Theocharous, and S. N. Mekhontsev. Solid– state detectors for infrared radiometry, Metrologia, 32, 609–613, 1995/96

63. N. P. Fox, Radiometry with cryogenic radiometers and semiconductor photodiodes, Metrologia, 32, 535–543, 1995

64. K. D. Stock, R. Heine, Spectral characterization of InGaAs trap detectors and photodiodes used as transfer standards, Metrologia, 37, 449-452, 2000

65. D. R. Taubert, Radiometrische Messung thermodynamischer Temperaturen und vergleich mit der Internationalen Temperaturskala (IST-90) im Bereich von 419 °C bis 660 °C, Dissertation, PhD Thesis, TU Berlin, Berlin, 2003

66. F. Rössler, Streulicht von Monochromatoren, OPTIK, 41(3), 293-308, 1974

67. J. Hartmann, High-temperature measurement techniques for the application in Photometry, Radiometry and Thermometry, Habilitation treatise, TU Berlin, Berlin, 2007

68. ORIEL INSTRUMENTS; Booklet of Grating Efficiency Curves

69. E. Collett, Polarized Light, Fundamentals and Applications, Marcel Dekker Inc., New York, 1993

70. F. Henning, H. Moser, Temperaturmessung, Springer, Berlin, S. 127, 1977

71. R. Friedrich, J. Fischer, M. Stock, Accurate calibration of filter radiometers against a cryogenic radiometer using a trap detector, Metrologia, 32, 509-513, 1995/96.

72. M. L. Baker, V. L. Yen, Effects of the Variation of Angle of Incidence and Temperature on Infrared Filter Characteristics, Appl. Opt., 6, 1343-1351, 1967

73. The infrared handbook, ed. W. L. Wolfe, G. J. Zissis, Washington DC, 4th Printing, S. 7-113, 1993

74. M. G. Cox, B. R. L. Siebert, The use of a Monte Carlo Method for evaluating uncertainty and expanded uncertainty, Metrologia, 43, 178-188, 2006

75. J. Hartmann, J. Fischer, J. Seidel: A non-contact technique providing improved accuracy in area measurements of radiometric apertures, Metrologia, 37, 637-640, 2000

76. E. Kosubek, private announcement, 2006

77. L. P. Boivin, Study of bandwidth effects in monochromator-based spectral responsivity measurements, Applied Optics 41(10), 1929-1935, 2002

78. M. F. Modest, Radiative Heat Transfer, McGraw-Hill Inc., New York, 1993

79. O. Brost, M. Groll, Liquid Metal Heat Pipe Applications: Thermometric Calibration Tools & Heat Transfer Components for Solar-Thermal Power Systems, in Proceedings of the 9th International Heat Pipe Conference, Ed. M A Merrigan (Los Alamos: Los Alamos National Laboratory), 110-115,1995

80. P. D. Dunn, D. A. Reay, Heat Pipes, 4th Edition, Elsevier Science Ltd, Oxford, 108, 1994

81. J. Fischer, J. Seidel and B. Wende, The double-heatpipe black body: a radiance and irradiance standard for accurate infrared calibrations in remote sensing, Metrologia, 35, 441-444, 1998

82. J. Hartmann, J. Fischer: Radiator standards for accurate IR calibrations in remote sensing based on heatpipe blackbodies, in Environmental Sensing and Applications, Proceedings of SPIE Vol. 3821, 395-403, 1999

83. V. I. Sapritsky, A. V. Prokhorov, Spectral effective emissivities of non-isothermal cavities calculated by the Monte Carlo method, Applied Optics, Vol. 34, 5645-5652, 1995

84. M. Stock, J. Fischer, R. Friedrich, H. J. Jung, B. Wende, "The double-heatpipe black body: a high accuracy standard source of spectral irradiance for measurements of $T-T_{90}$", Metrologia, 32, 441-444, 1995/96

85. L. Merz, Grundkurs der Regelungstechnik, Teil A, 2. Auflage, R. Oldenbourg, München, S. 35ff, 1964

86. G. Bönsch, E. Potulski, Measurement of the refractive index of air and comparison with modified Edlen's formulae, Metrologia, 35, 133-139,1998

87. A. V. Nikitin, V. F. Golovko, A. A. Chursin, Vl. G. Tyuterev, AIRSENTRY Software: Atmospheric Infra-Red Spectra for Emulating and Noting Transmission of Rays, Program and Manual, 1994

88. W. R. Blevin, Diffraction Losses in Radiometry and Photometry, Metrologia, 6, 39–44, 1970

89. J. M. Cowley, Diffraction Physics, North-Holland Publishing Company, Amsterdam, S. 16, 1975

90. W. H. Steele, M. De, and J.A. Bell, Diffraction corrections in radiometry. Journal of the Optical Society of America, (62 (9)):1099–1103, 1972

91. H. G. Nubbemeyer, High-temperature platinum resistance thermometers and fixed point cells for the realization of the ITS-90 in the range of 0°C to 961.78°C, TEMPERATURE, AIP, 199-202, 1990

92. Supplementary information for the International Temperature Scale of1990, BIPM, Pavillon de Breteuil, F-92310 SEVRES, S. 97 ff.,1990

93. P. J. Mohr and B. N. Taylor, CODATA recommended values of the fundamental physical constants:2002, Reviews of Modern Physics, Vol. 77, No. 1, pp41, 2005

Acknowledgements

First of all, I would like to express my deepest gratitude to Prof. Dr. Axel Hoffmann for his willingness to supervise this work, his continued guidance and the fruitful discussions helped a lot. I am indebted to Prof. Dr. Christian Thomsen who has accepted to act as a referee for this thesis.

At the Physikalisch- Technische Bundesanstalt I would like to thank Dr. Jörg Hollandt and especially Dr. Dieter Richard Taubert for their supervision, constant support, constructive comments and valuable teachings and for introducing me to the world of radiometry and radiation thermometry.

The help of Dr. Peter Meindl was essential for the spectral responsivity calibration of the transfer detectors. Very warm regards go to Dr. Rüdiger Friedrich for his support to bring me in close touch with the absolute calibration of the filter radiometers. The aperture area measurement was supported by Dr. Jürgen Hartmann and Elzbieta Kosubek. I am deeply indebted to Dr. Klaus Anhalt for his ongoing encouragement and friendship. His kindness will always be remembered.

I would like to thank my other colleagues form the working group temperature radiation, namely Thomas Schönebeck, Marco Schulz, Stephan Schiller, Beate Prußeit and Martina Becker who offered general help and support and I acknowledge the lively discussions with Berndt Gutschwager, Rolf Thomas, and Dr. Christian Monte.

The Ministry of Science and Technology Thailand and the National Institute of Metrology (Thailand) supported me by granting a Thai Government Science and Technology scholarship to do research in Germany.

Finally, I am most grateful to my wife Kanokwan, my son Donyapat and my parents for their continuous encouragement, constant care and assistance during my work in Germany.